

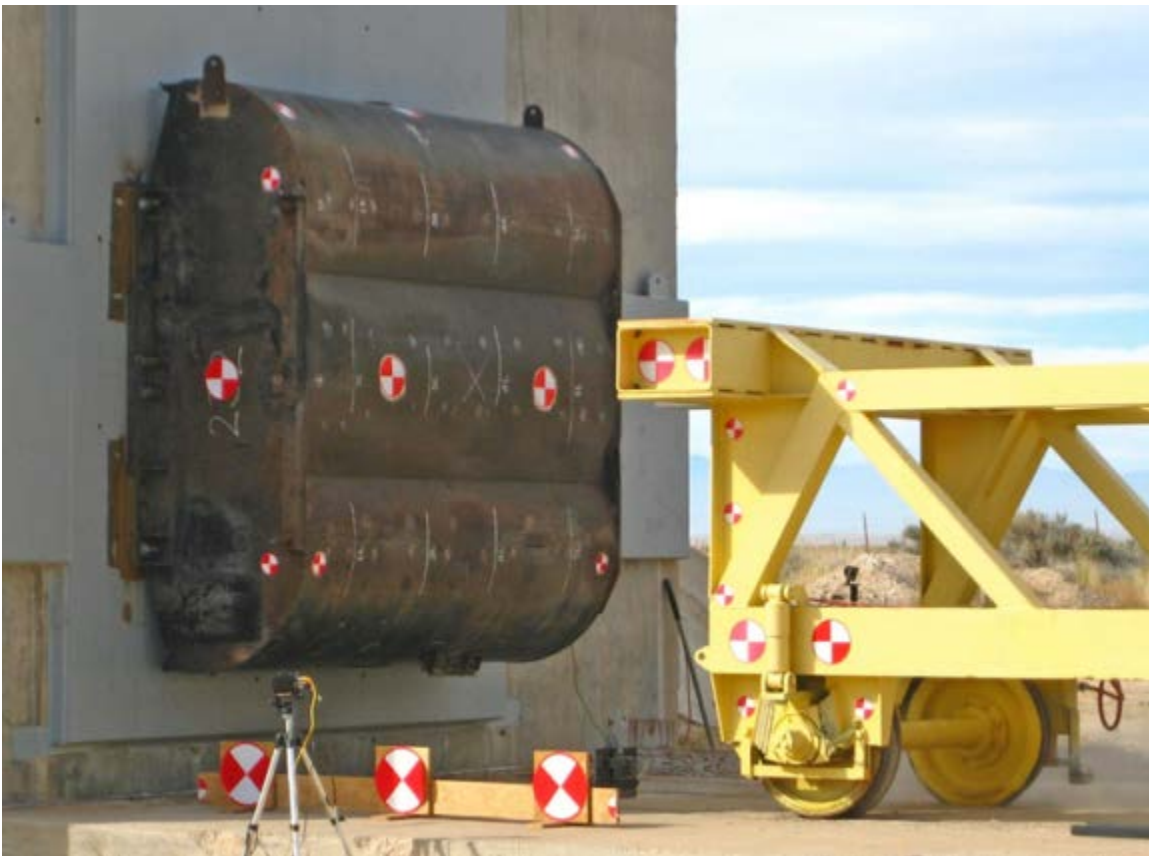


U.S. Department of
Transportation

**Federal Railroad
Administration**

Blunt Impact Tests of Retired Passenger Locomotive Fuel Tanks

Office of Research,
Development
and Technology
Washington, DC 20590



NOTICE

This document is disseminated under the sponsorship of the Department of Transportation in the interest of information exchange. The United States Government assumes no liability for its contents or use thereof. Any opinions, findings and conclusions, or recommendations expressed in this material do not necessarily reflect the views or policies of the United States Government, nor does mention of trade names, commercial products, or organizations imply endorsement by the United States Government. The United States Government assumes no liability for the content or use of the material contained in this document.

NOTICE

The United States Government does not endorse products or manufacturers. Trade or manufacturers' names appear herein solely because they are considered essential to the objective of this report.

REPORT DOCUMENTATION PAGEForm Approved
OMB No. 0704-0188

Public reporting burden for this collection of information is estimated to average 1 hour per response, including the time for reviewing instructions, searching existing data sources, gathering and maintaining the data needed, and completing and reviewing the collection of information. Send comments regarding this burden estimate or any other aspect of this collection of information, including suggestions for reducing this burden, to Washington Headquarters Services, Directorate for Information Operations and Reports, 1215 Jefferson Davis Highway, Suite 1204, Arlington, VA 22202-4302, and to the Office of Management and Budget, Paperwork Reduction Project (0704-0188), Washington, DC 20503.

1. AGENCY USE ONLY (Leave blank)		2. REPORT DATE August 2017	3. REPORT TYPE AND DATES COVERED Technical Report	
4. TITLE AND SUBTITLE Blunt Impact Tests of Retired Passenger Locomotive Fuel Tanks			5. FUNDING NUMBERS DTFR53-10-X-00061, RR28A3/NLL72	
6. AUTHOR(S) Michael Carolan, Przemyslaw Rakoczy, Karina Jacobsen			DTFR53-11-D-00008 Task Order 305	
7. PERFORMING ORGANIZATION NAME(S) AND ADDRESS(ES) Volpe National Transportation Systems Center, 55 Broadway, Cambridge, MA 02142 Transportation Technology Center, Inc., 55500 DOT Road, Pueblo, CO 81001			8. PERFORMING ORGANIZATION REPORT NUMBER	
9. SPONSORING/MONITORING AGENCY NAME(S) AND ADDRESS(ES) U.S. Department of Transportation Federal Railroad Administration Office of Railroad Policy and Development Office of Research, Development and Technology Washington, DC 20590			10. SPONSORING/MONITORING AGENCY REPORT NUMBER DOT/FRA/ORD-17/11	
11. SUPPLEMENTARY NOTES COR: Melissa Shurland				
12a. DISTRIBUTION/AVAILABILITY STATEMENT This document is available to the public through the FRA Web site at http://www.fra.dot.gov .			12b. DISTRIBUTION CODE	
13. ABSTRACT (Maximum 200 words) The Transportation Technology Center, Inc. conducted impact tests on three locomotive fuel tanks as part of the Federal Railroad Administration's locomotive fuel tank crashworthiness improvement program. Three fuel tanks, two from EMD F40PH locomotives and one from an EMD F40 locomotive, served as test specimens. A 14,075-pound impact cart equipped with a 12-inch by 12-inch impactor struck the tanks; fuel tanks 232 (F40PH) and 202 (F40) were impacted at their geometrical centers at 4.2 mph and 6.2 mph, respectively. Fuel tank 234 (F40PH) was offset from the center in the horizontal direction and impacted between the baffles at 11.2 mph. No fuel tanks ruptured. Results of the tests were eventually used for validation and refinements of finite element models developed by the John A. Volpe National Transportation Systems Center.				
14. SUBJECT TERMS Passenger locomotives, fuel tanks, impact testing, finite element analysis, diesel multiple unit, DMU, impact scenarios			15. NUMBER OF PAGES 92	
			16. PRICE CODE	
17. SECURITY CLASSIFICATION OF REPORT Unclassified	18. SECURITY CLASSIFICATION OF THIS PAGE Unclassified	19. SECURITY CLASSIFICATION OF ABSTRACT Unclassified	20. LIMITATION OF ABSTRACT	

NSN 7540-01-280-5500

Standard Form 298 (Rev. 2-89)
Prescribed by ANSI Std. Z39-18
298-102

METRIC/ENGLISH CONVERSION FACTORS

ENGLISH TO METRIC

LENGTH (APPROXIMATE)

- 1 inch (in) = 2.5 centimeters (cm)
- 1 foot (ft) = 30 centimeters (cm)
- 1 yard (yd) = 0.9 meter (m)
- 1 mile (mi) = 1.6 kilometers (km)

AREA (APPROXIMATE)

- 1 square inch (sq in, in²) = 6.5 square centimeters (cm²)
- 1 square foot (sq ft, ft²) = 0.09 square meter (m²)
- 1 square yard (sq yd, yd²) = 0.8 square meter (m²)
- 1 square mile (sq mi, mi²) = 2.6 square kilometers (km²)
- 1 acre = 0.4 hectare (he) = 4,000 square meters (m²)

MASS - WEIGHT (APPROXIMATE)

- 1 ounce (oz) = 28 grams (gm)
- 1 pound (lb) = 0.45 kilogram (kg)
- 1 short ton = 2,000 pounds (lb) = 0.9 tonne (t)

VOLUME (APPROXIMATE)

- 1 teaspoon (tsp) = 5 milliliters (ml)
- 1 tablespoon (tbsp) = 15 milliliters (ml)
- 1 fluid ounce (fl oz) = 30 milliliters (ml)
- 1 cup (c) = 0.24 liter (l)
- 1 pint (pt) = 0.47 liter (l)
- 1 quart (qt) = 0.96 liter (l)
- 1 gallon (gal) = 3.8 liters (l)
- 1 cubic foot (cu ft, ft³) = 0.03 cubic meter (m³)
- 1 cubic yard (cu yd, yd³) = 0.76 cubic meter (m³)

TEMPERATURE (EXACT)

$$[(x-32)(5/9)] \text{ } ^\circ\text{F} = y \text{ } ^\circ\text{C}$$

METRIC TO ENGLISH

LENGTH (APPROXIMATE)

- 1 millimeter (mm) = 0.04 inch (in)
- 1 centimeter (cm) = 0.4 inch (in)
- 1 meter (m) = 3.3 feet (ft)
- 1 meter (m) = 1.1 yards (yd)
- 1 kilometer (km) = 0.6 mile (mi)

AREA (APPROXIMATE)

- 1 square centimeter (cm²) = 0.16 square inch (sq in, in²)
- 1 square meter (m²) = 1.2 square yards (sq yd, yd²)
- 1 square kilometer (km²) = 0.4 square mile (sq mi, mi²)
- 10,000 square meters (m²) = 1 hectare (ha) = 2.5 acres

MASS - WEIGHT (APPROXIMATE)

- 1 gram (gm) = 0.036 ounce (oz)
- 1 kilogram (kg) = 2.2 pounds (lb)
- 1 tonne (t) = 1,000 kilograms (kg) = 1.1 short tons

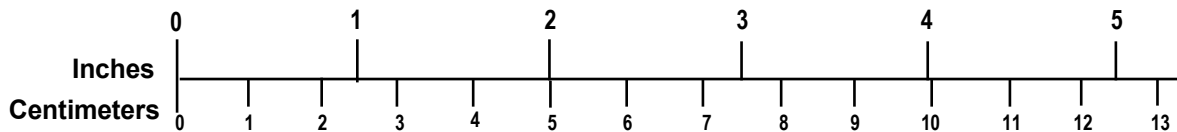
VOLUME (APPROXIMATE)

- 1 milliliter (ml) = 0.03 fluid ounce (fl oz)
- 1 liter (l) = 2.1 pints (pt)
- 1 liter (l) = 1.06 quarts (qt)
- 1 liter (l) = 0.26 gallon (gal)
- 1 cubic meter (m³) = 36 cubic feet (cu ft, ft³)
- 1 cubic meter (m³) = 1.3 cubic yards (cu yd, yd³)

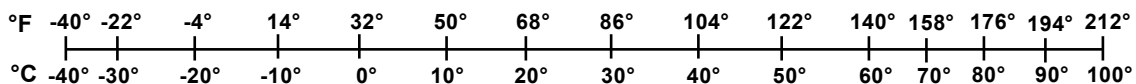
TEMPERATURE (EXACT)

$$[(9/5) y + 32] \text{ } ^\circ\text{C} = x \text{ } ^\circ\text{F}$$

QUICK INCH - CENTIMETER LENGTH CONVERSION



QUICK FAHRENHEIT - CELSIUS TEMPERATURE CONVERSION



For more exact and or other conversion factors, see NIST Miscellaneous Publication 286, Units of Weights and Measures. Price \$2.50 SD Catalog No. C13 10286

Updated 6/17/98

Acknowledgements

The John A. Volpe National Transportation Systems Center (Volpe) and the Transportation Technology Center, Inc. (TTCI) authors appreciate the technical advice provided by Jeff Gordon of FRA's Office of Research, Development and Technology. Volpe authors are grateful for the assistance of FRA Region 1 Administrator Les Fiorenzo, Deputy Regional Administrator Michelle Muhlinger, and MP&E Inspector Jere Miller for facilitating the field inspections. Volpe also acknowledges the Massachusetts Bay Transportation Authority and Consolidated Rail Corporation, and appreciates their cooperation in conducting the field inspections of the damaged fuel tanks.

Volpe authors gratefully acknowledge the contributions of their colleagues Patricia Llana and Laura Sullivan, who participated in the field inspections conducted during this research program and Dr. A. Benjamin Perlman for his invaluable advice in conducting purposeful research.

The TTCI author gratefully acknowledges the contributions of Adam Anderson, who supported tests from the engineering side and performed pre- and post-test surface scans of fuel tank 234.

Contents

Executive Summary	1
1. Introduction	2
1.1 Background	2
1.2 Objectives	2
1.3 Overall Approach	2
1.4 Scope	3
1.5 Organization of the Report	4
2. Regulations, Standards, and Field Study	5
2.1 Current Regulations and Standards in the United States	5
2.2 DMU Rail Equipment	9
2.3 Recent Incidents Involving Fuel Tank Puncture	11
3. Test Requirements and Methods	16
3.1 Test Overview	16
3.2 Test Setup	16
3.3 Test Methods	16
3.4 Test Instrumentation	19
4. Analysis Overview	24
4.1 Finite Element Models in Abaqus/Explicit	24
4.2 Modeling Phase 1: Before Tests of Tanks 202 and 232	30
4.3 Modeling Phase 2: After Tests of Tanks 202 and 232, Before Test of Tank 234	37
4.4 Modeling Phase 3: After Test of Tank 234	43
5. Results – Tests and Analyses	45
5.1 Tank 232 Impact Test Results	45
5.2 Tank 202 Impact Test Results	47
5.3 Tank 234 Impact Test Results	50
5.4 Tank 234 Post-test Puncture Model Results	54
6. Conclusion	58
7. References	59
Appendix A. Instrumentation Locations and Technical Specifications	61
Appendix B. Fuel Tank Materials	65
Appendix C. Test Data	73
Appendix D. Comparison Between Test Data and Finite Element Analysis Results	79
Abbreviations and Acronyms	83

Illustrations

Figure 1. Flowchart Diagram of Fuel Tank Research Methodology	3
Figure 2. Typical Fuel Tank Placement on Two Conventional Passenger Locomotives	10
Figure 3. Concord, MA, Locomotive Fuel Tank	11
Figure 4. Puncture on Bottom Sheet (Concord, MA).....	12
Figure 5. Joint Bar and Puncture (Concord, MA).....	12
Figure 6. Schematic View of Oak Island Raking Collision.....	13
Figure 7. Fractured Door Track on Trailing Boxcar (Oak Island).....	14
Figure 8. Damage to Trailing End Sheet and Side Sheet (Oak Island).....	14
Figure 9. Damage to Leading End of Fuel Tank, Side Sheet, and Baffles (Oak Island)	15
Figure 10. Test Fuel Tank Mounted on the Impact Wall.....	16
Figure 11. Test Setup	17
Figure 12. Fuel Tank 232.....	18
Figure 13. Fuel Tank 202.....	18
Figure 14. Fuel Tank 234.....	18
Figure 15. Impact Cart with Indenter Attached	19
Figure 16. Accelerometer Locations on Impact Cart for Tests of Tanks 202 and 232 (left) and Tank 234 (right)	20
Figure 17. Trigger Switch Arrangement for Tank 232 on Cart (left) and Ground (right).....	22
Figure 18. Trigger Switch Arrangement for Tank 202 on Cart (left) and Ground (right).....	23
Figure 19. Flowchart of Modeling and Testing Process	24
Figure 20. True Stress-True Plastic Strain Characteristics for Tanks 202 and 232, Post-test FE Models.....	28
Figure 21. Process for Derivation of Material Properties for Tank 234 Puncture Model	29
Figure 22. Pre-test Damage Initiation Envelopes for Tank 234	29
Figure 23. Post-test Damage Initiation Envelopes for Tank 234.....	30
Figure 24. Exterior and Baffle Arrangement for Tank 232 Pre-test Model.....	31
Figure 25. Solid Mesh on Tank 232 Pre-test Model.....	31
Figure 26. Model Setup in Pre-test Models of Tanks 202 and 232 (Tank 232 Shown)	32
Figure 27. Force-displacement Behavior from Tank 232 Pre-test Model	33
Figure 28. Deformed Shape of Tank 232 after 5 mph Impact, Pre-test Model (Contours of Displacement in inches).....	34
Figure 29. Exterior and Baffle Arrangement for Tank 202 Pre-test Model.....	35

Figure 30. Tank 202 Pre-test Model Solid Mesh.....	35
Figure 31. Tank 202 Pre-test Model Force-displacement Behavior	36
Figure 32. Deformed Shape of Tank 202 after 5 mph Impact, Pre-test Model (Contours of Displacement, in inches).....	37
Figure 33. Tank 202 Baffle Arrangement during Teardown (top) Pre-test Model (bottom left), and Post-test Model (bottom right).....	38
Figure 34. Tank 232 Baffle Arrangement during Teardown (top) Pre-test Model (bottom left), and Post-test Model (bottom right).....	39
Figure 35. Pre-test Rigid Impactor (left) and Post-test Deformable Impact Cart (right) Used in Models of Tanks 202 and 232.....	40
Figure 36. Tank-to-wall Attachment in Pre-test Model (top), Test (center), and Post-test Model (bottom).....	41
Figure 37. Comparison between Baffle Arrangement in Tank 232 Post-test FE Model (left) and Tank 234 Pre-test FE Model (right).....	42
Figure 38. Force-displacement Response from Tank 234 Pre-test Model, 11.2 mph Impact	42
Figure 39. Deformed Shape of Tank 234 after 11.2 mph Impact, Pre-test Model (Contours of Displacement, in inches).....	43
Figure 40. Tank 234 Baffle Arrangement during Teardown (top) Pre-test Model (bottom left), and Post-test Model (bottom right).....	44
Figure 41. Post-test View of Tank 232 from Test (left) and FE Model (right)	45
Figure 42. Tank 232 Force-time History from Test and Post-test FEA	46
Figure 43. Tank 232 Displacement-time History from Test and Post-test FEA.....	47
Figure 44. Post-test View of Tank 202 from Test (left) and FE Model (right)	48
Figure 45. Post-test View of Tank 202 Baffles from Test (left) and FE Model (right).....	48
Figure 46. Tank 202 Force-time History from Test and Post-test FEA	49
Figure 47. Tank 202 Displacement-time History from Test and Post-test FEA.....	50
Figure 48. Tank 234 Deformed Shape Comparison between FEA and Test.....	51
Figure 49. Deformation – Vertical Cross-section at the Impact Center	52
Figure 50. Tank 234 Force-time History from Test and Post-test FEA	53
Figure 51. Tank 234 Displacement-time History from Test and Post-test FEA.....	54
Figure 52. Deformed Shape of Tank 234 and Puncture Detail after 14.5 mph Impact Simulation (top) and 16 mph Impact Simulation (bottom)	55
Figure 53. Force-displacement Responses for 11.2, 14.5 and 16 mph FEA of Tank 234	56
Figure 54. Energy Dissipated During 14.5 and 16 mph Impact Simulations	57

Tables

Table 1. Locomotive Collision Scenarios and Related Fuel Tank Collision Modes	3
Table 2. Planned Fuel Tank Tests.....	4
Table 3. Definition of <i>Locomotive</i> in Two Parts of CFR.....	5
Table 4. Current Regulations and Industry Standards on Rail Vehicle Fuel Tanks	6
Table 5. Load Cases Specified in Each Regulation or Industry Standard	6
Table 6. Example DMU Operations in the United States.....	9
Table 7. Instrumentation Summary.....	20
Table 8. Impact Cart Accelerometers	21
Table 9. Pre-test Material Properties for Tank 232 FE Model	26
Table 10. Pre-test Material Properties for Tank 202 FE Model	26
Table 11. Locations of Fuel Tank Material Samples.....	27
Table 12. Summary of Fuel Tank Impact Tests.....	45

Executive Summary

The Federal Railroad Administration's (FRA) Office of Research, Development and Technology is currently conducting a research program into the puncture resistance of fuel tanks, with a particular focus on fuel tanks involved in passenger rail service. The focus of this research is on developing performance-based scenarios for evaluating the puncture resistance of modern fuel tank designs, such as the fuel tank found on a diesel multiple unit (DMU) locomotive. The Transportation Technology Center, Inc. (TTCI) and the John A. Volpe National Transportation Systems Center (Volpe) are supporting FRA in evaluating the crashworthiness of fuel tank designs. The overall FRA research program includes dynamic impact testing of fuel tank articles, analytical modeling of fuel tanks under dynamic loading conditions, and recommendations for improved fuel tank protection strategies.

In the project covered by this report, TTCI conducted three separate impact tests on typical locomotive fuel tanks. The team measured and characterized the tank's structural performance under dynamic impact loading conditions. Fuel tanks from Electro-Motive Diesel, Inc. (EMD) F40 and EMD F40PH locomotives served as specimens for tests that impacted the bottom of the tanks. The total weight of the impact cart with the 12-inch by 12-inch square indenter was 14,075 pounds. Tests were conducted on fuel tanks 232 and 202 on October 8 and 9, 2013, and on fuel tank 234 on August 20, 2014. The impact speeds were 4.5 mph for fuel tank 232, 6.2 mph for fuel tank 202, and 11.2 mph for fuel tank 234. All three tests resulted in permanent deformation to the fuel tanks, and no fuel tank was punctured. TTCI developed specialized hardware and procedures for testing locomotive fuel tanks during the project.

Test results were used to validate and refine computer simulations conducted by Volpe. These simulations consisted of a series of finite element analyses (FEA) that included nonlinear material responses. Some models also included additional parameters to simulate puncture by simulating material degradation and element removal. While pre-test models were used to help guide the instrumentation placement and overall test setup, complete details on the construction of the tanks (e.g., baffle layout and material properties) were not known until the post-test teardown. As a result, post-test models with additional details were compared with test results. In all tests, the post-test models were found to be in reasonable agreement with the measured test results.

1. Introduction

FRA is conducting fuel tank crashworthiness research in its Equipment Safety Research Program. This report describes a series of impact tests and companion computer simulations that were conducted by TTCI. These tests and analyses subjected retired passenger locomotive fuel tanks to blunt impact tests on their bottom sheets to characterize the behavior of the fuel tanks under dynamic loading conditions.

1.1 Background

The focus of this research is on developing performance-based scenarios that will evaluate the puncture resistance of modern fuel tank designs, such as fuel tanks on diesel multiple unit (DMU) locomotives. Since DMU locomotives place passengers in closer proximity to the tank, a tank that has been punctured and ignited during operation or a collision would pose a threat to passenger egress. All scenarios should ensure a level of puncture resistance equal to or greater than the level of puncture resistance provided by current fuel tank standards and regulations. These scenarios should also apply to a wide variety of designs, and take into consideration the particular conditions unique to DMU operations.

1.2 Objectives

The blunt impact tests were designed to impact each of three retired locomotive fuel tanks at designated locations and designated speeds, measure the resulting acceleration-time histories, characterize the influence of baffle arrangements on tank responses, and generate test measurements for calibrating finite element (FE) models. These tests were preliminary and were conducted on retired locomotive fuel tanks to assist in preparing for impact tests on fuel tanks of a modern design. In the process, the team developed test requirements, planned instrumentation, and used these tests as a “shakedown” of the test setup to identify any areas for potential improvement and maximizing success in future tests. Since future test series will be performed as destructive tests on modern fuel tank designs, it is important to have a thorough understanding of the test setup, instrumentation needs, and test parameters before tests are conducted on DMU fuel tanks or locomotive tanks with alternative designs.

1.3 Overall Approach

This research program included a combination of physical testing and computer simulations of a variety of fuel tank designs. Testing is planned to include fuel tanks of conventional, existing designs as well as tests of alternative designs. Testing on existing designs is intended to establish the baseline level of performance that would be expected to be met by an alternative fuel tank design. Figure 1 shows the overall flow of the passenger fuel tank crashworthiness research.

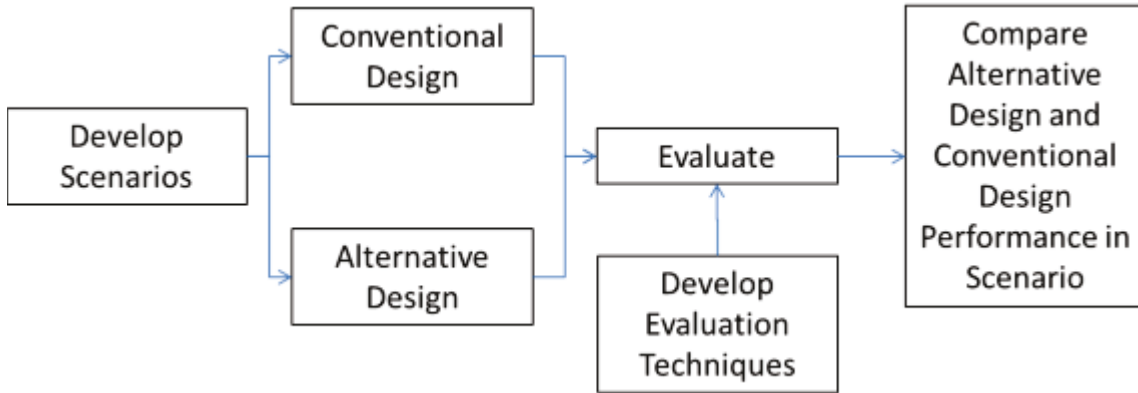


Figure 1. Flowchart Diagram of Fuel Tank Research Methodology

1.4 Scope

This research program focused on the response of the fuel tank to dynamic impact conditions. One key output of this series of full-scale tests was to understand the deformation pattern of a fuel tank under dynamic impact loads. The current requirements for fuel tanks require a series of static analyses, or specify minimum material and geometric requirements. The approach taken in this research program has been to consider the performance of the fuel tank under loading conditions that represent actual puncture threats to a fuel tank.

Through field inspections of damaged equipment and a general survey of rail incidents in the United States, the causes of fuel tank rupture in rail accidents have been identified and categorized into two general loading conditions. Table 1 summarizes the collision scenarios identified by Jacobsen [1].

Table 1. Locomotive Collision Scenarios and Related Fuel Tank Collision Modes

	Collision Scenario	Tank Collision Mode
1	Impact with surrounding railcar component	Blunt impact to end of tank
2	Oblique impact with another railcar	Raking of side of tank or Blunt impact to side of tank or Blunt impact to end of tank
3	Rollover and impact with another railcar	Blunt impact to bottom of tank
4	Grounding	Raking of bottom or side of tank or Blunt impact to side of tank
5	Impact with rail or other object in right-of-way	Blunt impact to bottom of tank

Table 1 indicates the exposed sides, ends, and bottom of a fuel tank are all vulnerable to impact over a wide range of collision scenarios that may occur. The ends of the fuel tank may be struck by a component on the railcar or locomotive to which it is attached during a collision, such as a

truck becoming detached and being pushed back into the fuel tank. The tank ends may also be struck by another railcar in the case of an oblique impact. The bottom of the tank may be struck in the event of a locomotive rollover following a collision or derailment, or may be struck by an object without locomotive derailment. The sides of the fuel tank may be impacted during an oblique collision or during a derailment where the locomotive comes to rest at least partially on its fuel tank. Finally, it is possible that more than one tank collision mode may occur during a single incident, placing demands on several impacted areas of the fuel tank at once.

The two scenarios of blunt impact to the bottom surface of the tank and a raking collision involving the side of the tank are planned for impact testing during the current program. Table 2 shows the target timeline for the proposed testing, which has been updated as the research has progressed.

Table 2. Planned Fuel Tank Tests

	Conventional Designs		Alternative Designs
	Passenger Locomotive	DMU	DMU
Blunt Impact to Bottom	October 2013 & August 2014	Winter 2015	Winter 2016
Raking Impact	TBD	TBD	

1.5 Organization of the Report

This report is organized into the following seven sections:

Section 1 is the introduction.

Section 2 presents the current regulations or standards applied to fuel tanks by the US general railroad system. It also provides examples of puncture modes observed during a field study of incidents involving punctured locomotive fuel tanks.

Section 3 describes the test requirements and the methodology employed in the blunt impact testing.

Section 4 provides an overview of the computer simulation that modeled the responses of the fuel tanks to the impacts.

Section 5 presents the results from the tests and the corresponding computer simulations, and compares these results to one another.

Section 6 contains some concluding remarks about the testing and analysis program.

Section 7 lists the references that are used in this report.

2. Regulations, Standards, and Field Study

This section discusses the current regulations and standards that are applied to locomotive fuel tanks in the general railroad system of the United States. This discussion covers regulations and standards for freight locomotives, passenger locomotives, and DMU locomotives. Additionally, observations from several field investigations of locomotive fuel tank punctures are presented.

2.1 Current Regulations and Standards in the United States

Rail vehicle fuel tanks are currently governed by Federal regulations and industry standards. The Code of Federal Regulations (CFR) contains several requirements for diesel fuel tanks in use in Tier I (up to 125 mph maximum operating speed) passenger rail service on the general railroad system of the United States. While the focus of this current research program is on passenger equipment, requirements applicable to freight locomotives are included in this section to provide a thorough discussion.

Within the CFR, the term “locomotive” is defined in both 49 CFR 229.5 and 49 CFR 238.5. [2,3] Both of those definitions are provided in Table 3 as a reference. In both cases, the term locomotive would apply to freight locomotives, passenger locomotives, and a passenger railcar with an onboard propelling motor (e.g., a DMU). Because a DMU is defined as a locomotive in these parts of the CFR, DMUs must comply with all regulations applicable to locomotives, unless a particular regulation specifies otherwise.

Table 3. Definition of *Locomotive* in Two Parts of CFR

49 CFR 229.5	49 CFR 238.5
<p><i>Locomotive</i> means a piece of on-track equipment other than hi-rail, specialized maintenance, or other similar equipment—(1) With one or more propelling motors designed for moving other equipment; (2) With one or more propelling motors designed to carry freight or passenger traffic or both; or (3) Without propelling motors but with one or more control stands.</p>	<p><i>Locomotive</i> means a piece of on-track rail equipment, other than hi-rail, specialized maintenance, or other similar equipment, which may consist of one or more units operated from a single control stand with one or more propelling motors designed for moving other passenger equipment; with one or more propelling motors designed to transport freight or passenger traffic, or both; or without propelling motors but with one or more control stands. This term does not include a locomotive propelled by steam power unless it is used to haul an intercity or commuter passenger train. Nor does this term include a freight locomotive when used to haul a passenger train due to failure of a passenger locomotive.</p>

Locomotive fuel tanks, whether on a freight locomotive, a conventional Tier I passenger locomotive, or a Tier I DMU, are subject to structural requirements in the form of Federal Regulations and industry standards (i.e., Association of American Railroads (AAR) Standard S-5506 and American Public Transportation Association (APTA) Standard SS-C&S-007-98). [2,3,4,5] Table 4 lists the current regulations and standards as applicable to each of the three types of rail vehicle fuel tanks.

Table 4. Current Regulations and Industry Standards on Rail Vehicle Fuel Tanks

Type of Vehicle	Federal Regulation	Industry Standard
Freight Locomotive	49 CFR 229.217 *[2]	AAR S-5506 [4] “Performance Requirements for Diesel Electric Locomotive Fuel Tanks”
Tier I Passenger Locomotive	49 CFR 238.223 [3]	APTA SS-C&S-007-98 [5] “Standard for Fuel Tank Integrity for Non-Passenger Carrying Passenger Locomotives”
Tier I DMU	49 CFR 238.223 ** [3]	No current industry standard

*49 CFR 229.217 incorporates AAR S-5506 by reference.

**External fuel tanks must comply with Appendix D to 49 CFR Part 238.

Each of the three regulations or standards listed in the previous table includes three scenarios (minor derailment, jackknifed locomotive, side impact) and a strength requirement (puncture resistance). While the load cases are substantially similar across all three regulations, there are minor differences in the way the loads are applied in each standard or regulation. The four load cases as considered in the three requirements are summarized in Table 5.

Table 5. Load Cases Specified in Each Regulation or Industry Standard

		AAR S-5506	APTA SS-C&S-007-98	49 CFR 238 App. D
Minor Derailment	Load Location	End Plate, within a +/-8-inch band above one rail	Any point on forward or aft end plate	End Plate, within a +/-8-inch band above one rail
	Load Magnitude	One-half the weight of the carbody at a 2G acceleration	One-half the total weight of the fully loaded carbody at 2G acceleration	One-half the weight of the carbody at a 2G acceleration
	Pass/fail Criterion	Without exceeding material’s ultimate strength	Without rupture of the fuel tank	Without exceeding material’s ultimate strength
	Additional Information	Consideration should be given in the design of the fuel tank to maximize the vertical clearance between the top of the rail and the bottom of the fuel tank.	This standard gives an exemption to this requirement for fuel tanks with a prescribed clearance above rail.	Consideration should be given in the design of the fuel tank to maximize the vertical clearance between the top of the rail and the bottom of the fuel tank.

		AAR S-5506	APTA SS-C&S-007-98	49 CFR 238 App. D
Jackknife	Load Location	Transversely at the center, supported on one rail, distributed between the longitudinal center line and the edge of the tank bottom, with a railhead surface width of 2 inches.	On one railhead surface with a width of two inches. The locomotive is assumed to be perpendicular to the track.	Transversely at the center, supported on one rail, distributed between the longitudinal center line and the edge of the tank bottom, with a rail head surface of 2 inches.
	Load Magnitude	One-half the weight of the locomotive at a 2G acceleration	One-half the weight of the locomotive at a 2G acceleration	One-half the weight of the locomotive at a 2G acceleration
	Pass/fail Criterion	Without exceeding the ultimate strength of the material	Without rupture of the fuel tank	Without exceeding the ultimate strength of the material
	Additional Information	---	This standard gives an exemption to this requirement for fuel tanks with a prescribed clearance above rail.	---
		AAR S-5506	APTA SS-C&S-007-98	49 CFR 238 App. D
Side Impact	Load Location	Longitudinal center of the fuel tank, 30 inches above the rail	Any location along fuel tank, 30 inches above the rail	Longitudinal center of the fuel tank, 30 inches above the rail
	Load Magnitude	200,000 pounds, distributed over a 6-inch by 48-inch area	200,000 pounds, distributed over a 6-inch by 48-inch area	200,000 pounds, distributed over a 6-inch by 48-inch area
	Pass/fail Criterion	Without exceeding the ultimate strength	Fuel tank must avert a rupture and fuel release	Without exceeding the ultimate strength

		AAR S-5506	APTA SS-C&S-007-98	49 CFR 238 App. D
Puncture Resistance	Sides, bottom sheet, and end plate requirements	Equivalent to a 5/16-inch steel plate with a 25,000 psi yield strength (where the thickness varies inversely with the square root of yield strength).	Equivalent to a 5/16-inch steel plate with a 25,000 psi yield strength (where the thickness varies inversely with the square root of yield strength).	Equivalent to a 5/16-inch steel plate with a 25,000 psi yield strength (where the thickness varies inversely with the square root of yield strength).
	Lower-third of End Plates	The lower one third of the end plates shall have the equivalent penetration resistance by the above method of 3/4-inch steel plate at 25,000 psi yield strength.	For fuel tanks less than 18 inches above the rail with fully worn wheels, the lower one third of the end plates shall have the equivalent penetration resistance of 3/4-inch steel plate at 25,000 psi yield strength.	The lower one third of the end plates shall have the equivalent penetration resistance by the above method of 3/4-inch steel plate at 25,000 psi yield strength.
	Additional Information	This may be accomplished by any combination of materials or other mechanical protection.	This may be accomplished by any combination of materials or other mechanical protection.	This may be accomplished by any combination of materials or other mechanical protection.

2.2 DMU Rail Equipment

A piece of DMU rail equipment is a self-propelled passenger rail vehicle with an onboard diesel engine. This type of rail vehicle, being capable of generating its own motive power, is capable of operating without the need for a dedicated, conventional locomotive. DMU vehicles may either be operated as a single vehicle or combined into a consist of multiple DMUs, each capable of powering itself. The DMU offers several advantages over conventional locomotive and coach passenger operations, including faster acceleration and deceleration times, potentially lower start-up costs, and increased operational flexibility. Under the current Tier I regulations in 49 CFR 238.233, a DMU is classified as a locomotive, and is therefore subjected to the same requirements as a conventional, non-passenger carrying locomotive.

Because of these advantages, several commuter rail services in the United States have acquired or announced plans to acquire DMU equipment. Several recent commuter rail operations to use DMU service are summarized in Table 6. Each operation has either procured DMU equipment that was designed to comply with the applicable regulations, or has applied for and received a waiver of one or more applicable regulations from FRA.

Table 6. Example DMU Operations in the United States

Operator	Start-up Date	Equipment Manufacturer	Compliant or Waiver
River Line Camden Co., NJ	March, 2004	Stadler	Waiver FRA-1999-6135
Sprinter San Diego Co., CA	March, 2008	Siemens	Waiver FRA-2002-11809
TriMET WES Portland, OR	February, 2009	Colorado Railcar	Compliant ¹ [6]
Capitol Metro Austin, TX	March, 2010	Stadler	Waiver FRA-2006-25040
A-train (DCTA) Denton Co., TX	June, 2011	Stadler	Waiver FRA-2010-0180
Sonoma-Marín Area Rail Transit (SMART) Sonoma-Marín Cos., CA	Target late 2016	Nippon-Sharyo	Compliant ¹ [7]

As Table 6 shows, current DMU operations in the United States use a variety of designs that comply with the CFR and designs that are operated under a waiver of a particular CFR

¹ “Compliant” indicates that the vehicle was designed to meet the applicable Federal Regulations and standards, but it does not mean that FRA or the authors of this report certify that the design meets these requirements.

requirement. For these particular operations occurring under a waiver, the vehicles have received a waiver of the existing Tier I fuel tank requirements in 49 CFR 238.223.

The railroad environment in which a DMU operates may be similar to the environment in which a conventional passenger locomotive is operated. If this is the case, then many of the hazards which exist for the fuel tank on a passenger locomotive may also exist for the fuel tank on a DMU. However, there are several details of DMU operation which may affect the overall risk of fuel tank puncture on a DMU.

DMU equipment typically carries less fuel than a conventional locomotive. According to Tofani and Walker, DMUs currently in operation within the U.S. have a fuel tank capacity of 250–600 gallons, while a typical passenger locomotive fuel tank has a capacity of 1,800–2,500 gallons [8]. Because of the smaller amount of diesel fuel carried onboard a DMU, a diesel fuel spill from a DMU fuel tank may have less severe consequences than a diesel fuel spill from a conventional fuel tank. However, since a DMU has the potential to carry more people than a conventional locomotive, the consequences of a fire in proximity to more people must be weighed against the decreased risk that comes from carrying less fuel.

An additional issue related to the capacity of the fuel tank and its proximity to more people is the actual location of the fuel tank on the vehicle. On a typical passenger locomotive, the fuel tank is suspended beneath the underframe of the locomotive, and it is adjacent to a truck and/or other pieces of underframe equipment. Two passenger locomotives are shown in Figure 2, with the fuel tanks indicated beneath the underframes. This placement renders the fuel tank exposed to loading both from a side impact (e.g., a highway vehicle at a grade crossing, or a raking impact), or from a detached piece of underframe equipment (e.g., a detached truck) for a sufficiently severe accident.

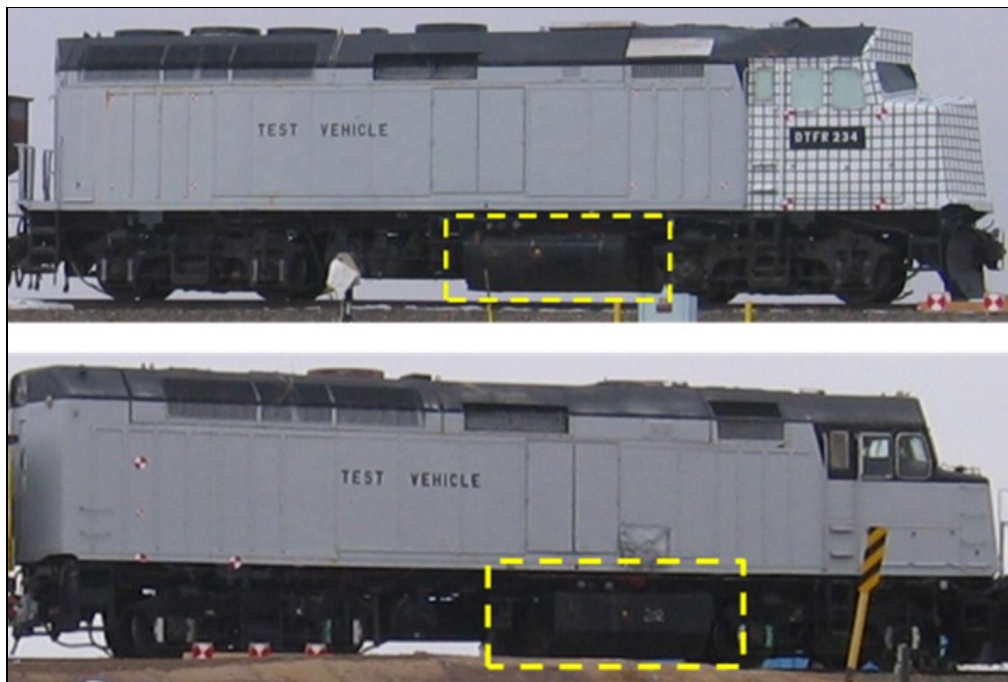


Figure 2. Typical Fuel Tank Placement on Two Conventional Passenger Locomotives

Because there are many different DMU designs in service, it is less apparent that there is a “typical” placement for the fuel tank on these vehicles. Because the fuel tank has a smaller capacity than a conventional locomotive fuel tank, there is additional flexibility offered to the manufacturer in terms of fuel tank placement. While generally, the fuel tanks are located low on the vehicle (e.g., beneath the underframe), the exact placement varies from DMU to DMU. DMU fuel tanks may be located inboard of the side structures of the underframe, potentially offering protection from a direct side impact into the tank. Dedicated shielding structures may also be used to prevent direct impact with the surface of the fuel tank.

2.3 Recent Incidents Involving Fuel Tank Puncture

As a part of this research program, surveys of damage to locomotive fuel tanks resulting in puncture and loss of fuel were conducted. [1] Additionally, field examinations of two damaged fuel tanks were conducted: one where a bottom impact occurred and one where a raking impact occurred. The purpose of these field examinations was to determine causes of fuel tank ruptures and evaluate existing fuel tank designs. These two field examinations, as well as the conclusions developed, are described in this section.

2.3.1 Bottom Impact: Concord, MA, September 5, 2010

On Sunday, September 5, 2010, a Massachusetts Bay Transportation Authority (MBTA) locomotive struck debris on the track, and the bottom sheet of the locomotive’s fuel tank was punctured [9]. FRA Region I personnel and Volpe staff conducted an examination of this locomotive fuel tank at MBTA’s Somerville, MA, locomotive shop. The locomotive involved in this incident was an F-40 type locomotive with a fuel tank of similar construction to tanks 232 and 234 in the impact testing program. This locomotive was constructed in the late 1970s, including this fuel tank. The fuel tank involved in the puncture is shown in Figure 3.



Figure 3. Concord, MA, Locomotive Fuel Tank

Examination of the fuel tank revealed a single puncture to its bottom sheet in the center lobe toward the leading end of the fuel tank. Judging from the marks on the bottom of the tank, it appeared that the struck debris scraped along the bottom surface of the tank until encountering the change-in-stiffness adjacent to the baffles, when it caused a puncture. This puncture occurred

adjacent to both a longitudinal and a lateral baffle, as Figure 4 shows. The damaged area also includes scuff marks on the bottom of the lateral baffle, which indicated apparent contact either between the struck object or the punctured bottom sheet and this baffle.

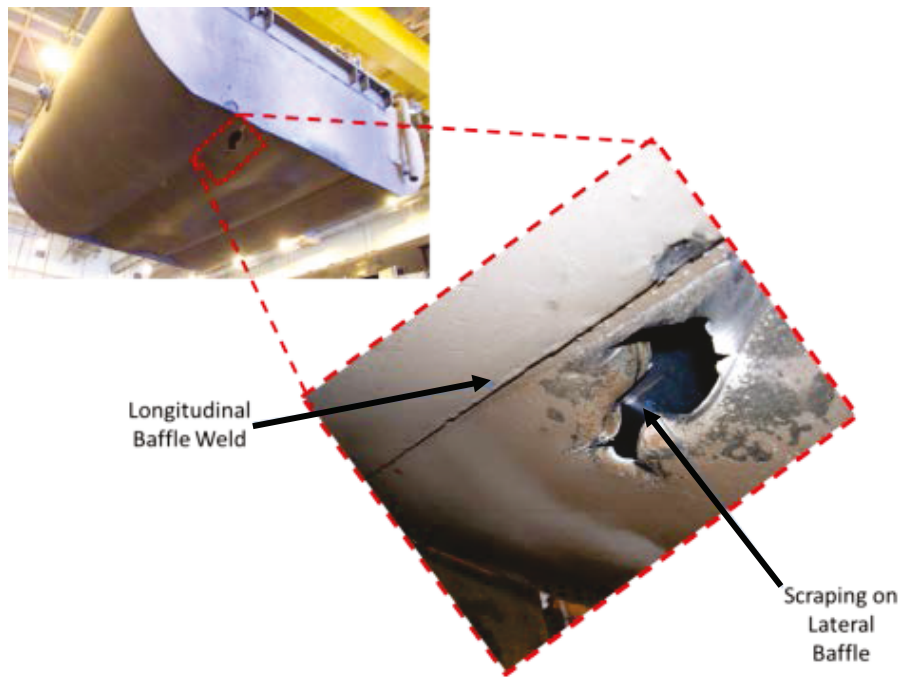


Figure 4. Puncture on Bottom Sheet (Concord, MA)

From examining the size and the shape of the punctured bottom sheet as well as discussions with MBTA personnel, it appeared that the puncture was caused by a joint bar which had been placed upon the track by vandals. Figure 5 shows an exemplar joint bar compared with the puncture. Unfortunately, it is not known at what speed the locomotive was traveling when this incident occurred.



Figure 5. Joint Bar and Puncture (Concord, MA)

2.3.2 Raking Impact: Oak Island Yard, NJ, April 28, 2012

On April 28, 2012, a raking impact collision occurred at Oak Island Yard in Newark, NJ. In this incident, two locomotives rolled into a switch while the trailing end of another freight consist was still passing through. Figure 6 shows a diagram of the accident. The freight consist that was traveling through the switch was moving at approximately 7 mph and the rolling locomotives were moving at approximately 4 mph at the time of collision. As a result of this collision, the lead locomotive's fuel tank (manufactured in 1977) was ruptured and the spilled diesel fuel ignited, resulting in a fire and damage to the leading locomotive.

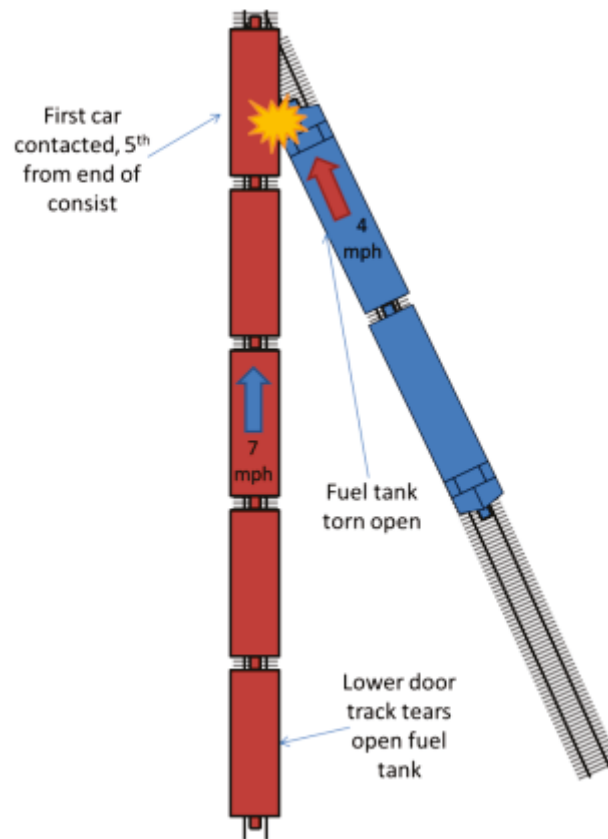


Figure 6. Schematic View of Oak Island Raking Collision

The last five cars of the moving consist struck the locomotives, and the door track on the last boxcar tore a gash into the locomotive fuel tank along nearly its entire length. Figure 7 shows this boxcar after the collision, with the missing length of door track indicated. The inset image shows the fractured end of the door track, which remained attached to the boxcar.



Figure 7. Fractured Door Track on Trailing Boxcar (Oak Island)

The door track struck the trailing end sheet of the lead freight locomotive, but did not puncture this sheet. The end sheet deformed, and the force on the end sheet appears to have buckled the side sheet, causing it to bulge outward. The door track then punctured the buckled portion of the side sheet as the boxcar continued to move past the locomotive. Figure 8 shows the trailing end of the punctured fuel tank.



Figure 8. Damage to Trailing End Sheet and Side Sheet (Oak Island)

The door track tore through several baffles and tore the lead end sheet away from the side sheet of the fuel tank. The portion of door track that had been torn away from the boxcar was found inside the lead locomotive's fuel tank. Figure 9 shows the torn side sheet and the lead end sheet. As can be seen in this image, the lead sheet itself did not tear. The separation occurred either through tearing of the side sheet or the weld between the side sheet and the leading end sheet.

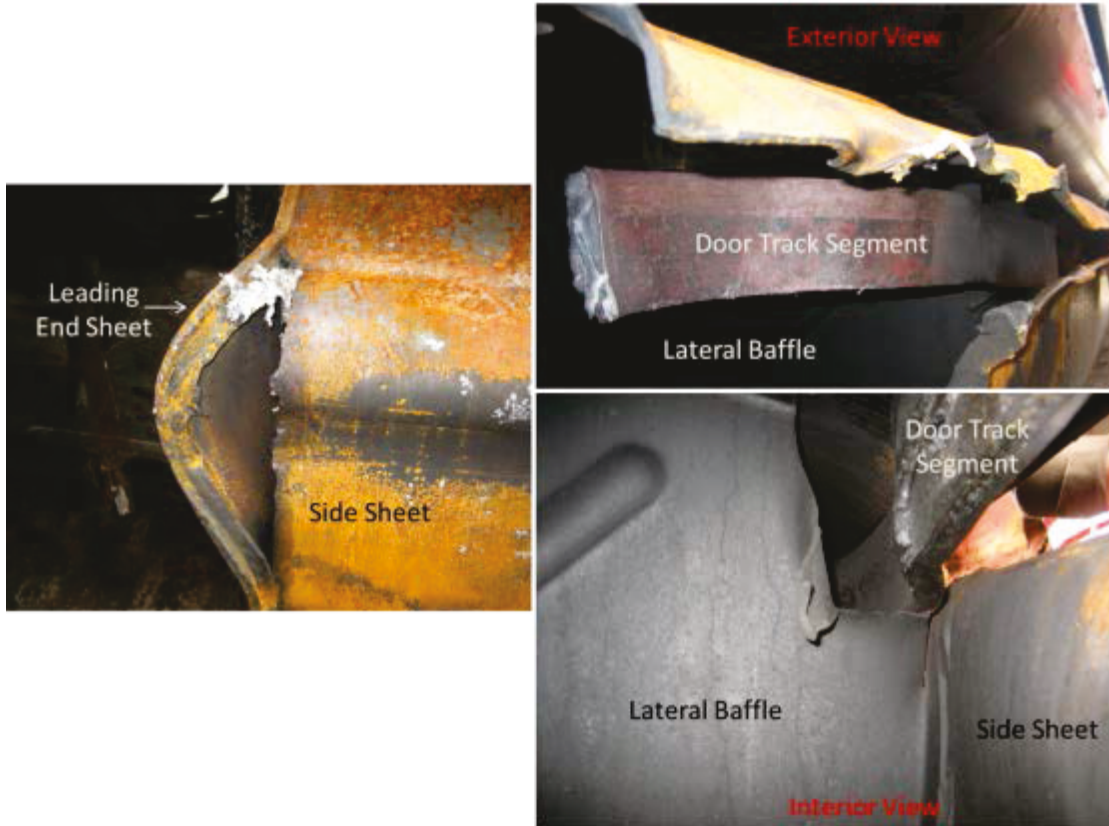


Figure 9. Damage to Leading End of Fuel Tank, Side Sheet, and Baffles (Oak Island)

3. Test Requirements and Methods

3.1 Test Overview

Transportation Technology Center, Inc. (TTCI) conducted three separate impact tests on typical locomotive fuel tanks to measure and characterize their structural performances under dynamic impact loading conditions. Fuel tanks from EMD F40 and EMD F40PH locomotives, which were built by Electro-Motive Diesel, Inc. (EMD), were the test specimens for tests that impacted the bottom of the tanks. Results of the tests were used to validate and refine computer simulations conducted by Volpe.

3.2 Test Setup

All fuel impact tests were conducted on the impact wall at the Transportation Technology Center (TTC). Mounting brackets were built by TTCI to support the fuel tanks on the impact barrier face. The brackets were aligned with the existing connections on each fuel tank, and the mounting method created a support condition similar to what would occur for a fuel tank installed under a locomotive. Figure 10 shows a test fuel tank that had been mounted on the impact wall.



Figure 10. Test Fuel Tank Mounted on the Impact Wall

3.3 Test Methods

FRA, Volpe, and TTCI collectively developed the test requirements contained in this report. Three fuel tanks were set up for individual impact tests. The fuel tanks were supported directly on the impact wall as described in Section 3.1. Two of the fuel tanks (202 and 232) were positioned to align with a 12-inch by 12-inch indenter for the center impact. Fuel tank 234 was offset from the center in the horizontal direction. Figure 11 illustrates the test setup and fuel tank mounted to the impact wall.



Figure 11. Test Setup

All fuel tank alignments provided for impacts on the bottom surface of the tank. Removal of the fuel tanks' fill and vent tubes permitted the top surface of the tanks to be mounted relatively close to the impact barrier face. The impact location on the first fuel tank, tank 232 (taken from an EMD F40PH), was at its geometrical center. The geometric center of tank 232 is centered between transverse and longitudinal baffles. Figure 12 shows dimensions and baffle layout of fuel tank 232. The impact location on the second fuel tank, tank 202 (taken from an EMD F40), was at its geometrical center, which corresponds to impact centered between two longitudinal baffles and on the middle transverse baffle. Fuel tank 202 was a custom-made replacement for the original fuel tank. Figure 13 shows dimensions and baffle layout of tank 202. The impact location on the third fuel tank, tank 234 (taken from an EMD F40PH), was offset from the center in the horizontal direction and centered between transverse and longitudinal baffles. Figure 14 shows the baffle layout of tank 234.



Fuel Tank 232 – Baffle Layout

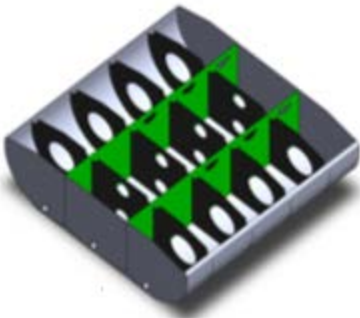


Figure 12. Fuel Tank 232



Fuel Tank 202 – Baffle Layout

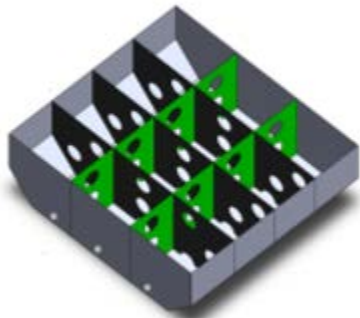


Figure 13. Fuel Tank 202

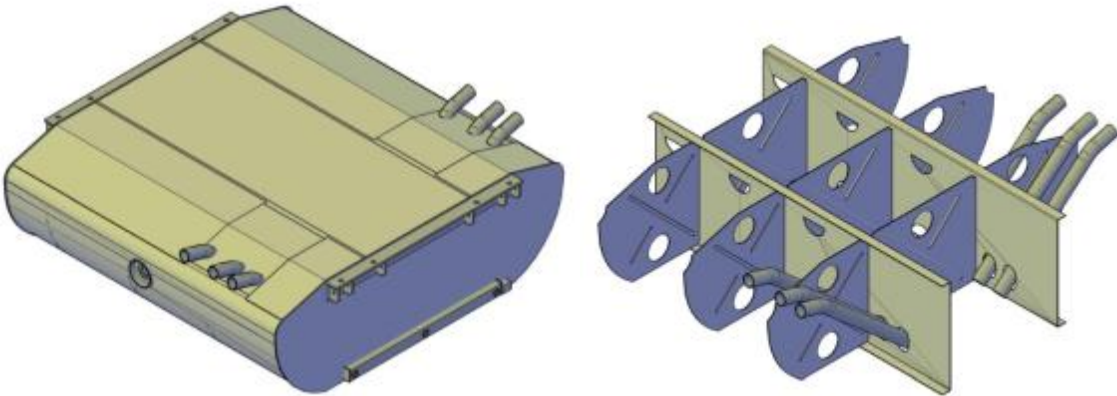


Figure 14. Fuel Tank 234

Figure 15 shows the 12-inch by 12-inch square indenter as it was attached to the moving impact cart. The total weight of the impact cart, including indenter, was 14,075 pounds. The target impact speeds were specified (using preliminary analyses) to be within the estimated puncture range for each fuel tank. The impact cart release location was determined from a series of speed

calibration runs carried out beforehand on the adjacent Precision Test Track at TTC and adjusted on the basis of the wind speed and the wind direction before the start of the test. During these speed calibration runs, a radar speed measuring system was used to precisely measure the speed of the impact cart.



Figure 15. Impact Cart with Indenter Attached

The data collected during the test included accelerations, impact speed, and both high-speed and real time video recordings.

3.4 Test Instrumentation

3.4.1 Definition of Coordinate Axes

All local acceleration and displacement coordinate systems are defined relative to the impact vehicle. Positive x, y, and z directions are forward, left, and up relative to the lead end of the impact vehicle.

3.4.2 Impact Cart Accelerometers and Speed Sensors

Two similar, but slightly different instrumentation arrangements were used on the impact cart during this program. For the tests of tanks 202 and 232, four triaxial accelerometers were mounted at the two ends, at the middle of the right side sill and close to the middle of the impact cart along its centerline. One additional longitudinal accelerometer was mounted at the middle of the left side sill.

Data analysis from the first two tests on fuel tanks 202 and 232 showed that accelerometer BA2C, located along the centerline of the impact cart on a lateral member, experienced a ringing behavior due to insufficient stiffness of the lateral member. Instrumentation for the last test on fuel tank 234 was therefore modified. Accelerometers at location BA2C were removed, and all other accelerometer locations featured triaxial accelerometers.

TTCI installed redundant speed sensors, which were mounted on each side of the impact cart to accurately measure the cart speed within 2 feet of the impact point. The speed traps were reflector-based sensors, which used ground-based reflectors separated by a known distance and vehicle-based light sensors that triggered as the impact cart passed over the reflectors. The last reflector was within 1 in of the impact point. The time interval between passing the reflectors was recorded. Speed was then calculated from distance and time. TTCI also used a handheld radar gun to take supplemental speed measurements. Table 7 shows the summary of instrumentation, Table 8 shows the accelerometer details, and Figure 16 illustrates the sensor locations used in all three tests.

Table 7. Instrumentation Summary

Type of Instrumentation	Channel Count
Accelerometers	13 (12 for 3rd test)
Speed Sensors	2 (all tests)
Total Data Channels	13 (14 for 3rd test)

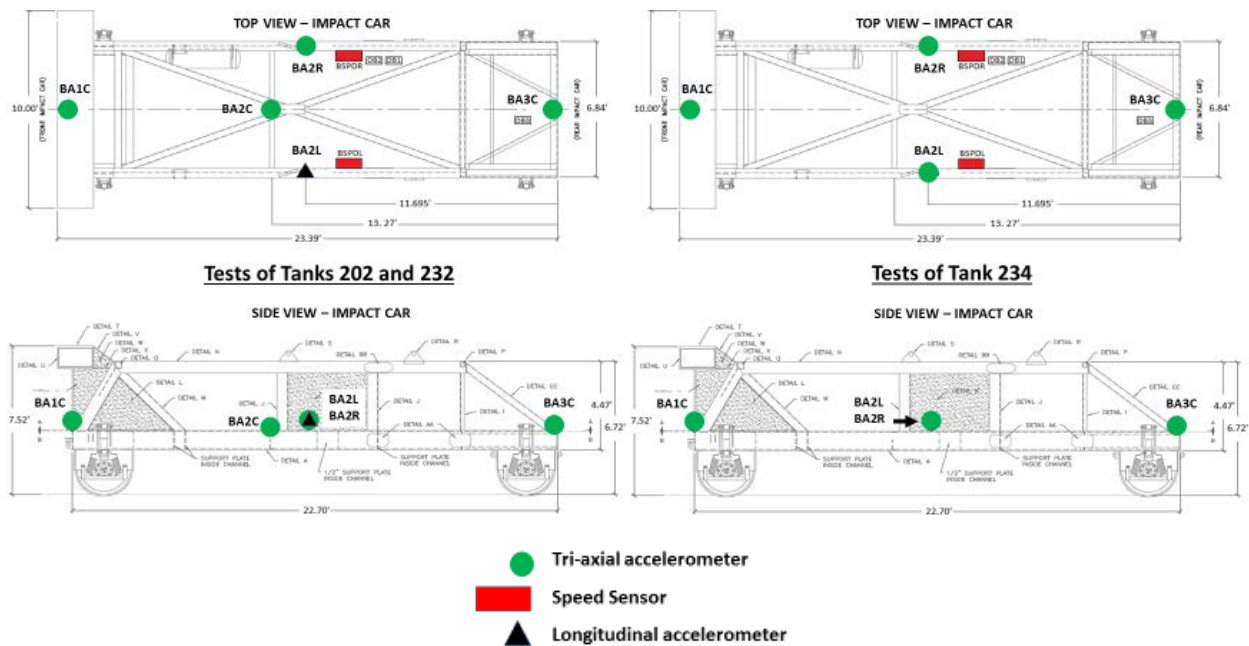


Figure 16. Accelerometer Locations on Impact Cart for Tests of Tanks 202 and 232 (left) and Tank 234 (right)

Table 8. Impact Cart Accelerometers

Channel Name	Sensor Description	Range
BA1CX (all tests)	Leading end, Centerline, X Accelerometer	100 g
BA1CY (all tests)	Leading end, Centerline, Y Accelerometer	100 g
BA1CZ (all tests)	Leading end, Centerline, Z Accelerometer	100 g
BA2LX (all tests)	Middle, Left Side X Accelerometer	100 g
BA2LY (Test 3)	Middle, Left Side Y Accelerometer	100 g
BA2LZ (Test 3)	Middle, Left Side Z Accelerometer	100 g
BA2CX (Test 1 & 2)	Middle, Centerline, X Accelerometer	50 g
BA2CY (Test 1 & 2)	Middle, Centerline, Y Accelerometer	50 g
BA2CZ (Test 1 & 2)	Middle, Centerline, Z Accelerometer	50 g
BA2RX (all tests)	Middle, Right Side X Accelerometer	100 g
BA2RY (all tests)	Middle, Right Side Y Accelerometer	100 g
BA2RZ (all tests)	Middle, Right Side Z Accelerometer	100 g
BA3CX (all tests)	Trailing end, Centerline, X Accelerometer	200 g
BA3CY (all tests)	Trailing end, Centerline, Y Accelerometer	200 g
BA3CZ (all tests)	Trailing end, Centerline, Z Accelerometer	200 g

3.4.3 Real Time and High-Speed Photography

Three high-speed and three real time high definition video cameras documented the impact event. Appendix A contains a schematic that documents the camera positions and the locations of the targets on the fuel tank and on the impact cart.

3.4.4 Data Acquisition

A set of 8-channel battery powered onboard data acquisition systems recorded data from instrumentation mounted on the impact cart. These systems provided excitation to the instrumentation, performed analog anti-aliasing filtering on the signals, did analog-to-digital conversion, and recorded each data stream.

The data acquisition systems were GMH Engineering DataBRICK2 units, which comply with the appropriate sections of SAE J211 [10]. Data from each channel were anti-alias filtered at 1,735 Hz then sampled and recorded at 12,800 Hz. Data recorded on the DataBRICK2 units were synchronized to time zero at initial impact. The zero-time reference was triggered from closure of tape switches on the front of the indenter. The DataBRICK2 units can withstand shock loading up to at least 100 g. Onboard battery power was provided by GMH Engineering 1.7 amps per hour 14.4-Volt NiCad battery packs. Tape Switches, Inc., model 1201-131-A tape switches provided the timing of the initial contact event.

Software in the DataBRICK2 unit was used to determine zero levels and calibration factors rather than relying on set gains and expecting no zero drift. The DataBRICK2 units recorded 1 second of data before initial impact and 4 seconds of data after initial impact.

During the test of fuel tank 232, the tape switches onboard the impact cart and on the ground were arranged as shown in Figure 17. Tape switches on the impact cart, which were used to activate data storage and indicate $t=0$ for the onboard instrumentation, were installed below the cart on an arm that was designed to break away from the cart at a fairly low level of force, thereby reducing the kinetic energy of the impact cart by a negligible amount. A separate plate was attached securely to the ground, with tape switches used to trigger high-speed cameras. On each plate, the tape switches were offset from the plate by a 0.5-inch thick piece of plywood. The wood was arranged to result in shear of the tape switches when the switches on the impact cart made contact with the switches on the ground.



Figure 17. Trigger Switch Arrangement for Tank 232 on Cart (left) and Ground (right)

This trigger arrangement did not work perfectly. During the test, not all of the high-speed cameras triggered, because not all of the tape switches on the ground-mounted plate were activated. Additionally, a review of the test data and comparisons with the FE results created doubts that the trigger at $t=0$ corresponded to the instant at which the impactor surface made first contact with the bottom of the tank.

The trigger arrangement was modified for the subsequent tests of tanks 202 and 234. In order to increase the certainty that all switches would trigger and that triggering would occur at the same time for all switches, the wooden block on the ground plate was replaced with a steel L-section, which was arranged (Figure 18) to form a peak behind the switches. The plywood behind the switches on the cart was replaced with a piece of solid wood that spans a larger area. Originally,

the mechanism for activating the switches in the test of tank 232 was shear resulting from an offset between the plywood on the cart and on the ground. However, the mechanism for triggering in subsequent tests relied on the sharp peak formed by the steel section pinching the switches against the wooden block.

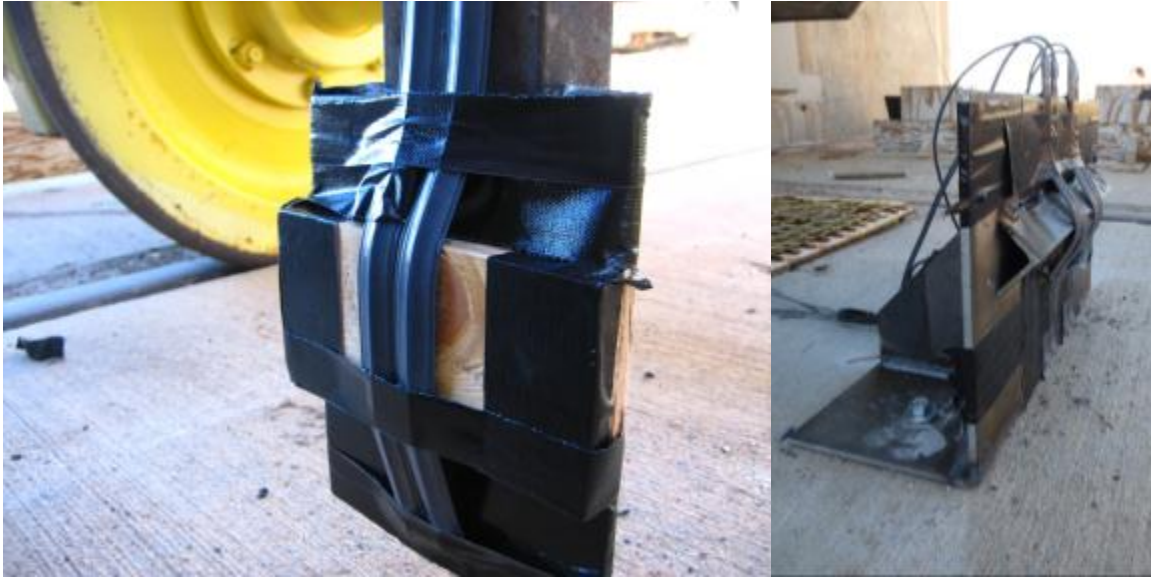


Figure 18. Trigger Switch Arrangement for Tank 202 on Cart (left) and Ground (right)

The trigger switch setup used in the test of tank 202 successfully activated the instrumentation and cameras and reduced the uncertainty associated with timing of the triggers. A similar setup to this one was used when tank 234 was tested.

4. Analysis Overview

In this program, a combination of FE modeling and impact testing was used to study the impact response of several retired locomotive fuel tanks of different designs. Because the tested fuel tanks came from locomotives that were donated to FRA for impact testing, much of the material and geometric information that served as inputs to the models had to be measured or estimated from the fuel tanks themselves, as opposed to from drawings or material specifications. Therefore, the modeling and analysis program followed a somewhat different path than if the fuel tanks being tested were of a new design, with supporting documentation that could be used to generate FE models.

Following each test, post-test modeling was performed to include newly discovered information about each tank. The new data was generated from post-test teardown of the test article such as internal geometry details and material properties. Because a major goal of this program was to evaluate the test setup and test conditions, the testing program was conducted in two phases. This allowed the team to take lessons learned in the first phase of testing and implement them in the second phase. Figure 19 contains a flowchart of the overall process of generating model input through measurements, pre- and post-test modeling, and impact testing.

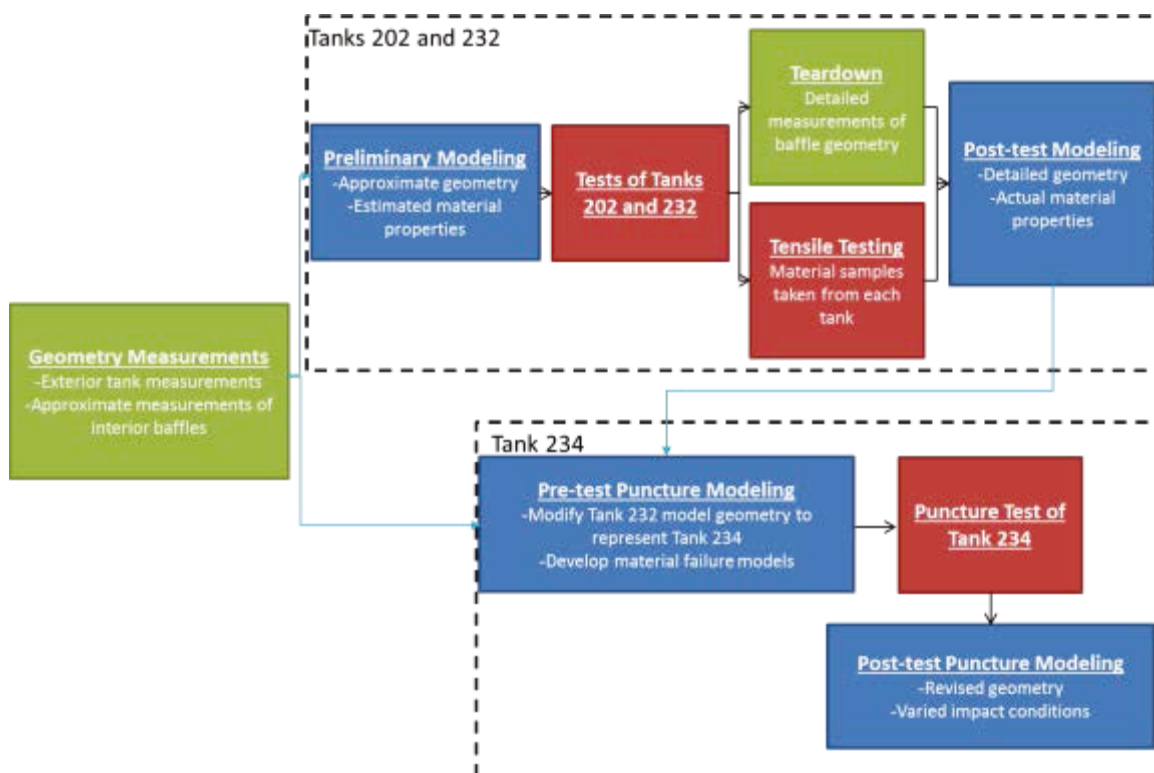


Figure 19. Flowchart of Modeling and Testing Process

4.1 Finite Element Models in Abaqus/Explicit

The FE models were preprocessed using Abaqus/CAE and executed using the Abaqus/Explicit solver [11]. Abaqus/Explicit is a commercially-available nonlinear dynamic explicit FE solver.

Because manufacturer drawings for the tanks were not available to this program, the major dimensions of each fuel tank had to be manually measured. TTCI performed measurements of the major external dimensions, material thicknesses, approximate baffle locations, and approximate baffle geometries inside each fuel tank. Using these measurements, pre-test models were constructed for tanks 202, 232, and 234. Following each test, the tank was cut open to permit an examination of the internal damage and deformation patterns of the baffles. With the tanks cut open, more detailed measurements of the baffle geometry could be made. For each tank, new information on the baffle arrangement was discovered during the post-test examination. This new information caused the team to change each model after the test, so it could more accurately represent the tested tank's geometry.

Similarly, data on the materials of construction for each tank were not available during this research program. Because cutting material coupons from each tank before testing would have compromised the structural integrity of the tank, the only pre-test material measurements taken were hardness measurements. These measurements could not be taken on the bottom surface of any tanks or on the internal baffles. Since tank 234 was tested at a later date than tanks 202 and 232, the material data measured from tank 232 was used as inputs to the pre-test model of tank 234.

Because of the limitations on materials and geometries, the pre-test models offered coarse approximations of the behaviors expected during the actual tests. While the information used to construct the pre-test models is included in this section, the focus of these discussions is on the post-test modeling. The post-test modeling used the actual geometry and material data derived from tensile tests, and it offers more relevant information on the performance of the tested fuel tanks during their respective tests.

4.1.1 Materials in Pre-test Models of Tanks 232 and 202

Before the October 2013 impact tests of tanks 232 and 202, limited material characteristics were available for these fuel tanks. Original manufacturer specifications and drawings were not available during this program, so estimated material thickness and strength properties had to be used in the pre-test FE models. Of particular importance, in modeling the response of the tank, was the thickness and plastic response of the bottom sheet of the tank. The thicknesses of the baffles and their plastic responses were also important characteristics to capture within the FE models. Material coupons could not be cut from the tanks without compromising their structures, so hardness measurements were used to estimate the ultimate strength of a given material. Then, assumptions were made regarding the relationship between yield strength and ultimate strength as well as the strain at failure for these materials.

TTCI conducted Brinell hardness (HB) testing on several surfaces for each tank. These hardness measurements were then used to estimate the ultimate strength of each corresponding material with the relationship:

$$515 \times \text{HB} = S_u \quad [12]$$

It was then assumed that the tanks were made of materials with a yield-to-ultimate ratio of approximately 0.65, approximating a plain carbon steel. Within the pre-test FE models, the materials were given an elastic perfectly plastic behavior, where the material behaved elastically until the yield strength was reached. The material then continued to experience plastic strain

without an increase in stress. The materials used in these models are summarized in Table 9 and Table 10.

Table 9. Pre-test Material Properties for Tank 232 FE Model

Tank 232				
Section	Hardness (Brinell)	Yield (ksi)	Ultimate (ksi)	Yield/Ultimate Ratio
Top	110	36	56.7	0.65
End 1	130	43.3	67	0.65
End 2	130	43.3	67	0.65
Side	113	36	58.2	0.65
*Bottom	113	36	58.2	0.65
*Baffles (lateral)	113	36	58.2	0.65
*Baffles (longitudinal)	113	36	58.2	0.65
*Drain box	110	36	56.7	0.65

*No measurements made; properties were estimated using lowest measured properties

Table 10. Pre-test Material Properties for Tank 202 FE Model

Tank 202				
Section	Hardness (Brinell)	Yield (ksi)	Ultimate (ksi)	Yield/Ultimate Ratio
Top	85	28.3	43.775	0.65
End 1	85	28.3	43.775	0.65
End 2	85	28.3	43.775	0.65
Side	85	28.3	43.775	0.65
*Bottom	85	28.3	43.775	0.65
*Baffles (lateral)	85	28.3	43.775	0.65
*Baffles (longitudinal)	85	28.3	43.775	0.65
*Drain box	110	36	56.7	0.65

*No measurements made; properties were estimated using lowest measured properties

A simplified approach to modeling element failure was included in the pre-test models of tanks 202 and 232. Because material stress-strain behaviors were not known prior to the impact tests, a more detailed failure criterion (e.g., Bao and Wierzbicki) would not offer a better representation of failure, as the key inputs for calculating the criterion come from the properties of the materials themselves. Instead, the tank bottom sheet area in the vicinity of the impact was modeled using solid (hexahedral) elements. When the equivalent plastic strain (PEEQ) reached 40 percent in one of these elements, the element was removed from the model. This value of PEEQ strain assumed a fairly ductile material for the bottom sheets of both tanks, since it used the material strengths derived from the hardness measurements. This element removal technique approximates material failure and fracture, and it can be used to estimate the puncture resistance of a thin sheet under specified impact conditions.

4.1.2 Materials in Post-test Models of Tanks 232 and 202

Following the impact tests of tanks 232 and 202, material coupons were cut from several structures within each tank. After the impact tests, a total of 15 samples were cut from the test articles and sent out for testing according to ASTM E8M-13a [13]. The analysis showed that the yield strengths of the fuel tank steels were higher than those in the initial FE analyses. Table 11 lists the location of each material sample taken from the fuel tanks.

Table 11. Locations of Fuel Tank Material Samples

Fuel Tank	Location on Fuel Tank	ID of Tested Samples	Number of Tested Samples
No. 202	Bottom Plate	202 Bottom	3
	Baffle	202 Baffle	3
No. 232	Bottom Plate	232 Bottom	3
	Longitudinal Baffle	232 Baffle Long	3
	Stamped (Lateral) Baffle	232 Stamped Baffle	3

The material properties obtained through tensile testing were used to update the post-test models of the respective tanks. A complete description of the tensile test results and the implementation of the material behaviors within the FE models can be found in Appendix B. Figure 20 shows the true stress-true plastic strain behaviors that were input into the post-test models of tanks 202 and 232.

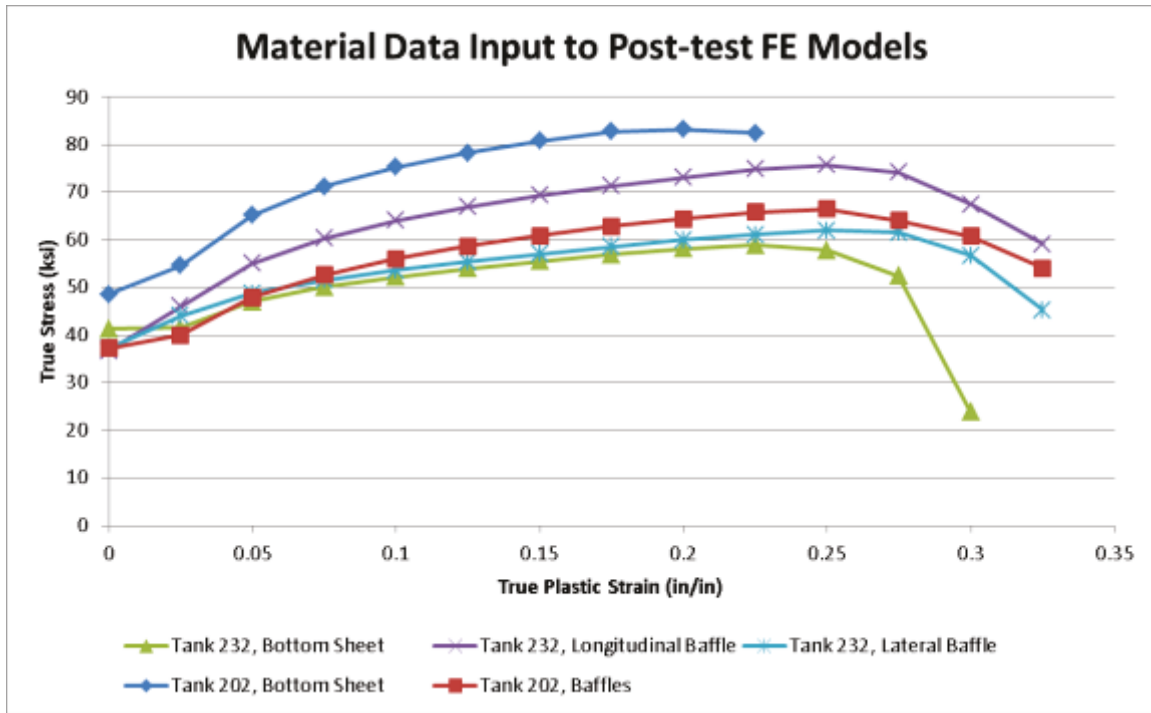


Figure 20. True Stress-True Plastic Strain Characteristics for Tanks 202 and 232, Post-test FE Models

4.1.3 Materials in All Models of Tank 234

Since tanks 232 and 234 had similar shapes and exterior dimensions, the team assumed that they were constructed from the same materials. Therefore, the material properties used in the post-test model of tank 232 were used as a starting point for developing the material models used in tank 234 models. Because the test of tank 234 was planned to occur at a higher speed than the tests of tanks 202 or 232, puncture was a likely outcome. The material properties used to describe the bottom sheet of the tank required additional parameters for describing a damage initiation envelope within the model to enable elements to fail and be removed. The use of a damage initiation envelope is a more sophisticated modeling technique than simply defining a uniform PEEQ value at which elements begin to fail. The particular damage initiation envelope used in this program featured a PEEQ where damage initiated that varied with the triaxiality of the strains contributing to that PEEQ. Additionally, because the tank 234 model was meshed entirely out of shell elements, an adjustment had to be applied to the damage initiation envelope to compensate for some limitations of shell elements.

Previous FRA-sponsored impact testing and analysis programs in the field of tank car puncture [14] and end frame integrity [15] included FE modeling of material failure. In both efforts, the failure model chosen uses a combination of PEEQ strain and triaxiality to determine when material fracture has initiated. This approach is referred to as the Bao and Wierzbicki (B-W) method. [16] Figure 21 diagrams the overall approach to material modeling used by Volpe in this research program. This technique involved tensile testing, FE modeling of the tensile testing using solid and shell elements, and refinement of the material parameters used in the FE model of the tensile tests until a suitable agreement was reached between the model and the actual tests.

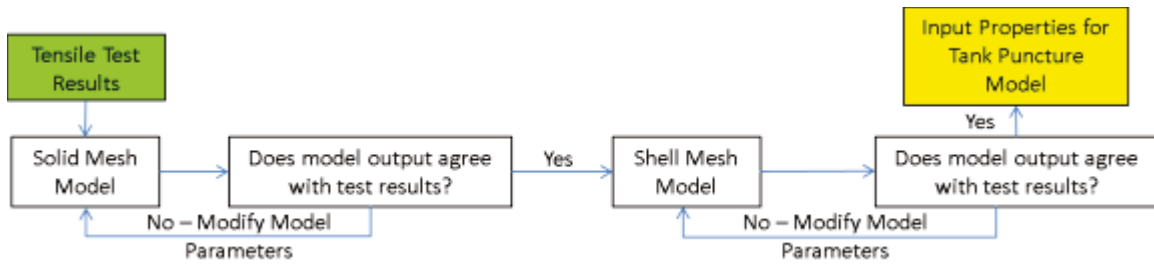


Figure 21. Process for Derivation of Material Properties for Tank 234 Puncture Model

The pre-test material modeling for tank 234 used an approach derived from the B-W method that had been previously employed in tank car research that utilized a “quick calibration” method of deriving the baseline B-W envelope using the results of a uniaxial tensile test. [17] Several adjustments were made to the baseline failure initiation envelope that resulted from the modified quick-calibration method. As had been done with previous B-W envelopes developed during tank car research performed by Volpe, the cusp shown on Figure 22 was manually adjusted to occur at a triaxiality of one-third [18]. A second adjustment to the curve was made to enable use of this failure initiation technique with shell elements in the FE model. The baseline B-W characteristic was derived using the average measured reduction in area of the tested material coupons, which was approximately 75 percent. In order to use the B-W envelope with shell elements, the effective reduction in area was varied until the results of the simulation of the tensile test were in good agreement with the results of the tensile tests themselves. Figure 22 shows the initial 75 percent reduction in area envelope as compared with the 55 percent reduction in area envelope, which was found to give the best agreement in a shell element model.

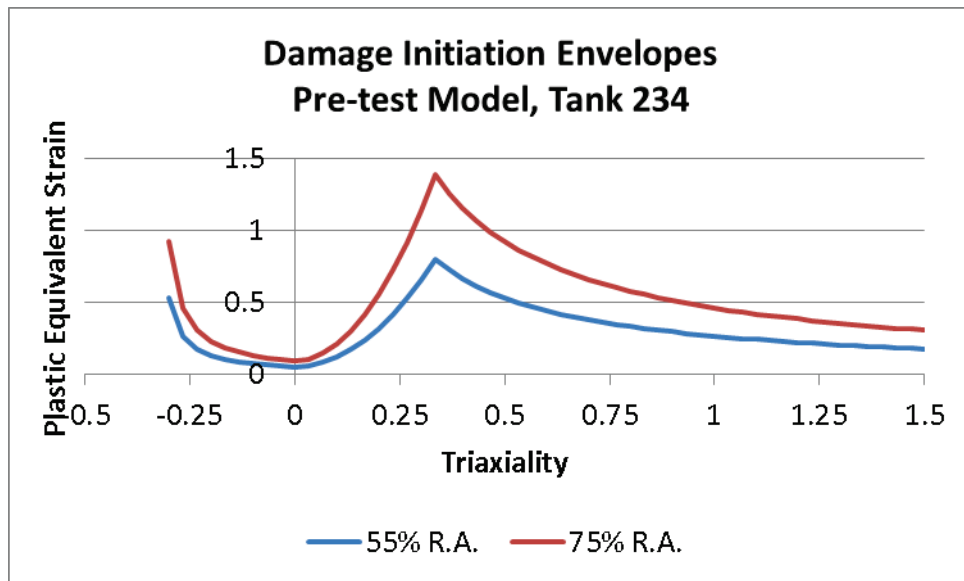


Figure 22. Pre-test Damage Initiation Envelopes for Tank 234

Following the test, a second derivation of the B-W envelope was made. This second derivation is described in greater detail in Appendix B. This approach more closely followed the procedure given by Lee and Wierzbicki [17]. Notably, this second derivation did not force the cusp to occur at a triaxiality of one-third, but permitted it to occur at its calculated location. The baseline characteristic was then modified for use with shell elements by shifting the curve vertically (i.e.,

with respect to PEEQ), following a similar process as shown in Figure 21. Figure 23 shows the post-test B-W envelopes used for tank 234. The best agreement resulted from a PEEQ shift of 0.1.

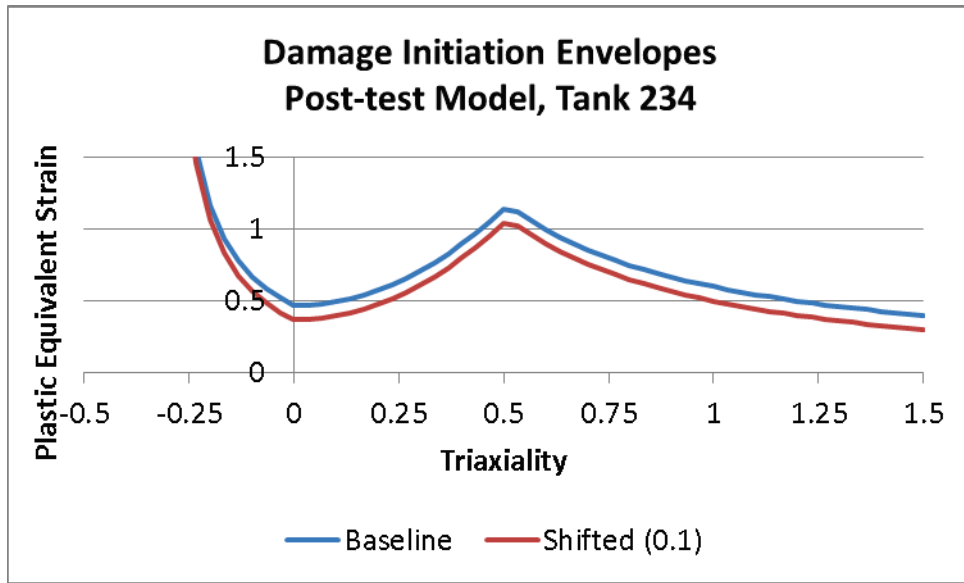


Figure 23. Post-test Damage Initiation Envelopes for Tank 234

4.2 Modeling Phase 1: Before Tests of Tanks 202 and 232

Pre-test models of tanks 202 and 232 were built using the geometric and material information that was available at the time. There were known limitations to these models, since key parameters such as material stress-strain characteristics were unknown. These models were used to help guide the placement of instrumentation and to evaluate different test setups, since this type of fuel tank impact testing had not previously been performed.

4.2.1 Pre-test Model of Tank 232

The pre-test model of tank 232 was previously described by Jacobsen, Carolan, and Llana [19]. This research program did not have access to fairly basic information that would be available during analysis of a tank that has been newly constructed, such as material specifications and layout drawings. Therefore, model inputs needed to be measured on the fuel tanks themselves or approximated when measurement was not possible or not practical.

The exterior geometry of tank 232 and its internal baffle arrangement, as implemented in the pre-test model, are shown in Figure 24. In this image, the fuel tank has been inverted from its normal operating position when attached to a locomotive. This tank featured three distinct lobes on its bottom sheet. Internally, a longitudinal (parallel to the rails) baffle ran the length of the tank at the intersection of each side lobe with the center lobe. Tank 232 featured four lateral baffles with approximately equal spacing along the length of the tank. These baffles featured cutouts to permit fuel to flow from one compartment to the next. Additionally, there was a gap between the lowest point of each bottom sheet lobe and the lowest point of each lateral baffle, presumably to permit fuel to flow beneath each baffle.

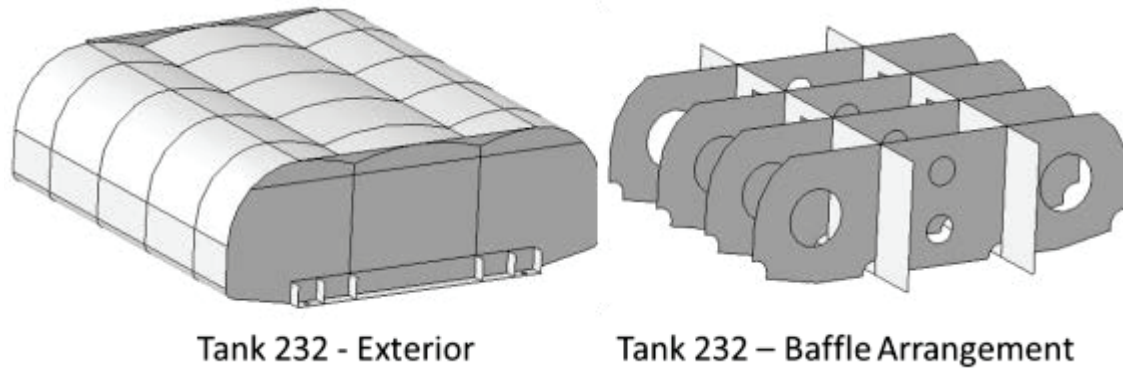


Figure 24. Exterior and Baffle Arrangement for Tank 232 Pre-test Model

In the pre-test model of tank 232, a simple shear failure criterion was used to allow element removal to occur, simulating puncture of the tank. Solid (hexahedral) elements were used to model the impact zone on the bottom sheet of the tank, where puncture could potentially occur. Two solid elements were meshed through the thickness of the tank. Outside of the impact zone, shell elements were used to model the remainder of the tank. At the interface between the solid mesh and the shell mesh, a technique known as shell-to-solid coupling was employed to attach the two different mesh types to one another. The impact zone of tank 232 is shown in Figure 25. This figure also shows the rigid 14-kip 12-inch by 12-inch impactor used to strike the tank.

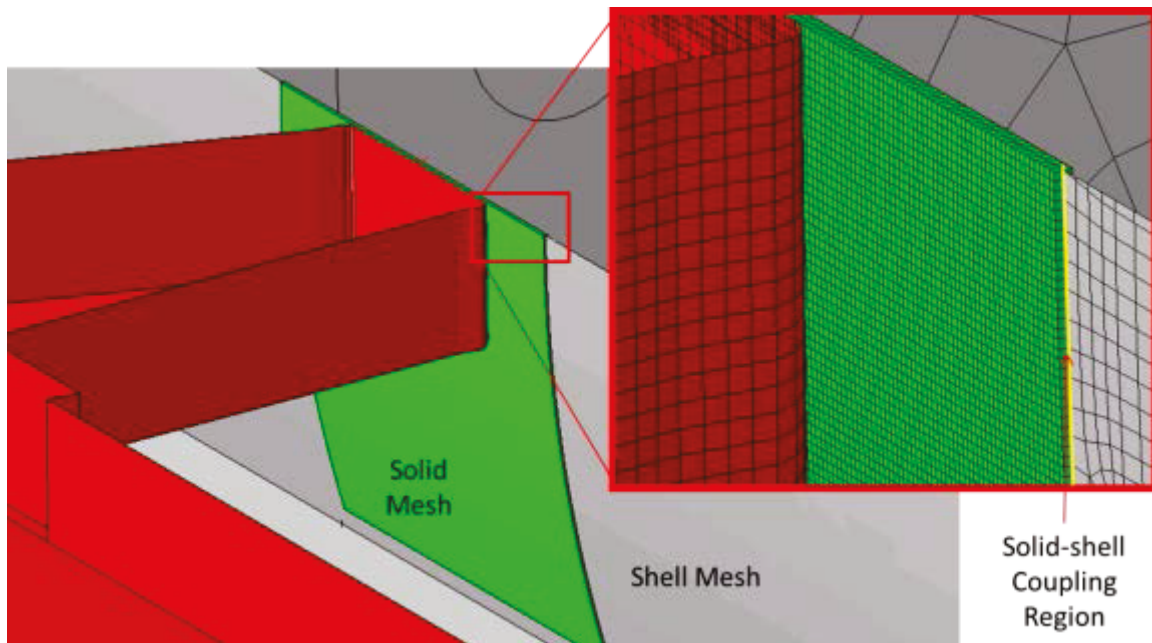


Figure 25. Solid Mesh on Tank 232 Pre-test Model

In the pre-test model, the fuel tank was separated from a rigid test wall with a 2-inch by 2-inch rigid rectangular member. The test wall and the mounting blocks were rigid bodies with no degrees of freedom (DOF). This modeling condition was intended to represent the use of a similar arrangement on the test wall at TTC, which itself was intended to simulate the support condition of a fuel tank suspended beneath a locomotive. In the FE model, zero-displacement boundary conditions were applied to the translational DOF each of the four bolt holes on the

sides of the tank, effectively pinning the tank against its mounting blocks. A rigid representation of a 12-inch by 12-inch impactor, which had a weight of 14 kips, was given an initial velocity and allowed to contact the bottom surface of the tank. The rigid impactor was only permitted longitudinal motion, with boundary conditions preventing vertical or lateral motion. The impactor did not have any rotational DOF. The test setup used in the pre-test simulation of tank 232 is shown in Figure 26.

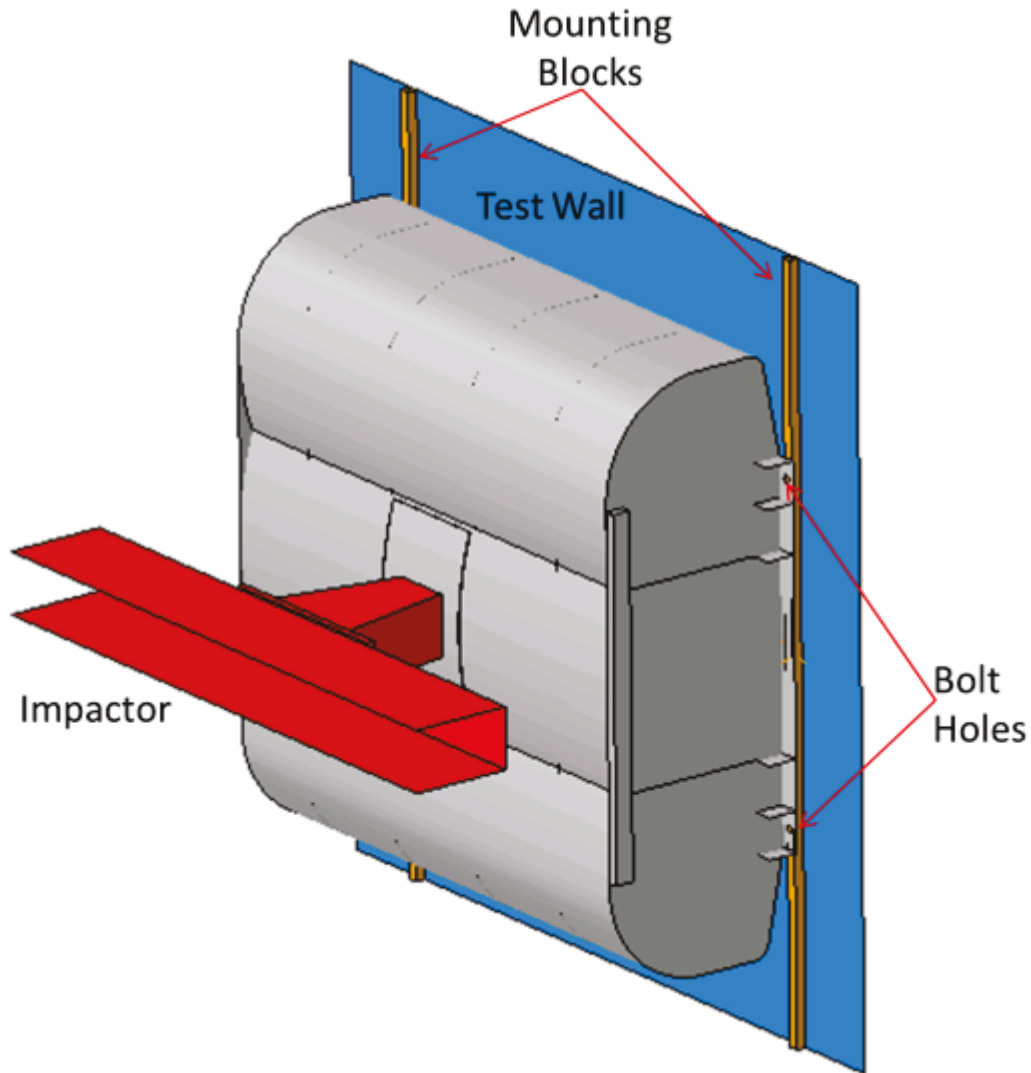


Figure 26. Model Setup in Pre-test Models of Tanks 202 and 232 (Tank 232 Shown)

The impact simulation was first run with an initial velocity of 10 mph on the rigid impactor. This resulted in the puncture of the tank, according to the simplified puncture characterization employed in this model. The simulation was repeated with an initial velocity of 5 mph. In the 5 mph impact case, the bottom sheet of the tank has a tear in it, but the impactor rebounded from the tank. The force versus displacement responses of the tank under both impact speeds are shown in Figure 27.

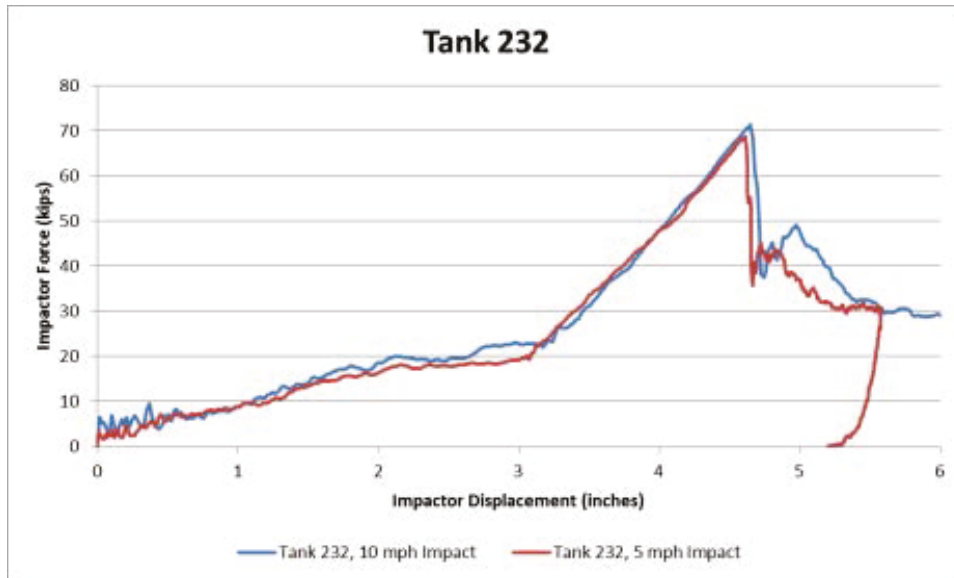


Figure 27. Force-displacement Behavior from Tank 232 Pre-test Model

In both models, the resulting force-displacement responses are both qualitatively and quantitatively similar. The initial response is fairly soft, as only the bottom sheet is being deformed. After approximately 3 inches of displacement, the inside of the bottom sheet makes contact with the bottom of the lateral baffles and results in a stiffening of the force-displacement response. The response continues up a fairly constant slope until failure of the bottom sheet occurs. In the 5 mph case, the tear does not extend around the full perimeter of the impactor. The impactor is reflected after approximately 5.5 inches of indentation. However, in the 10 mph case, the impactor fully punctures the bottom sheet and continues moving in the same direction. The deformed shape of the 5 mph model is shown in Figure 28, with contours of displacement in inches illustrating the indentation. This image is taken just after the puncture has begun to occur in the model.

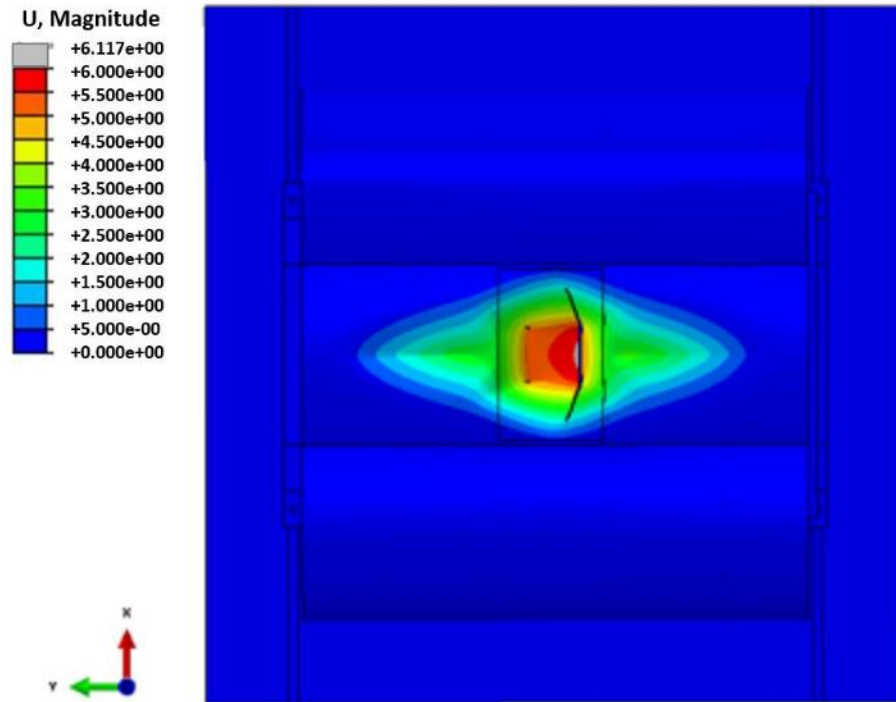


Figure 28. Deformed Shape of Tank 232 after 5 mph Impact, Pre-test Model (Contours of Displacement in inches)

The pre-test model of tank 232 demonstrated that the baffles could play a key role in the impact response of the tank. For impacts of sufficient energy to close the gap between the bottom sheet and the bottom surface of the baffles, the loading conditions on the bottom sheet will change. Initially, the bottom sheet is loaded like a plate that is supported at its edges, far from the impacted zone. However, once contact is made with the baffles, the load is being transferred through the bottom sheet directly into the baffles. These baffles are able to deform and dissipate some portion of the impactor's kinetic energy.

4.2.2 Pre-Test Model of Tank 202

The pre-test model of tank 202 was previously described by Jacobsen, Carolan, and Llana. [19] Similar to the pre-test model of tank 232, drawings and material specifications were not provided for this tank. The material and geometric information used for model inputs were either measured or estimated from the actual tank.

The exterior geometry of tank 202 and its internal baffle arrangement, as implemented in the pre-test model, are shown in Figure 29. In this image, the fuel tank has been inverted from the normal operating position that it takes when attached to a locomotive. This tank featured a distinctly different external shape and internal baffle arrangement than either tank 232 or tank 234. Whereas tanks 232 and 234 featured a rounded shape with distinct lobes, tank 202 had a square bottom and angled sides. As seen in the right side of Figure 29, the baffles included two longitudinal and three lateral baffles. Unlike the other tanks, there is no large gap between the bottom sheet of the tank and the bottom of the baffles. Rather, the baffles are attached directly to the bottom sheet. Tank 202 featured cutouts in the baffles to permit fuel to flow between chambers, similar to the other tanks.

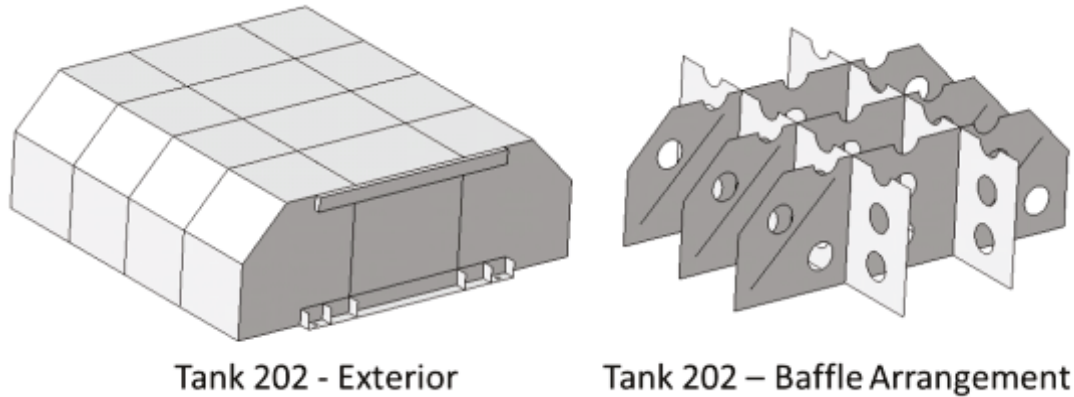


Figure 29. Exterior and Baffle Arrangement for Tank 202 Pre-test Model

Similar to the pre-test model of tank 232, a simple shear failure criterion was used to permit elements to be removed from the analysis. A mesh of solid elements was used in the region directly below the impactor. Because of this particular baffle arrangement at this impacted location, it was necessary to employ solid elements both in the bottom sheet of the tank and in the baffle directly beneath the impactor. Shell-to-solid coupling was used to attach the solid region to the shell mesh used to model the remainder of the tank, as seen in Figure 30.

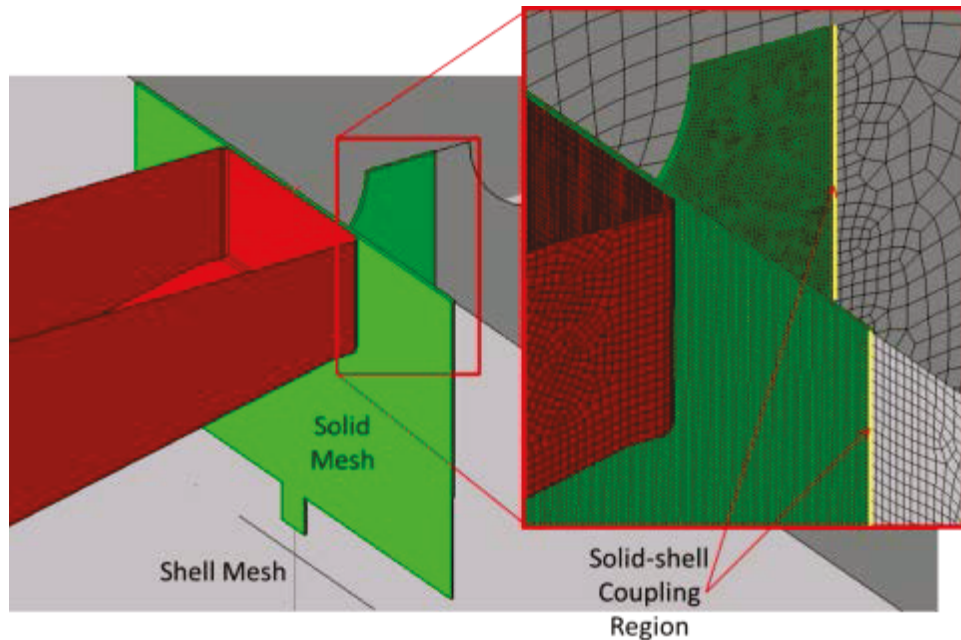


Figure 30. Tank 202 Pre-test Model Solid Mesh

The boundary and support conditions used in the pre-test model of tank 202 are the same as those for tank 232. While the impactor struck tank 232 centered between four baffles, the impact location chosen for tank 202 placed the impactor directly above a lateral baffle. Similar to the pre-test simulation of tank 232, the pre-test model of tank 202 was executed for both a 5 mph and a 10 mph initial velocity on the rigid impactor. In both the 5 mph and 10 mph cases, the bottom sheet of the tank begins to experience tearing, but the tear does not extend around the full

perimeter of the impactor. The force-displacement behaviors resulting from both impact speeds are shown in Figure 31.

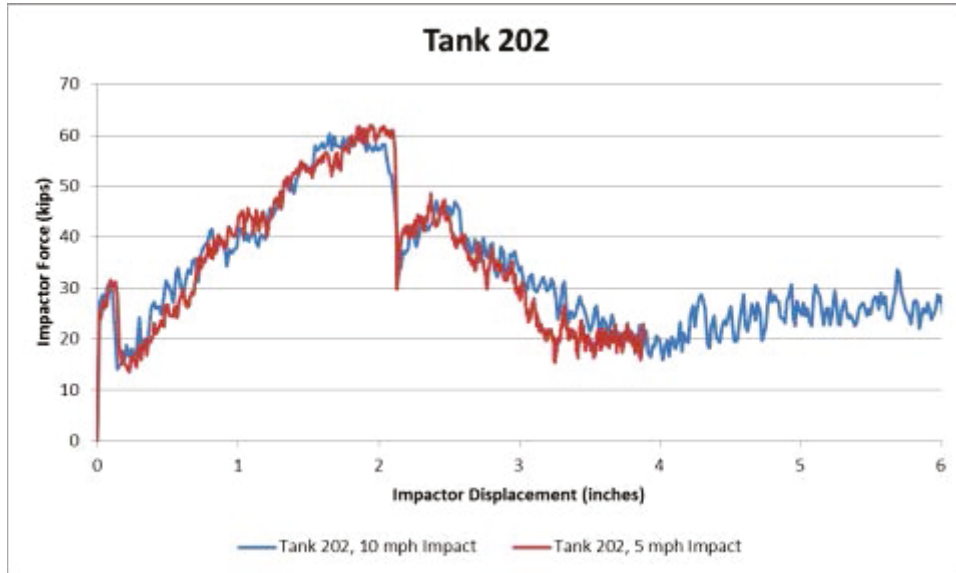


Figure 31. Tank 202 Pre-test Model Force-displacement Behavior

The force-versus-displacement results from tank 202 pre-test model are distinctly different from those obtained using the pre-test model of tank 232. Results show the response of tank 202 is initially stiff; the force quickly reaches 30 kips with very little impactor displacement. This is followed by a decrease in load, likely caused by folding of the baffle directly beneath the impacted location. As the baffle folds and contact is made between the bottom sheet of the tank and the folded portion of the baffle, the force resumes increasing. After a load of approximately 60 kips is reached, tearing of the bottom sheet begins, and it results in a drop in load. However, because the tear is limited to the vicinity of the attachment between the baffle and the bottom sheet, the force level does not drop to zero. Rather, the impactor continues to move forward while the baffle is in contact with the bottom sheet, keeping the resistance force above 20 kips.

Figure 32 contains a contour plot of displacement, in inches, for tank 202 from its pre-test model. This image is taken near the end of the 5 mph pre-test simulation. At this time, elements have been removed along the baffle (oriented vertically in this figure) as well as running laterally at the top and bottom of the impactor. The tank continues to offer resistance to further impactor travel through contact between the internal baffle and the bottom sheet of the tank.

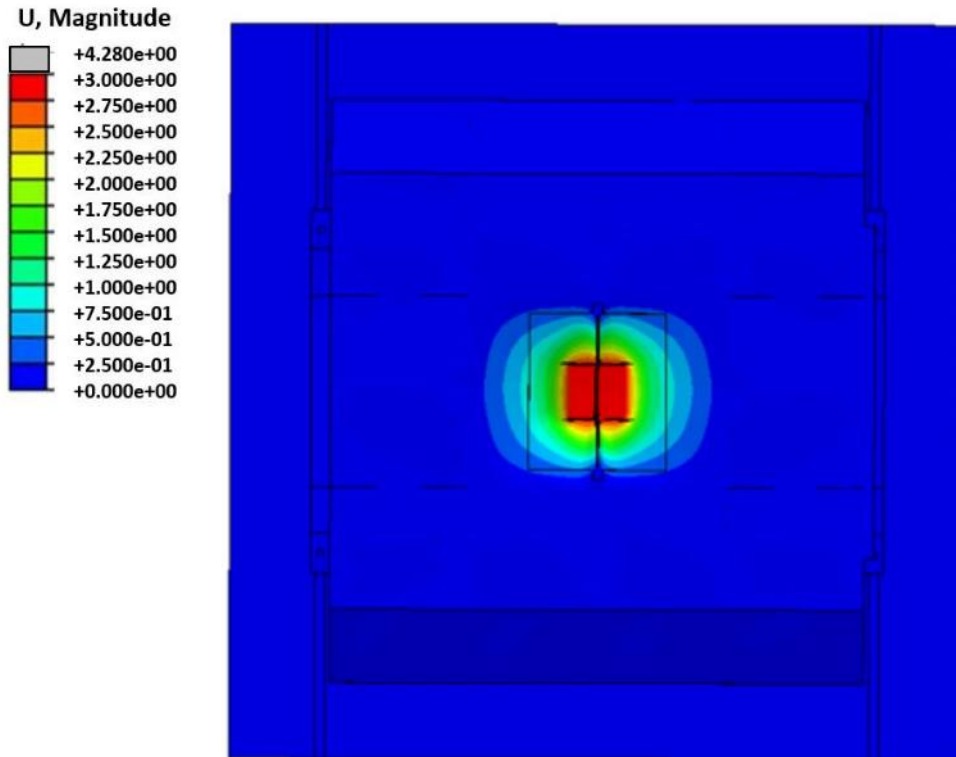


Figure 32. Deformed Shape of Tank 202 after 5 mph Impact, Pre-test Model (Contours of Displacement, in inches)

The pre-test model of tank 202 indicated that the force-displacement response could be significantly different for an impact at a baffle, compared with an impact between baffles. Additionally, the attachment of the baffles to the bottom sheet of the tank would change the behavior of the tank's response, compared with an arrangement where there is initially a sizable gap between the bottom sheet of the tank and the bottom of the baffles.

4.3 Modeling Phase 2: After Tests of Tanks 202 and 232, Before Test of Tank 234

Following the tests of tanks 232 and 202, material samples were cut from various structures on each tank to be used in tensile testing. Because of the high computational expense of solid elements, the patch of solid elements in the impact zone was abandoned after the tests of tanks 202 and 232. Future models used shell elements throughout the model, with refined meshes in the impact zone for puncture simulations. Appropriate adjustments needed to be made to the damage initiation envelopes to compensate for known limitations when used with shell elements, compared to solid elements. Additionally, more detailed information on the internal baffle arrangements of each tank was gathered after the test. These updates to materials and geometry were implemented within the post-test models to more closely approximate the actual conditions of the tanks in the tests. The improvements made to the post-test models of tank 202 and tank 232 were implemented within the pre-test model of tank 234. Results of analysis with updated models were compared to test results in Section 5.

4.3.1 Post-test Models of Tank 232 and Tank 202

After the impact tests of tanks 202 and 232 were performed, several modifications were made to the FE models of these tanks. Some of these modifications had been planned before the test, while some modifications became necessary after the test was observed. These changes are discussed in this section.

Internal Structure

During the post-test teardown of tanks 202 and 232, several geometric differences were noted between the pre-test measurements and the actual structures of the tank. Specifically, the baffle arrangements and their attachments within each tank were slightly different from what had been included in the pre-test FE models. Correspondingly, the baffle structures in each model had to be updated to reflect the actual baffle geometry found within each tank.

On tank 202, the pre-test model featured a continuous attachment between the bottom of each baffle and the bottom sheet of the tank. Within tank 202, post-test examination indicated that the baffles were only intermittently connected to the outer shell of the fuel tank, using a series of angles. The pre-test FE model baffles, the post-test FE model baffles, and a photograph of the baffles within the tank are shown in Figure 33.

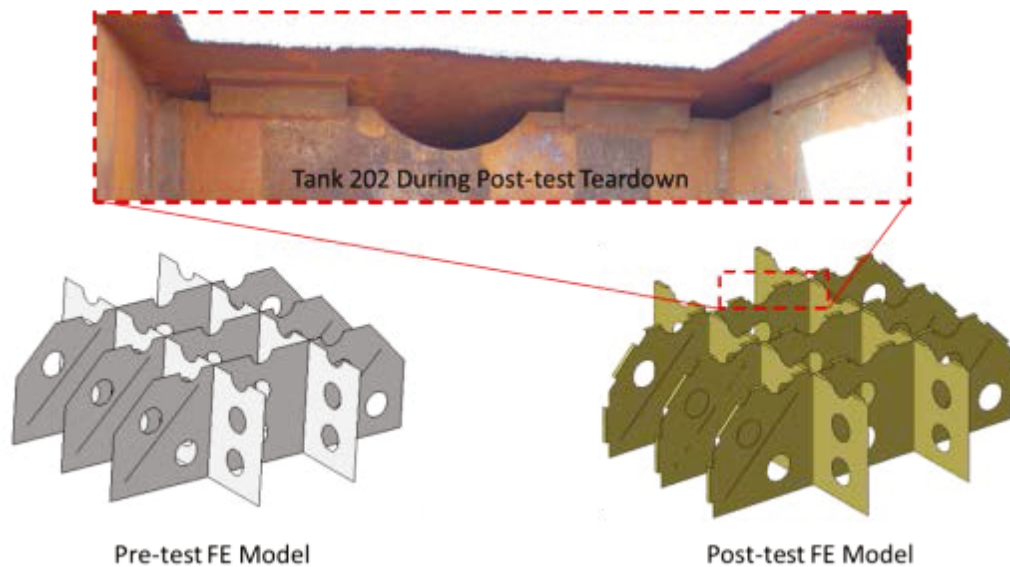


Figure 33. Tank 202 Baffle Arrangement during Teardown (top) Pre-test Model (bottom left), and Post-test Model (bottom right)

On tank 232, the pre-test model featured the lateral and longitudinal baffles terminating at the same distance from the bottom sheet of the tank. During teardown, it was apparent that while the longitudinal baffles spanned the full height of the tank's interior, the lateral baffles terminated below the height of the longitudinal baffles. This serves to increase the distance from the bottom sheet of the tank to the bottom flange of the lateral baffles. Figure 34 shows the pre-test FE model baffle arrangement, a detail from teardown showing the lateral baffle terminating below the height of the longitudinal baffle, and the implementation of this geometry in the post-test FE model.

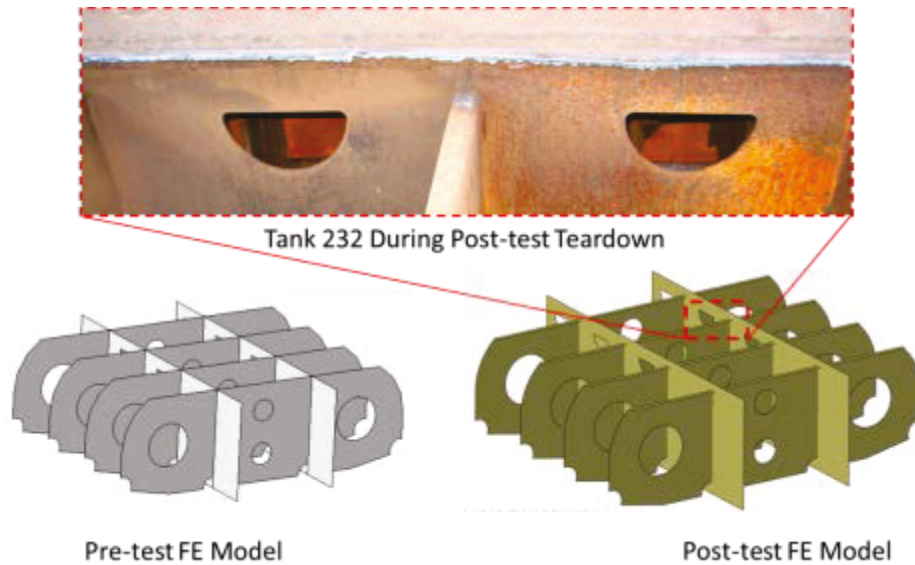


Figure 34. Tank 232 Baffle Arrangement during Teardown (top) Pre-test Model (bottom left), and Post-test Model (bottom right)

Impactor Details

In the pre-test models, a rigid 12-inch by 12-inch impactor was modeled, and a single acceleration-time history was calculated at its reference point. After examining the test data, it was apparent that the impact cart was not as rigid as had initially been thought. Therefore, a deformable model of the cart was incorporated within the post-test FE models of tanks 202 and 232. This deformable cart model was derived from a model initially developed in a previous FRA-sponsored research program, in which the impact cart was used to impart dynamic loads on a passenger railcar end frame [20]. A deformable 12-inch by 12-inch impactor was developed by TTCI for this fuel tank impact program. TTCI provided the drawings of this impactor to Volpe, and the impactor was incorporated into the model of the deformable cart. The pre-test and post-test representations of the impactors are shown in Figure 35.

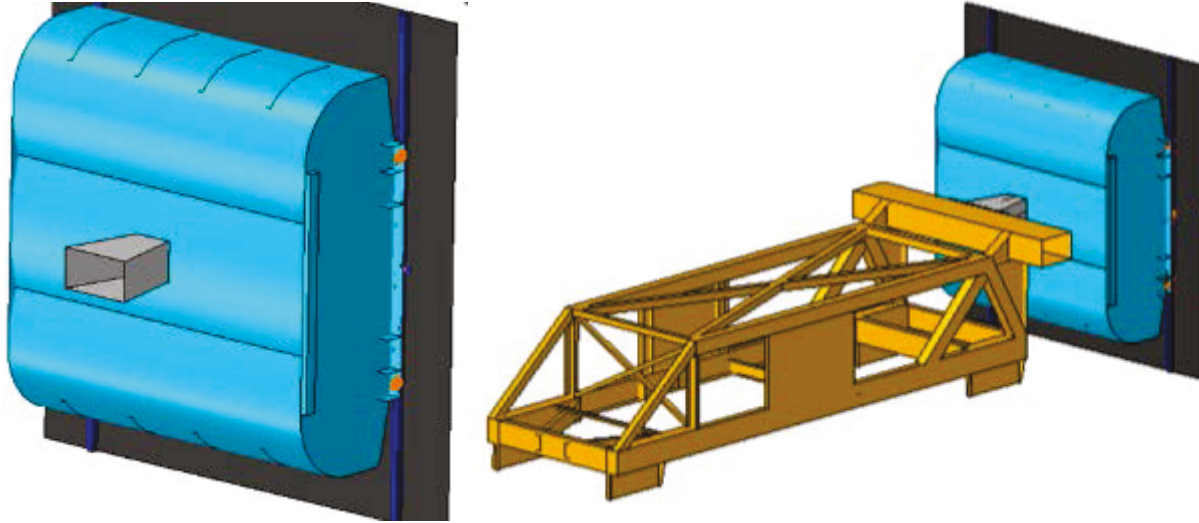


Figure 35. Pre-test Rigid Impactor (left) and Post-test Deformable Impact Cart (right) Used in Models of Tanks 202 and 232

Material Properties

Changes to the material properties in the post-test models of tanks 202 and 232 are described in Section 4.1.2 as well as Appendix B. Material coupons were cut from the tanks after their respective tests. Tensile tests were performed on these coupons to generate stress-strain curves. These material properties were assigned to the corresponding regions in the post-test models of tanks 202 and 232.

Wall to Tank Attachment

In the pre-test FE model, the tank was positioned adjacent to the rigid wall and rigid mounting blocks. The displacements of the nodes making up each of the four bolt holes on the tank were then constrained. The intention of this boundary condition was to mimic the constraint afforded by the bolts attaching the tank to the mounting blocks in the actual test. However, examination of the FE results from the pre-test model indicated that the zero-displacement boundary condition at the bolt holes was overly constraining the model and resulted in a different timing to the peak accelerations measured in the impact cart. In the post-test models, these boundary conditions were removed and replaced with a rigid body representing the bolt and washer passing through the bolt holes of the tank. Contact was defined between the rigid bolt and washer part, and the mounting bracket on the fuel tank. This method of modeling the tank attachment offered a closer representation of the actual constraint offered by the bolts in the physical tests without introducing an artificial constraint to the model.

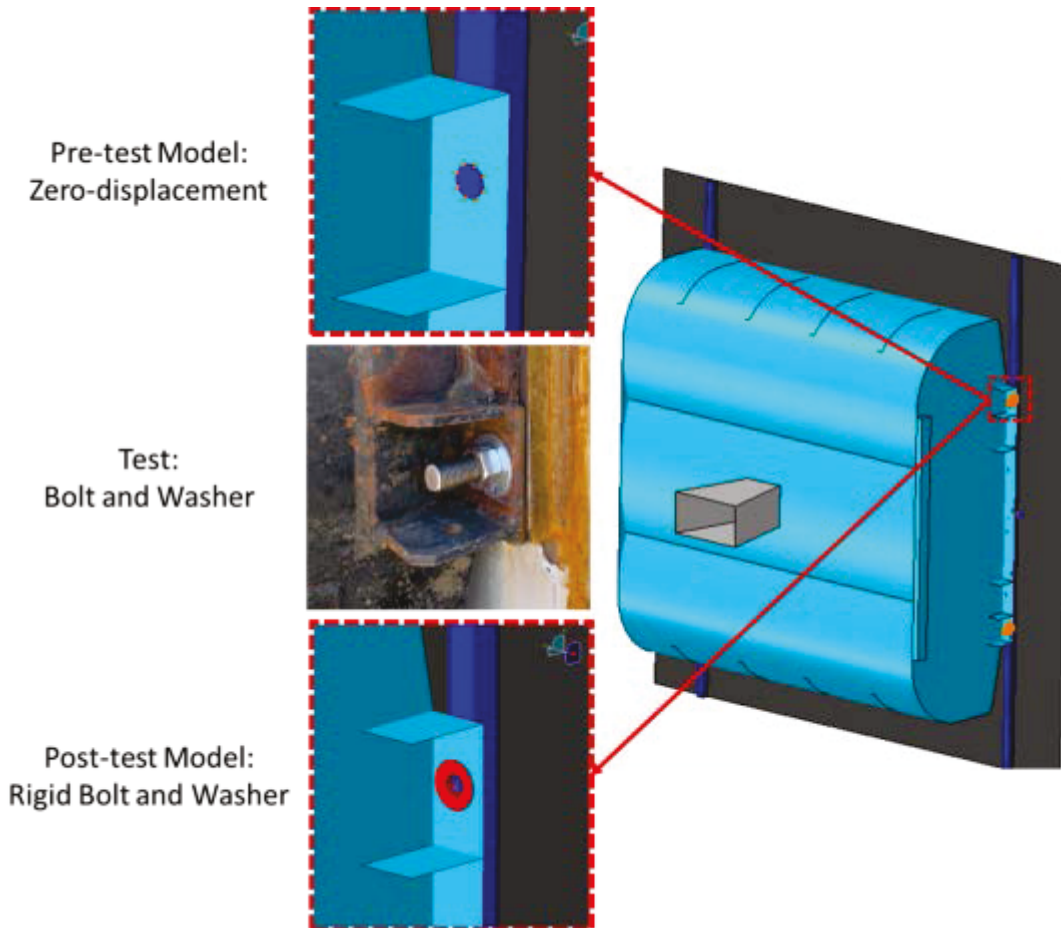


Figure 36. Tank-to-wall Attachment in Pre-test Model (top), Test (center), and Post-test Model (bottom)

4.3.2 Pre-test Model of Tank 234

As illustrated in the flowchart shown in Figure 19, the pre-test model of tank 234 was assembled beginning with the post-test model of tank 232. As a result, several of the modifications made to the post-test model of tank 232 were incorporated within the pre-test model of tank 234. A detailed discussion of the changes implemented in the post-test models of tank 232 is in Section 4.3.1. The pre-test model of tank 234 used the deformable impact cart, the material properties derived from tensile tests, the rigidly bolted attachment, and the updated geometry that had been implemented in the post-test model of tank 232.

While tanks 232 and 234 are substantially similar to one another, there were some differences that were known to exist before the test of tank 234. The placement of the lateral baffles within tank 234 was measured before the test, and they did not correspond to the baffle placement within tank 232. Therefore, the model was updated to reflect the actual baffle placement within tank 234. Figure 37 compares the baffle arrangements in the post-test model of tank 232 and the pre-test model of tank 234.

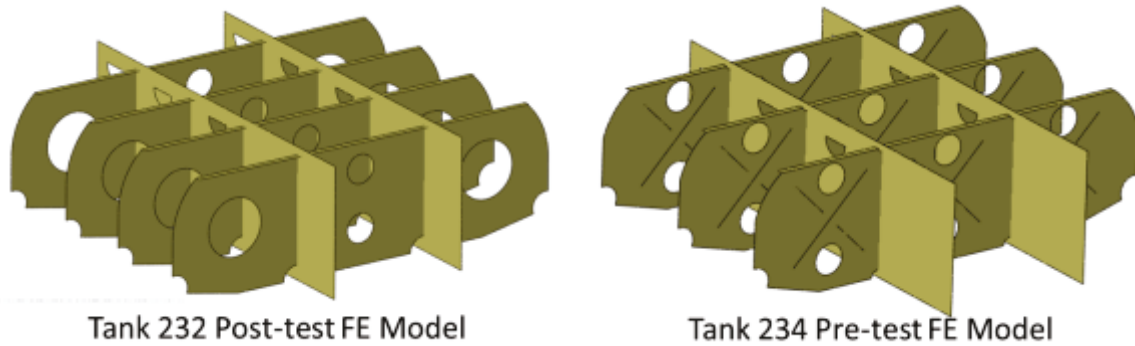


Figure 37. Comparison between Baffle Arrangement in Tank 232 Post-test FE Model (left) and Tank 234 Pre-test FE Model (right)

The pre-test model of tank 234 was run at various impact speeds before the impact test to assist in determining the target impact speed. Because the actual impact occurred at 11.2 mph, the pre-test model was re-run at this speed following the test. The average force-displacement response from the pre-test model of tank 234, from an 11.2 mph impact, is shown in Figure 38. Note that because this model included a deformable impact cart, the accelerations calculated in the model have been filtered using a channel frequency class (CFC) 60 filter.

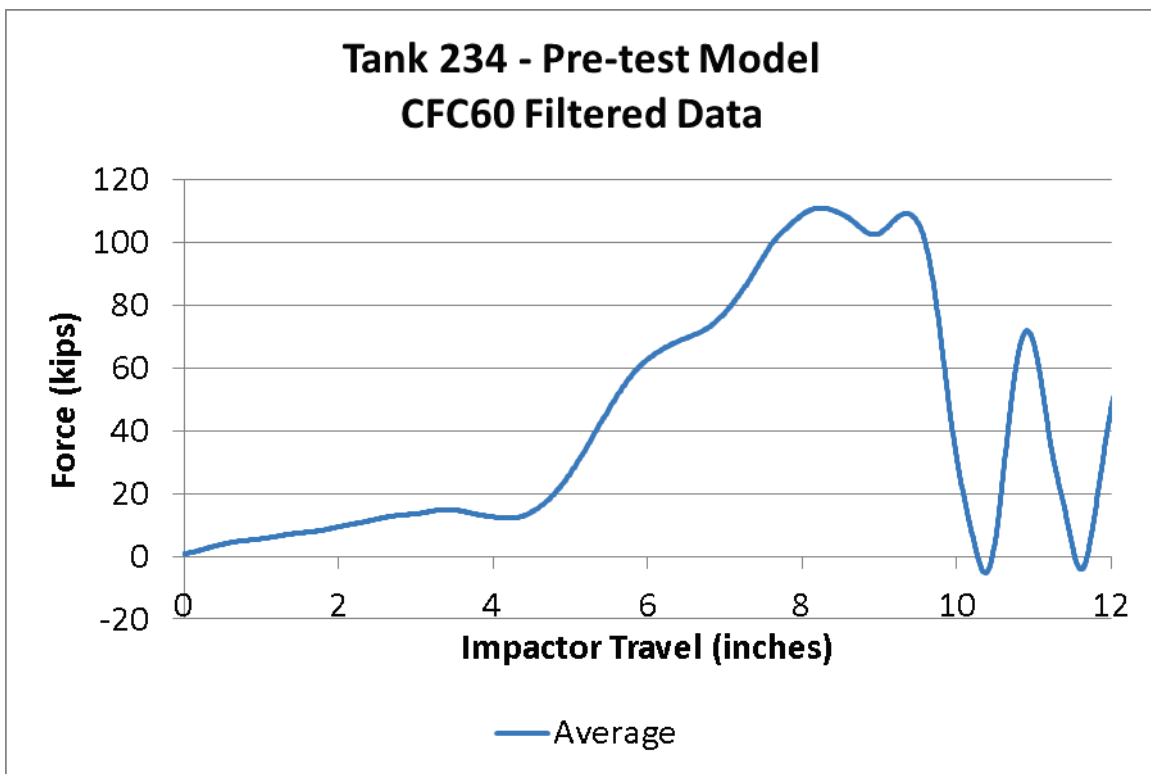


Figure 38. Force-displacement Response from Tank 234 Pre-test Model, 11.2 mph Impact

The deformed shape of tank 234 in the pre-test model, just before the onset of puncture, is shown in Figure 39. Some tearing of the material around the perimeter of the impactor is apparent in this image.

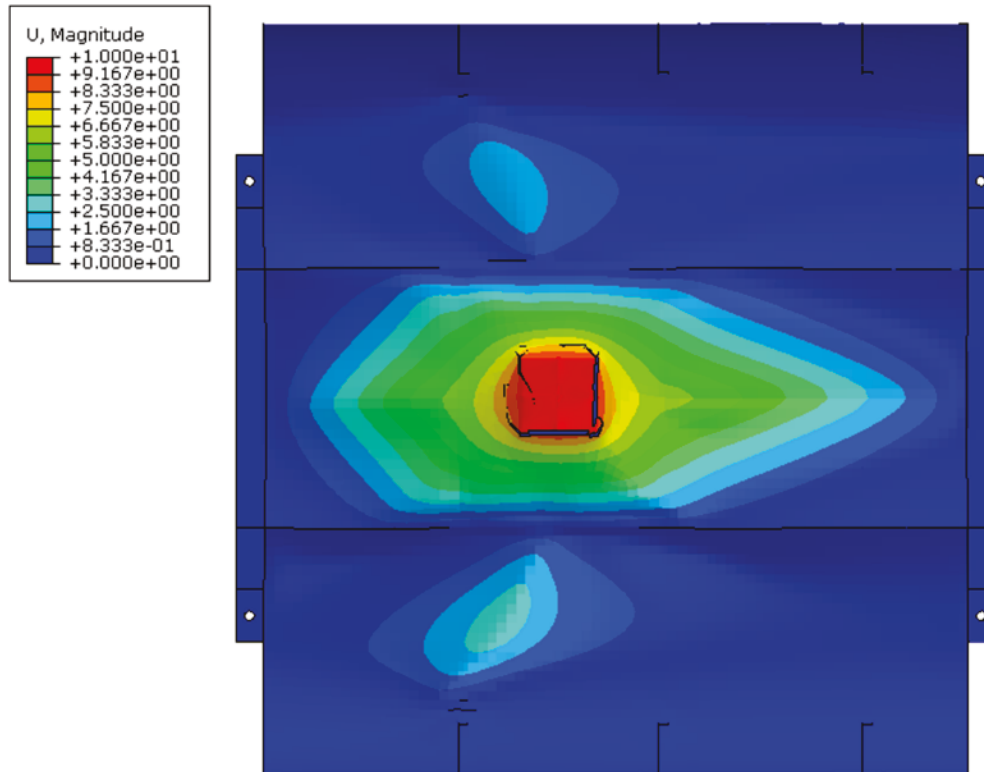


Figure 39. Deformed Shape of Tank 234 after 11.2 mph Impact, Pre-test Model (Contours of Displacement, in inches)

On the basis of the pre-test modeling, an 11.2 mph impact was expected to cause puncture of the tank. A target speed of 12.5 mph was selected for the test of tank 234 to provide some tolerance for reduction in impact speed caused by test conditions (e.g., wind). As will be discussed in the following section, post-test changes to the material failure behavior and geometry of the tank’s baffles were made to the model.

4.4 Modeling Phase 3: After Test of Tank 234

Following the test of tank 234, additional information on the internal baffle arrangement was obtained, resulting in changes to the structure of the model. The material behavior associated with damage initiation was also re-visited in the post-test FE model.

4.4.1 Post-test Model of Tank 234

The test of tank 234 did not result in puncture of the tank. This outcome led to close scrutiny of the tested tank and resulted in changes to the pre-test model. Changes were made to the material properties as well as to the geometry of the baffles within the impacted zone. The changes to the material properties in the post-test model are discussed in Section 4.1.3 and Appendix B. The changes to the geometry of the model are discussed in this section.

Before the test of tank 234, external measurements were made for the overall tank. These measurements were found to be nearly identical to tank 232. Additional information on the baffles of tank 234 was gathered before the test. The number of baffles and their lateral locations

within the tank were estimated by external measurements. Additionally, a small camera was inserted into the side lobe of the tank through the hole previously occupied by the fuel gage. This camera allowed the external measurements of the baffle locations to be confirmed, and it allowed further measurements of the baffle geometry to be made. This information was used to generate the pre-test FE model of tank 234.

Following its impact test, tank 234 was cut open to permit examination of the interior damage. During this teardown, it was discovered that the baffle arrangement within the center lobe of the tank differed both from the baffle arrangement of companion tank 232 and from the baffle arrangement in its own side lobes. The baffle arrangement within tank 232, within the side lobes of tank 234, and within the tanks examined in the field inspections (Oak Island, NJ and Concord, MA), all feature an L-shaped extension welded to the tops of the lateral baffles. However, in the center lobe of tank 234, this L-shaped extension was at the bottom of the lateral baffles, adjacent to the struck bottom sheet of the tank.

The lateral baffle geometries from the pre- and post-test FE models of tank 234 are shown in Figure 40. The top photograph shows the bottom of the center lobe baffles during the post-test teardown of tank 234; it is one of the lateral baffles that did not experience permanent deformation during the test. The lower left image shows the pre-test baffle arrangement from tank 234 FE model. The L-shaped baffle extension is highlighted in the post-test model, at the bottom right of this figure.

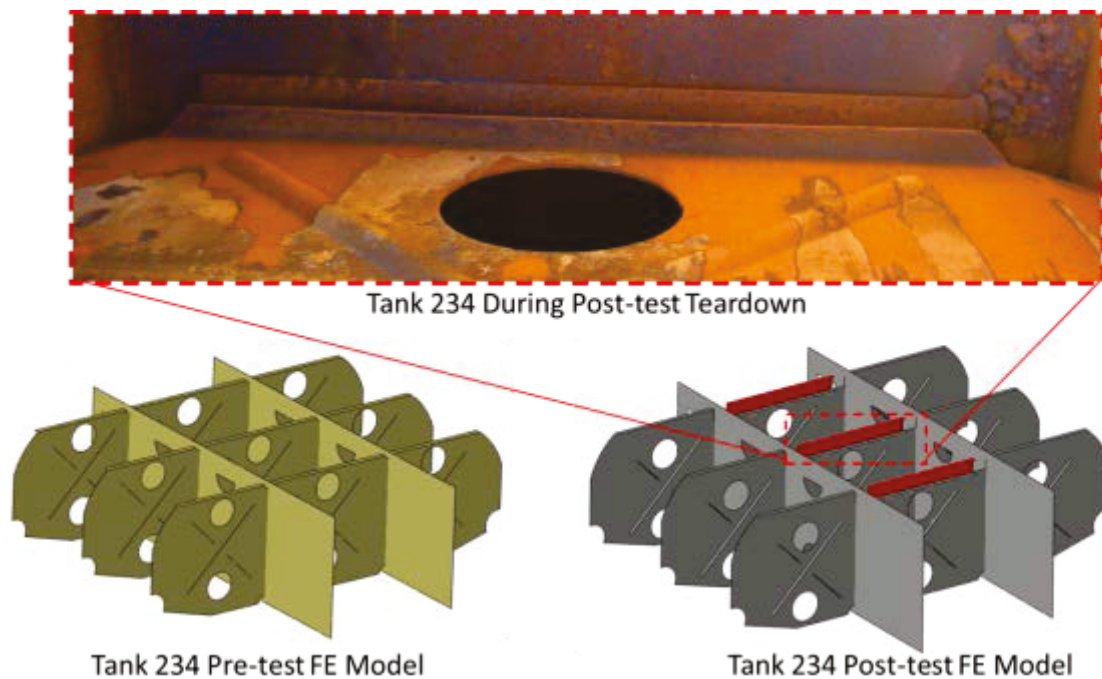


Figure 40. Tank 234 Baffle Arrangement during Teardown (top) Pre-test Model (bottom left), and Post-test Model (bottom right)

5. Results – Tests and Analyses

The results of the three impact tests are summarized in Table 12. In this section, the post-test FE models are discussed unless otherwise specified. The complete set of test and analysis results can be found in Appendices C and D.

Table 12. Summary of Fuel Tank Impact Tests

Tank	Test Date	Target Speed	Impact Speed	Impact Energy	Result
202	October 9, 2013	7 mph	6.2 mph	~18,100 ft-lb	~1.5 inch residual dent No puncture
232	October 8, 2013	6 mph	4.5 mph	~9,500 ft-lb	~5 inch residual dent No puncture
234	August 20, 2014	12.5 mph	11.2 mph	~59,000 ft-lb	8.5 inch residual dent No puncture

5.1 Tank 232 Impact Test Results

The tank 232 impact test was conducted on October 8, 2013. Just before the test, the temperature was recorded as 62°F, with a wind speed of 6 mph W. Tank 232 was impacted at a speed of 4.5 mph and the impact was centered on the bottom of the tank itself, which corresponded to an impact centered between two lateral and two longitudinal baffles. Figure 41 shows a post-test image of the deformed shape of tank 232 on the left and the deformed shape of the FE model on the right. The FE model shows contours of residual indentation depth. The tested tank had a residual dent of approximately 5 inches, and the FE model had a residual dent of approximately 4.8 inches.

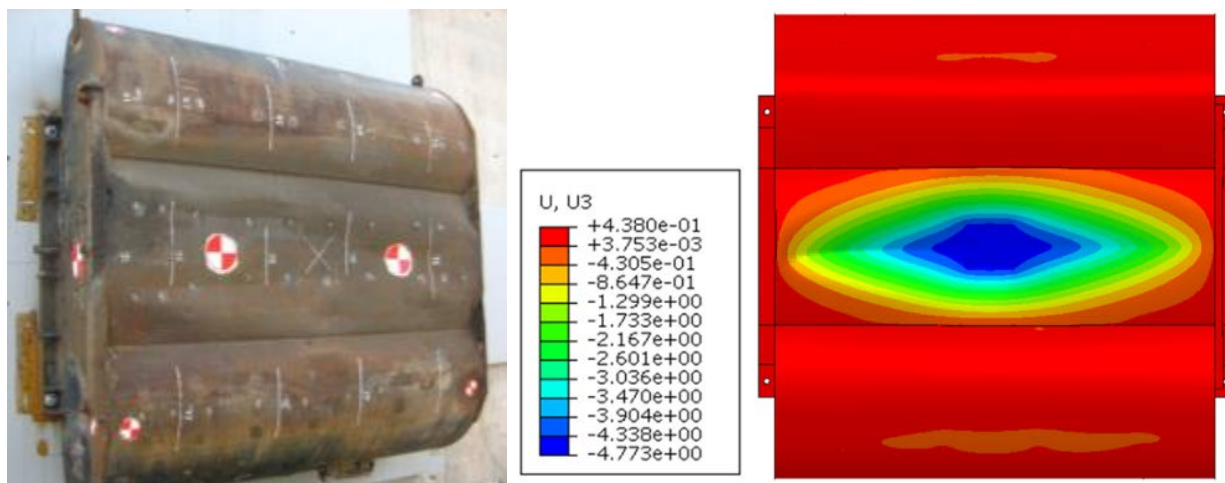


Figure 41. Post-test View of Tank 232 from Test (left) and FE Model (right)

The longitudinal acceleration of the impact cart was measured at five locations. Two post-test FE models were also analyzed for tank 232. One model used a fully-deformable cart, the other used a rigid representation of the impactor. In both models, the impacting object had the same mass. In the model using the deformable cart, acceleration-time history was requested at corresponding locations to the instrumented locations in the test. Because of persistent ringing, the longitudinal accelerations measured at location BA2C were excluded from the average acceleration calculated for both the test and the FE model using the deformable impactor.

The acceleration at the four remaining locations from the test and from the FEA were filtered using a CFC60 Hz filter in accordance with SAE J211 [10], with the filtered results then averaged to obtain a single acceleration-time history for the cart. For the FE model using a rigid impactor, a single acceleration-time history was generated at the rigid body reference point. For the test and two FE model results, the impact force was obtained by multiplying the entire mass of the cart by the average acceleration. For both FE models of tank 232, the impactor was initially offset from the tank at $t=0$ seconds. This was done to compensate for the uncertainty between the triggering of the instrumentation and the actual contact of the impactor with the tank, as discussed in Section 3.4.4. In the FE model, this corresponded to a time offset of 0.015 second, or approximately 1 in. The average force-time responses from the test, the deformable cart FE model, and the rigid impactor model are shown in Figure 42. Appendices C and D contain plots of all data channels.

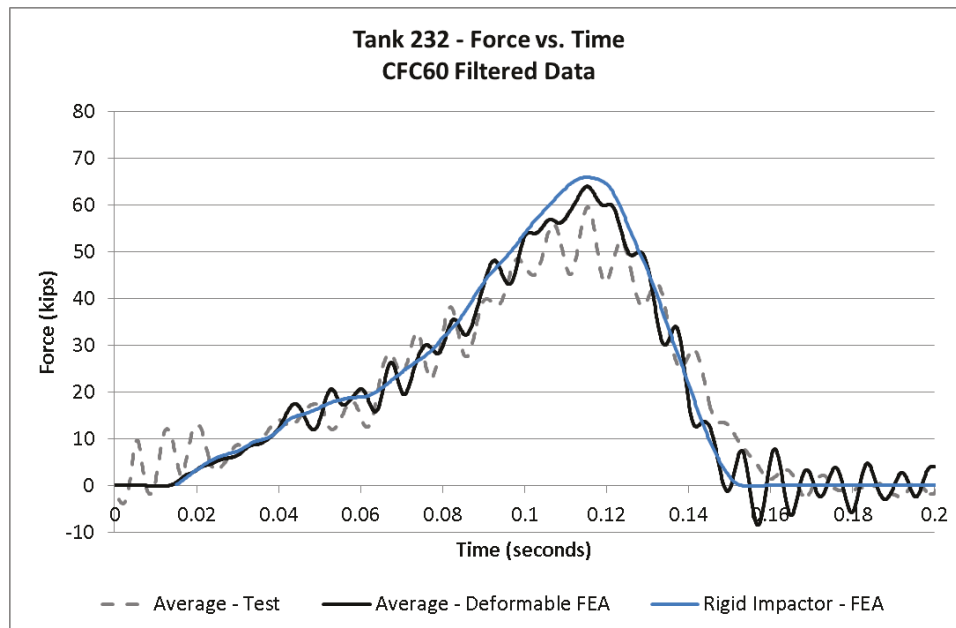


Figure 42. Tank 232 Force-time History from Test and Post-test FEA

In tank 232, there was an initial gap between the interior of the bottom sheet of the tank and the bottom of the lateral baffles. During the initial phase of the impact event, the bottom sheet was deforming freely as the impactor made contact with the tank. Eventually, the gap was closed and the interior of the bottom sheet made contact with the lateral baffles. This caused an apparent stiffening of the tank, since the impactor was now pressing against the bottom sheet and the baffles acting together. However, before significant deformation of the baffles could occur, the

impactor had come to a stop and the cart was reflected away from the tank. The impact cart had rebounded fully from the tank by approximately 0.15 second in all the series plotted above.

Figure 43 shows the displacement-time history from the average of the test accelerometers, the average of the corresponding locations on the impact cart in the deformable FE model, and the displacement of the rigid impactor. Tank 232 had a maximum indentation of approximately 6.8 inches in the test, a maximum indentation of approximately 7 inches in the deformable cart FE model, and approximately 6.9 inches in the rigid impactor FE model.

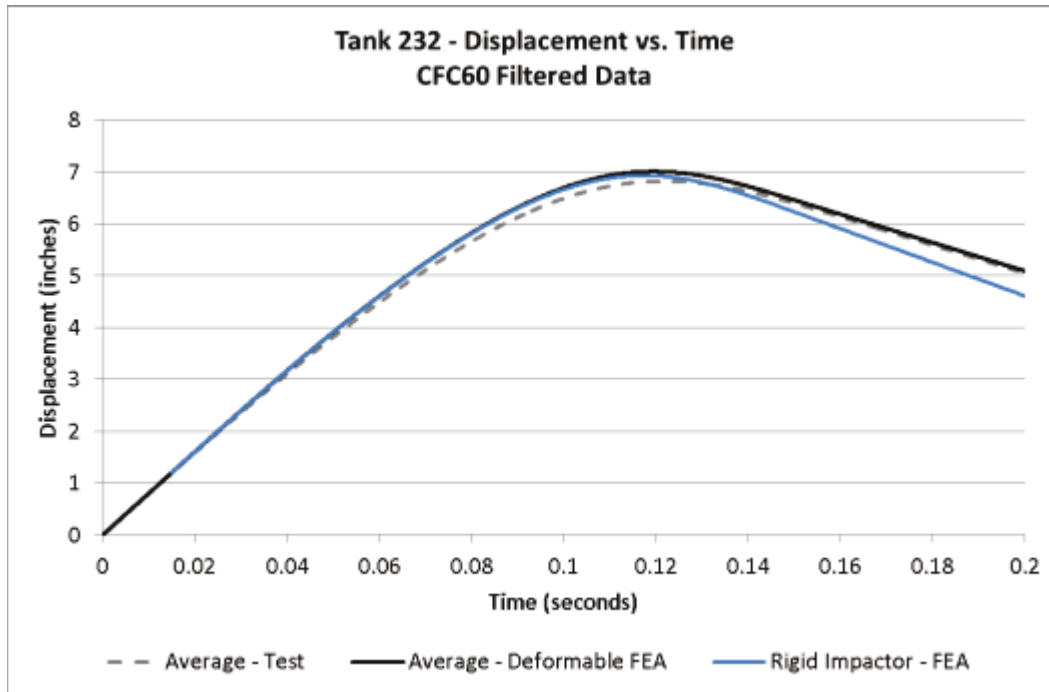


Figure 43. Tank 232 Displacement-time History from Test and Post-test FEA

Generally, there is good agreement between the test and the FE models. There is better agreement with the test results for the deformable cart FE model than for the rigid impactor FE model. While the intent of the impact cart was to act as a rigid impactor, it is apparent that the cart itself was deforming slightly during the impact event. While a rigid impactor is suitable for approximating the behavior of the cart-tank system during the impact test, some of the details in the force-time history come about because of deformation of the cart. Therefore, those details will not be seen in an FE model without a deformable impactor.

5.2 Tank 202 Impact Test Results

The tank 202 impact test was conducted on October 9, 2013. Just before the test, the temperature was recorded as 62°F, with a wind speed of 10 mph ENE. Tank 202 was impacted at a speed of 6.2 mph. The impact was centered on the bottom of the tank itself, which corresponded to an impact centered between two longitudinal baffles and on the middle transverse baffle. Figure 44 shows a post-test image of the deformed shape of tank 202 on the left and the deformed shape of the FE model on the right. The FE model shows contours of residual indentation depth. The tested tank had a residual dent of approximately 1.5 inches, and the FE model had a residual dent of approximately 2.2 inches.

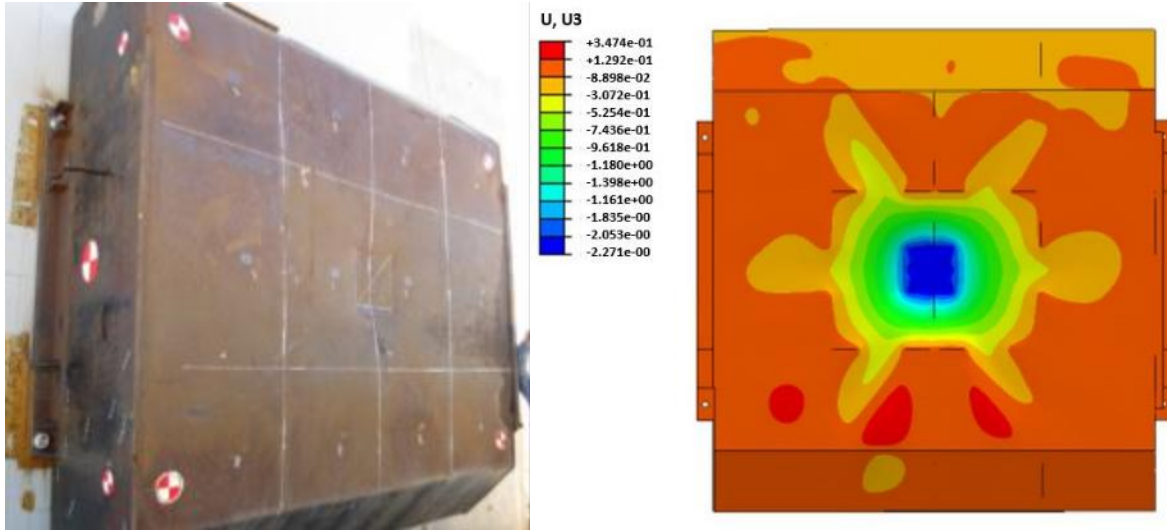


Figure 44. Post-test View of Tank 202 from Test (left) and FE Model (right)

In both the test and the FE model, the deformation pattern of the bottom sheet was very similar. The outline of the impactor was clearly visible on the bottom sheet of the fuel tank in both the test and the modeled tanks. Outside of the immediate impact zone, the indentation formed a roughly “x” shaped pattern. This pattern of indentation corresponds to the intermittent baffle-to-bottom sheet connections within the tank, where regions of deeper indentation correspond to areas without a connection between the baffles and the sheet.

Following the test, tank 202 was cut open and the interior damage was examined. One observed mode of deformation was buckling of the L-shaped brackets used to attach the lateral and longitudinal baffles to the bottom sheet of the tank. These L-brackets tended to flatten as the bottom sheet was pushed inward by the impactor. Additionally, the baffle to which these brackets were attached also buckled in the area surrounding cutouts in the baffles. Figure 45 shows this mode of deformation on the left for the tested article, and on the right for the FE model.



Figure 45. Post-test View of Tank 202 Baffles from Test (left) and FE Model (right)

Similar to the data from tank 232, the longitudinal accelerations measured at location BA2C were excluded from the average acceleration calculated for both the test and the FE model using the deformable impactor because of persistent ringing. The acceleration at the four remaining

locations from the test and from the FEA model were filtered using a CFC60 filter in accordance with SAE J211 [10], with the filtered results then averaged to obtain a single acceleration-time history for the cart. The average acceleration was multiplied by the full mass of the impact cart to obtain the force-versus-time response. Figure 46 shows the force-time history from the test of tank 202, the FE model using a deformable cart, and the FE model using a rigid impactor. Similar to the results of tank 232, there is better agreement between the test results and the deformable cart FE model.

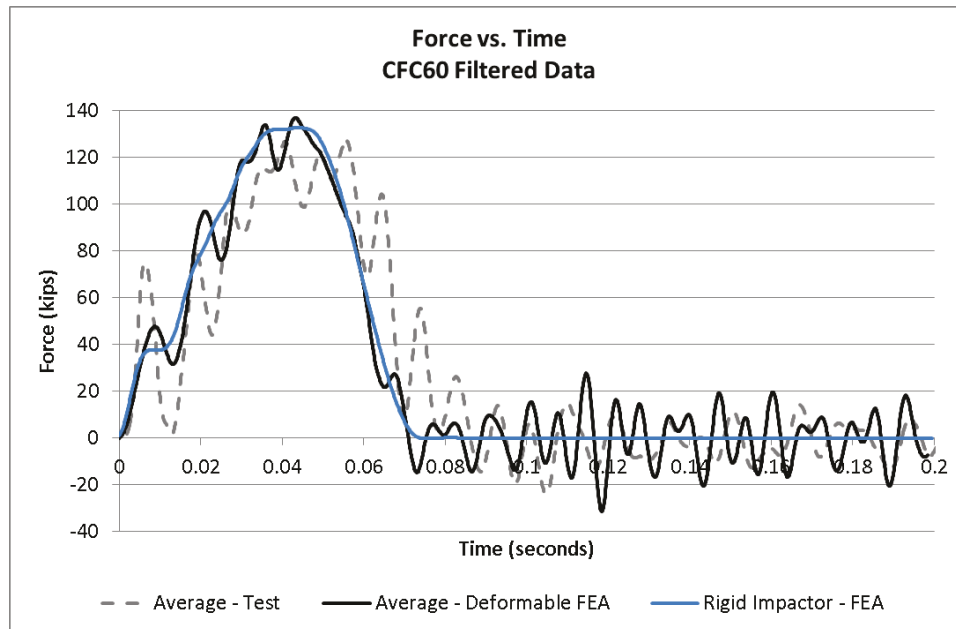


Figure 46. Tank 202 Force-time History from Test and Post-test FEA

Tank 202 was of a different design than either tank 232 or 234. In tank 202, the longitudinal and lateral baffles were attached to the bottom sheet using an intermittent series of L-shaped brackets welded between the two structures. While there was a gap between the baffles and the bottom sheet, the gap was much smaller than that of tanks 232 or 234. In addition to differences in construction, the test setup was intentionally chosen to strike tank 202 directly above a baffle.

The combination of differences in geometry and impact site caused a significantly different impact response than was seen in tank 232. Because the bottom sheet was attached to the baffles, the force response was initially stiff. However, there is some buckling that quickly occurred either to the baffles themselves or to the L-brackets attaching the baffles to the bottom sheet. This caused the first drop in load at approximately 0.015 second. The load was quickly able to resume climbing as the impactor continued moving forward. The load reached a much higher peak level than was seen during tank 232 test. The impact cart was fully rebounded from the tank by approximately 0.1 second in the test and both FE model simulations.

In the test, the dent reached a maximum depth of approximately 3.6 inches before the cart began rebounding from the tank. In the post-test FE model with a deformable cart, the maximum dent depth was approximately 3.4 inches before the cart was rebounded. In the post-test FE model with the rigid cart, the maximum dent depth was approximately 3.3 inches.

Figure 47 shows the average displacement-time histories from the test, the FE model that used the deformable impact cart, and the FE model that used the rigid impactor.

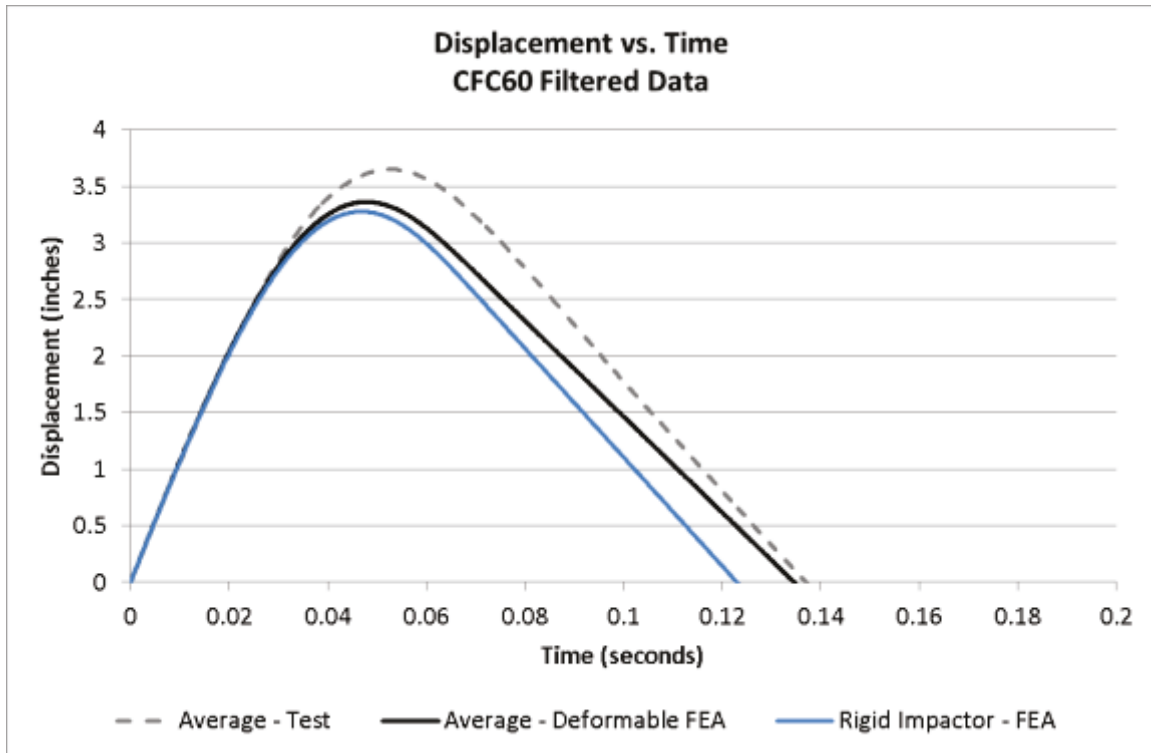


Figure 47. Tank 202 Displacement-time History from Test and Post-test FEA

Similar to the results of tank 232 test and simulations, there was better agreement between the test measurements and the FE model that used the deformable impact cart. There was generally good agreement between the test and both FE models for such key results as force response, maximum displacement, and deformed shape.

5.3 Tank 234 Impact Test Results

The tank 234 impact test was conducted on August 20, 2014. Just before the test, the temperature was recorded as 80.8°F, with a wind speed of 5 mph WNW. Tank 234 was impacted at a speed of 11.2 mph. The impact occurred at the target location, which was offset from the centerline of the tank. This location was chosen to result in an impact centered between two vertical and two horizontal baffles. The maximum residual indentation of the tank, measured as the difference between the initial and final shape, was approximately 8.5 inches. A comparison between the deformed shape of tank 234 and its deformed contours from the FE model is shown in Figure 48. This figure includes pre-impact images for the FEA, the laser-mapped tank, and a photograph of the tank itself. Because the tank had several pre-existing dents on its bottom, it was important to document the existing damage before the impact so that the damage caused by the test could be determined.

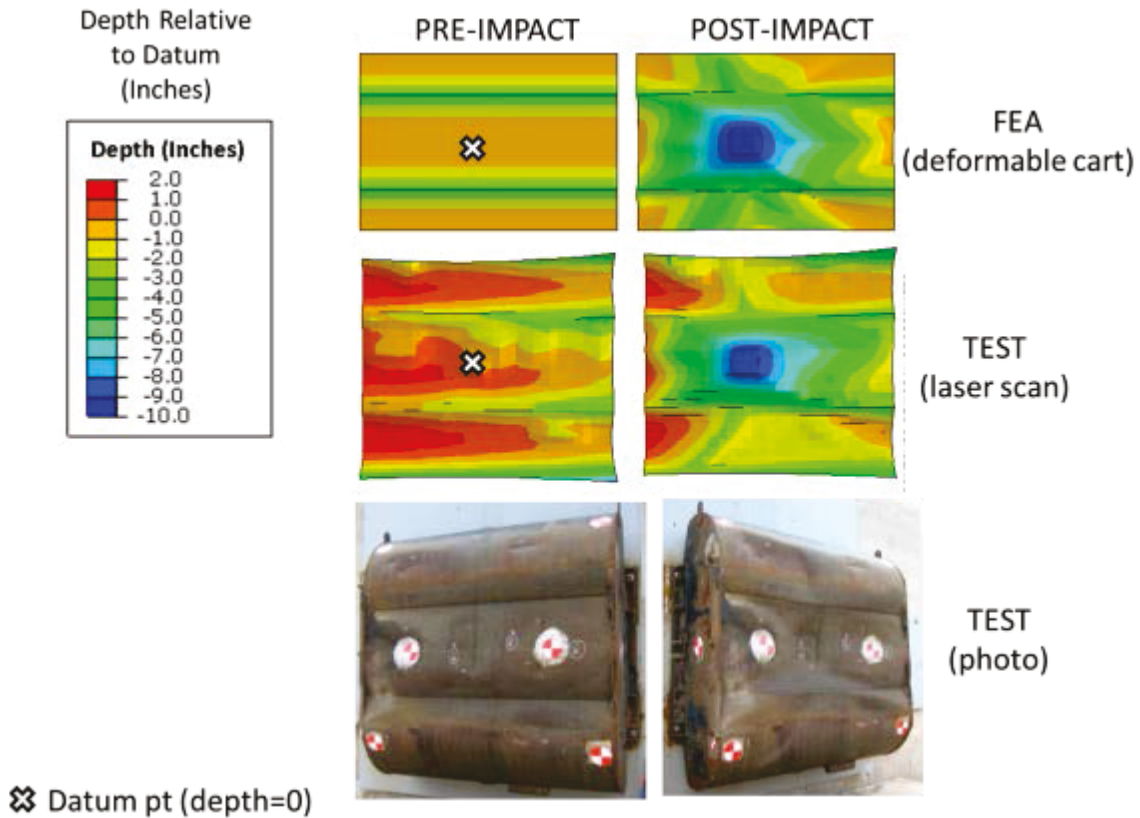


Figure 48. Tank 234 Deformed Shape Comparison between FEA and Test

There is very good agreement between the deformed shape, measured on the tested tank and the post-test FE results. The deformation extends across the width of the tank on the center (impacted) lobe of the bottom sheet. At the top and bottom lobes, both the test and the FEA have diagonal dents extending away from the impacted zone. Figure 49 shows the original and final profiles of the tank taken at a section passing through the point of impact. This figure shows the difference between the initial and final dent depth to be approximately 8.5 inches.

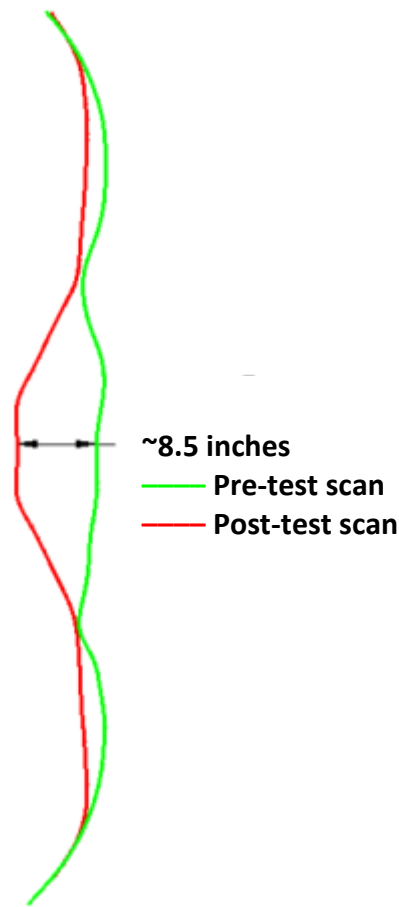


Figure 49. Deformation – Vertical Cross-section at the Impact Center

For the test of tank 234, the test accelerations and the deformable FE accelerations were filtered using a CFC60 filter. The acceleration data from accelerometer BA1CX (located directly beneath the impactor) was excluded from the average owing to high amplitude peaks that persisted even with filtering. High amplitude peaks in accelerometer BA1CX are due to its proximity to the impact surface and a higher impact force than in the two previous tests, which increased the dynamic response of the impact cart. Figure 50 contains a plot of the force-time histories from the test, the FEA using a deformable impact cart, and the FEA using a rigid impactor.

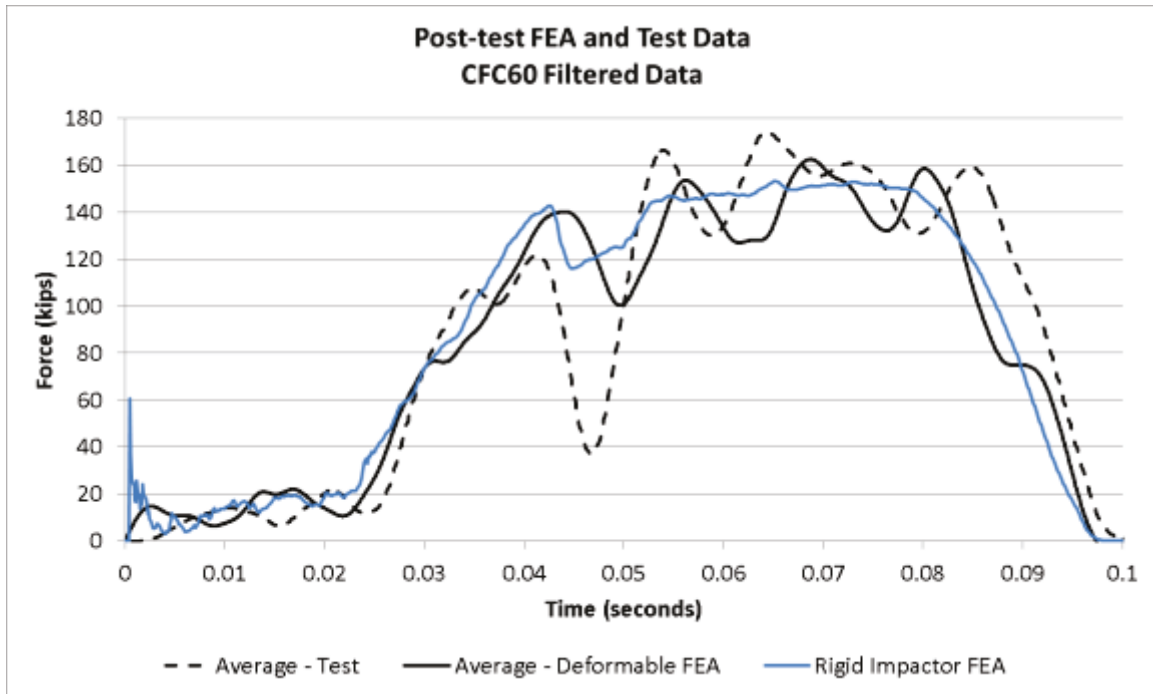


Figure 50. Tank 234 Force-time History from Test and Post-test FEA

Similar to the design of tank 232, tank 234 had a gap between the inside of the bottom sheet of the tank and the bottom of the baffles. The force needed to deform the bottom sheet of the tank is initially low. Once the bottom sheet makes contact with the bottom of the baffle extensions, the force necessary to increase the indentation becomes larger. The force continues to increase until approximately 0.04 seconds. At this point, it is believed that the baffle extensions begin to fold over, allowing the force to drop. Once the baffle extensions have folded over completely, the force resumes its climb, as the bottom sheet remains in contact with the baffles. The force level remains fairly constant until the impact is rebounded from the tank. In the test and in the simulations, the impactor is reflected at just prior to 0.1 seconds.

Figure 51 shows the displacement-time histories from the test of tank 234, the post-test FE model using a deformable cart, and the post-test FE model using a rigid impactor. The test measurements recorded a maximum indentation of 11.1 inches before the impact cart was rebounded from the tank. The deformable cart FE model calculated a maximum indentation of approximately 10.7 inches. The FE model using a rigid representation of the impactor calculated a maximum indentation of approximately 10.4 inches.

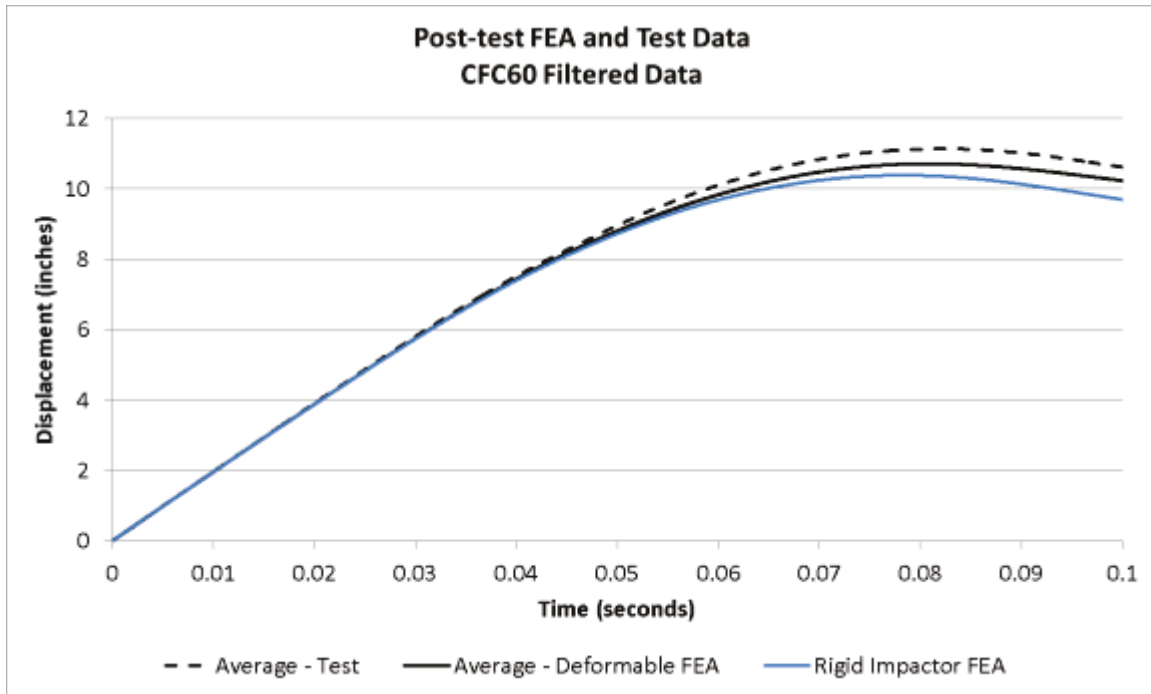


Figure 51. Tank 234 Displacement-time History from Test and Post-test FEA

There is generally good agreement between the test results and the post-test FEA. While the FEA that used a rigid impactor gives a generally similar shape to the test measurements, there is better agreement between the test results and the FEA that used a deformable impact cart. The force response, maximum indentation, and deformed shapes of the tested article and models are all in fairly good agreement with each other.

5.4 Tank 234 Post-test Puncture Model Results

Using the post-test FE model of tank 234, additional simulations were performed to estimate the speed-to-puncture for the tank in the impact condition that was tested. With the exception of changing the impact speed, the post-test model of tank 234 was otherwise unchanged. Note that these simulations were run with a rigid impactor rather than the deformable impact cart that was used to compare test and FE results previously.

While a significantly high-speed impact would cause puncture, the desired outcome of this modeling effort was to run the model at a speed slightly above the speed necessary to cause puncture. Running a model at an extremely high impact speed will guarantee puncture and decrease simulation time, but it is not likely to give an accurate representation of the performance of the tank when struck in the vicinity of its threshold puncture speed. The desired result of this modeling extrapolation is to estimate the maximum speed at which the tank can be struck without causing puncture. Therefore, it is important to examine not only the energy the tank has absorbed at the time of puncture, but also the residual kinetic energy that has not been dissipated. Ideally, at the critical puncture speed, puncture will occur with very little residual kinetic energy in the impactor.

The post-test model was run at two speeds higher than the test speed. At 14.5 mph, the impactor was rebounded from the tank. At this speed, a small number of elements on the bottom of the

tank, under the impactor's corners, had experienced failure. This result indicates that a 14.5 mph impact is at the threshold puncture speed for this tank in this impact condition.

The simulation was then run at 16 mph to establish a speed at which the tank would be unable to stop the impactor (i.e. complete puncture). The top of Figure 52 shows the deformed shape of tank 234 after a 14.5 mph impact, and the bottom shows the shape after a 16 mph impact. While both speeds were sufficient to cause elements to be removed from the tank, at 14.5 mph the impactor rebounded from the tank, while at 16 mph the impactor continued to penetrate the tank but with little residual kinetic energy.

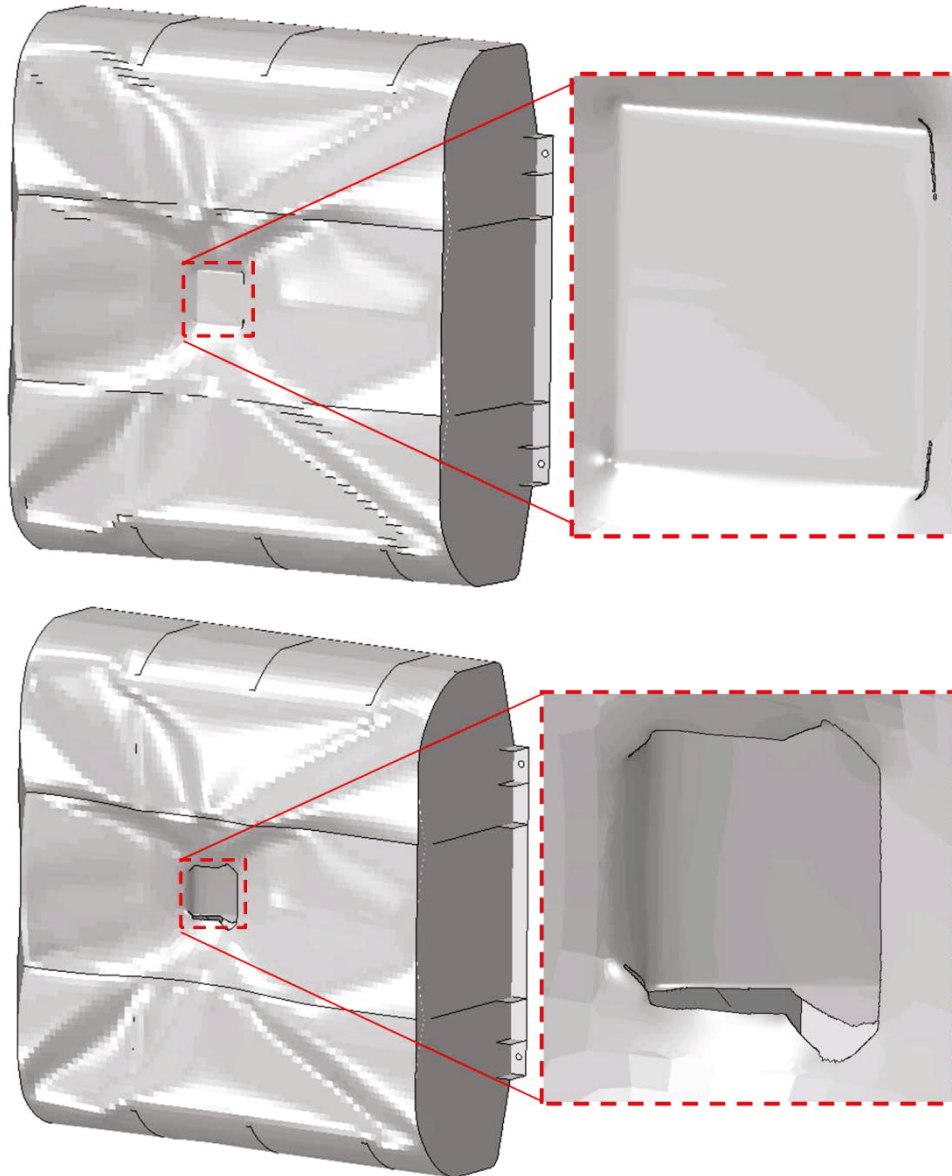


Figure 52. Deformed Shape of Tank 234 and Puncture Detail after 14.5 mph Impact Simulation (top) and 16 mph Impact Simulation (bottom)

Figure 53 shows the force-versus-displacement responses from the post-test FE models of tank 234 when subjected to an 11.2 mph (test speed), 14.5 mph, and 16 mph impact. In all cases, the

plot was derived from the accelerometers on the simulated rigid impactor. Because a rigid impactor was used and the results exhibit very little high-frequency noise, these results have not been filtered. While generally the responses are similar, there are some important differences between them. In the 11.2 mph impact, the impactor stops and is rebounded from the tank after reaching approximately 11 inches of indentation without causing any elements to experience material failure. This case is the only case to exhibit the force drop at approximately 7.5 inches, where the baffle buckling occurs. While the baffles buckle in the other two simulations, the impactor is moving at a higher speed at that point, and the drop in force is not “seen” by the impactor. In the 14.5 mph impact, the impactor is also rebounded from the tank, although elements have begun to be removed from the simulation. However, in the 16 mph impact, the impactor continues to move forward as the force drops after nearly 14 inches of travel. This is an indication that puncture is occurring in the model. As elements are removed from the simulation under the impactor, the tank’s resistance to further impactor travel decreases. Because the impactor still contains some kinetic energy that has not been dissipated during the impact, it will continue to push into the now-punctured tank.

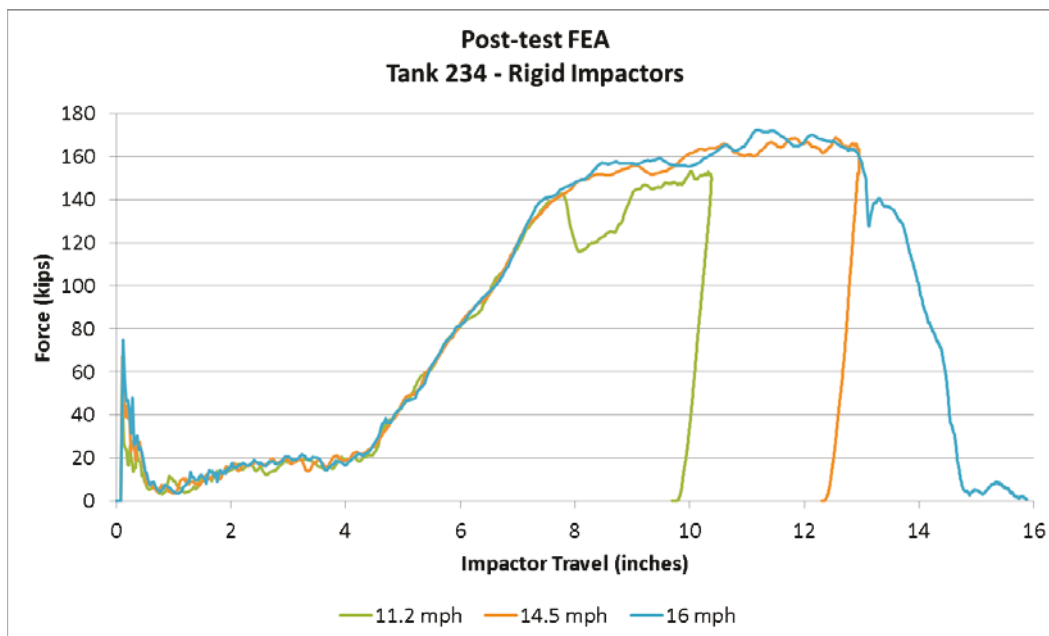


Figure 53. Force-displacement Responses for 11.2, 14.5 and 16 mph FEA of Tank 234

The energy dissipated by the tank during the calculated as the area beneath the force versus displacement characteristic. The energy-displacement history is plotted in Figure 54. This figure also shows the initial kinetic energy of the cart for the 14.5 and 16 mph simulations where puncture occurred. From this figure, it can be seen that the dissipated energy of the 16 mph impact is slightly less than the initial kinetic energy. This indicates that the impact cart is still moving forward as the tank punctures. Because the residual kinetic energy is small, the impact at 16 mph is occurring at a slightly higher speed than the tank could resist without the impactor continuing to travel through the tank after puncture.

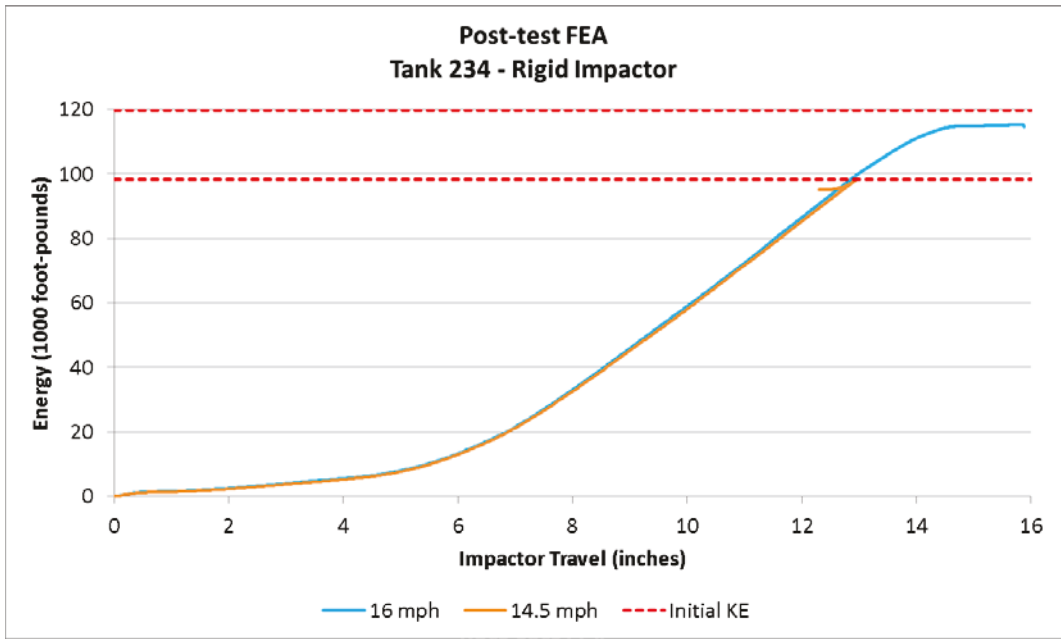


Figure 54. Energy Dissipated During 14.5 and 16 mph Impact Simulations

6. Conclusion

FRA sponsored research into the puncture resistance of passenger locomotive fuel tanks, subjected to blunt impacts on their bottom sheets, is currently underway. This program includes FE modeling performed by Volpe and impact testing performed by TTCI. This research is intended to guide the development of scenarios for evaluating the performance of DMU fuel tanks under a variety of impact conditions. The first phase of this research included three impact tests of retired F40 passenger locomotive fuel tanks. These first tests were intended to help evaluate the test setup, instrumentation needs, and modeling techniques that will eventually be applied to DMU fuel tanks of various designs.

These first tests have proven very useful to developing information on the test setup, instrumentation needs, and modeling techniques necessary to further this research program. Additionally, these preliminary tests provided valuable information and understanding of the structural response of the fuel tanks. In particular, the contribution of the baffles to the overall puncture resistance of the fuel tank has been revealed through these first tests. After refinements, all developed FE models produced results that matched the tests.

In the first phase of this program, TTCI conducted impact tests on three locomotive fuel tanks, which provided data for Volpe to use in developing its FE models of the fuel tanks. Speeds for all impact tests were below target speeds, but were within the pre-test tolerance of ± 2 mph. The impacts did not puncture the fuel tanks. Post-test material tests showed that the yield strengths of the fuel tank steels were higher than those used in the initial FE analyses. Additionally, post-test examination of the fuel tanks revealed differences in the baffle arrangements and their connections in each of the three tanks used.

7. References

1. Jacobsen, K. "Fuel Tank Crashworthiness: Loading Scenarios." Paper No. JRC2011-56077, in *Proceedings 2011 American Society of Mechanical Engineers Joint Rail Conference*, Pueblo, CO. March 2011. Available at: http://ntl.bts.gov/lib/37000/37900/37914/JRC2011-56077_Fuel_Tank_Crashworthiness.pdf
2. Federal Railroad Administration. Code of Federal Regulations. 49—Transportation Part 229—Railroad Locomotive Safety Standards. Washington, DC. Available at: http://www.ecfr.gov/cgi-bin/text-idx?SID=01e6ba5ad7bf36569b42f6697cd558f7&mc=true&node=se49.4.229_15&rgn=div8
3. Federal Railroad Administration. Code of Federal Regulations. 49—Transportation Part 238—Passenger Equipment Safety Standards. Washington, DC. Available at: http://www.ecfr.gov/cgi-bin/text-idx?SID=01e6ba5ad7bf36569b42f6697cd558f7&mc=true&node=se49.4.238_15&rgn=div8
4. Association of American Railroads. "Performance Requirements for Diesel Electric Locomotive Fuel Tanks – Standard S-5506." Adopted as Recommended Practice: 1995; Upgraded to Standard: 2001.
5. American Public Transportation Association. "APTA SS-C&S-007-98, Rev. 1. Standard for Fuel Tank Integrity on Non Passenger Carrying Locomotives." Edited February 13, 2004.
6. Sonoma-Marín Area Rail Transit. "SMART Vehicle Technology Assessment – Final Draft Report." Prepared by LTK Engineering Services. July 2009. Available at: <http://www2.sonomamarintrain.org/userfiles/file/Vehicle%20LTK%20Study%20for%20web.pdf>
7. Sonoma-Marín Area Rail Transit. "SMART Technical Specification for Diesel Multiple Units (DMUs)." Industry Review Draft. January 20, 2010. Available at: <http://www2.sonomamarintrain.org/userfiles/file/Vehicles%20-Draft%20DMU%20Technical%20Specification%201-20-10.pdf>
8. Tofani, T., and Walker, C. "Development of an Alternative Fuel Tank Standard for DMUs." 2012 APTA Rail Conference, Dallas, TX, June 3-6, 2012. Available at: <http://www.apta.com/mc/rail/previous/2012/presentations/Presentations/Tofani-Walker-Development-of-an-Alternative-Fuel-Tank-Standard-for-DMUs.pdf>
9. Ball, P. "Ruptured fuel tank causes MBTA train to stop by Concord depot." WickedLocal.com. Posted September 16, 2010. Available at: <http://www.wickedlocal.com/x560105612/Ruptured-fuel-tank-causes-MBTA-train-to-stop-by-Concord-depot>

10. SAE International. Standard J211-1: 2007. "Instrumentation for Impact Test – Part 1 – Electronic Instrumentation."
11. Abaqus Version 6.13. Dassault Systems Simulia Corp, Providence, RI. 2013.
12. "Material Hardness." Center for Advanced Life Cycle Engineering – Test Services and Failure Analysis Laboratory. 2001. Available at: http://www.calce.umd.edu/TSFA/Hardness_ad_.htm
13. ASTM E8 / E8M-13a, Standard Test Methods for Tension Testing of Metallic Materials. ASTM International, West Conshohocken, PA. 2013.
14. Tang, Y.H., Yu, H., Gordon, J.E., Jeong, D.Y., Perlman, A.B. "Analysis of Railroad Tank Car Shell Impacts Using Finite Element Method." JRC2008-63014, in *Proceedings of the 2008 IEEE/ASME Joint Rail Conference*, Wilmington, DE. April 2008. Available at: http://ntl.bts.gov/lib/47000/47300/47391/Tang_Analysis_RR_Tank_Car_Shell.pdf
15. Stringfellow, R., Paetsch, C. "Modeling Material Failure during Cab Car End Frame Impact." Paper No. JRC2009-63054, in *Proceedings 2009 American Society of Mechanical Engineers Joint Rail Conference*, Pueblo, CO. March 2009. Available at: <http://ntl.bts.gov/lib/47000/47300/47322/09-63054.pdf>
16. Bao, Y., Wierzbicki, T. "On fracture locus in the equivalent strain and stress triaxiality space." *International Journal of Mechanical Sciences* 46, pp. 81–98. January 2004.
17. Lee, Y.W. and Wierzbicki, T. "Quick Fracture Calibration for Industrial Use." *Impact & Crashworthiness Laboratory Report No. 115*, Massachusetts Institute of Technology. August 2004.
18. Jeong, D.Y., Yu, H., Gordon, J.E., Tang, Y.H. "Finite Element Analysis of Unnotched Charpy Impact Tests." *Proceedings of the Materials Science & Technology Conference and Exhibition*. October 2008. Available at: http://ntl.bts.gov/lib/47000/47500/47511/Jeong_finite_element.pdf
19. Jacobsen, K., Carolan, M., Llana, P. "Test Requirements of Locomotive Fuel Tank Blunt Impact Tests." RTDF2013-2701, *Proceedings of the 2013 ASME Rail Transportation Division Fall Technical Conference*, Altoona, PA. October 2013. Available at: <http://ntl.bts.gov/lib/48000/48500/48594/RTDF2013-4701.pdf>
20. Priante, M., Llana, P., Jacobsen, K., Tyrell, D., Perlman, A.B. "A Dynamic Test of a Collision Post of a State-of-the-Art End Frame Design," Paper No. RTDF2008-74020, *Proceedings of ASME 2008 Rail Transportation Division Fall Technical Conference*, Chicago, IL. September 2008. Available at: <http://ntlsearch.bts.gov/tris/record/ntl/43043.html>

Appendix A. Instrumentation Locations and Technical Specifications

Video Setup

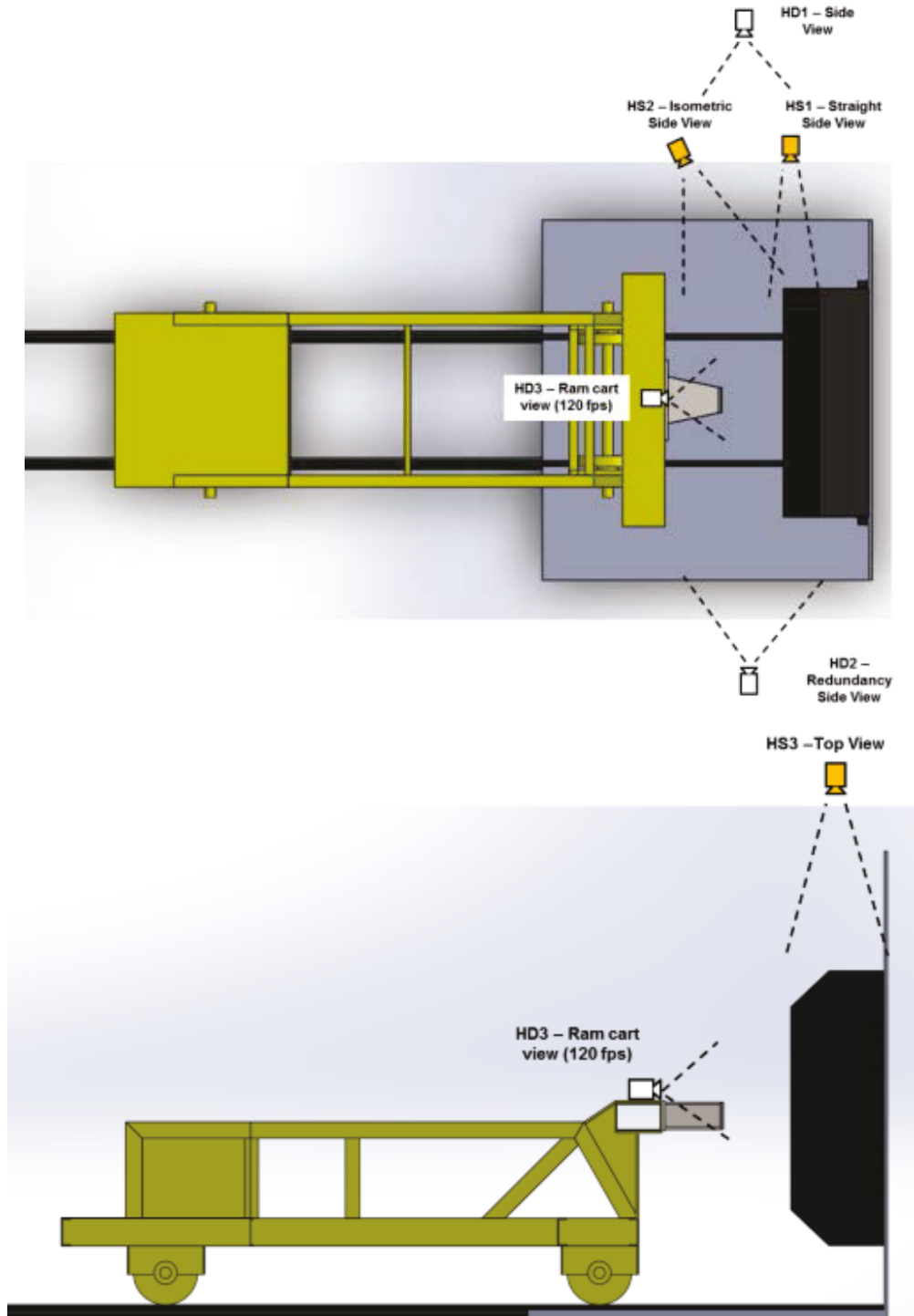


Figure A1. Camera Views

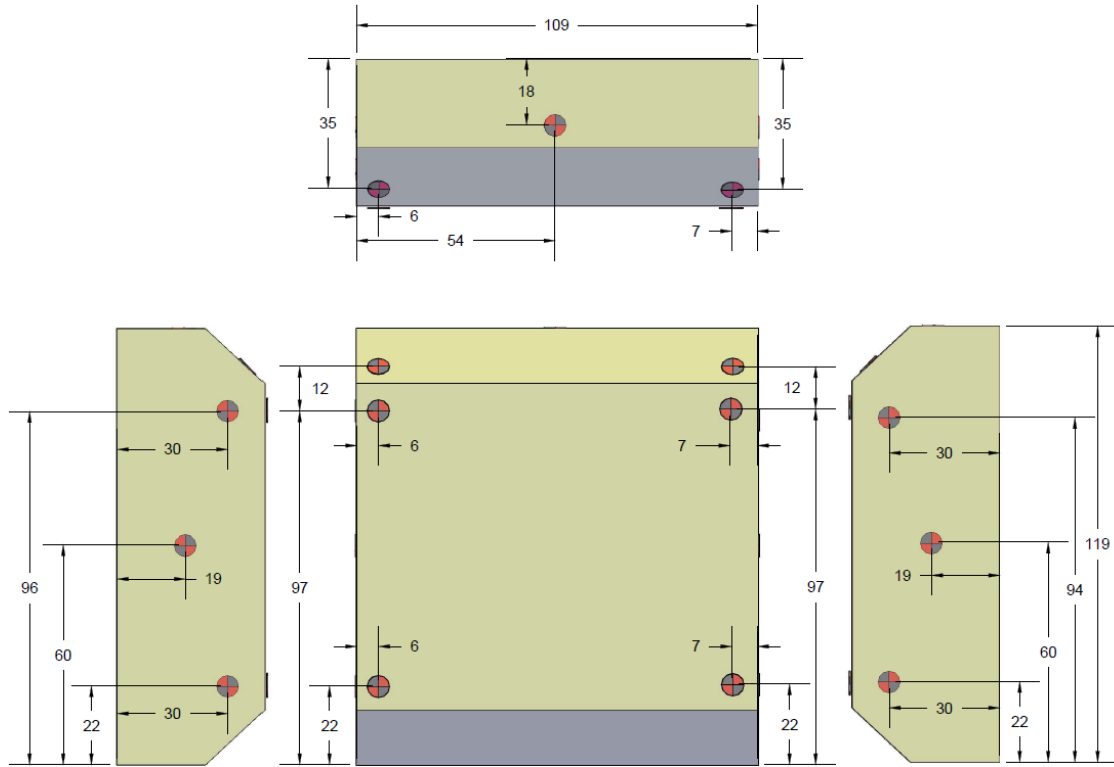


Figure A3. Target Locations (Tank 202)

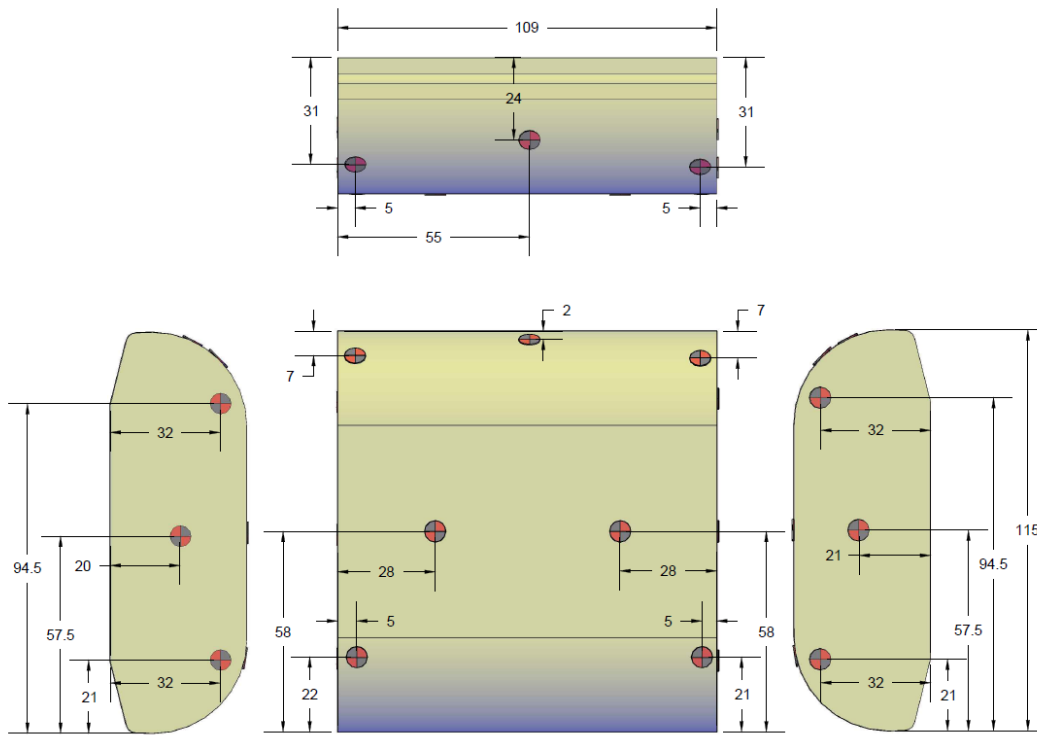


Figure A4. Target Locations (Tank 232)

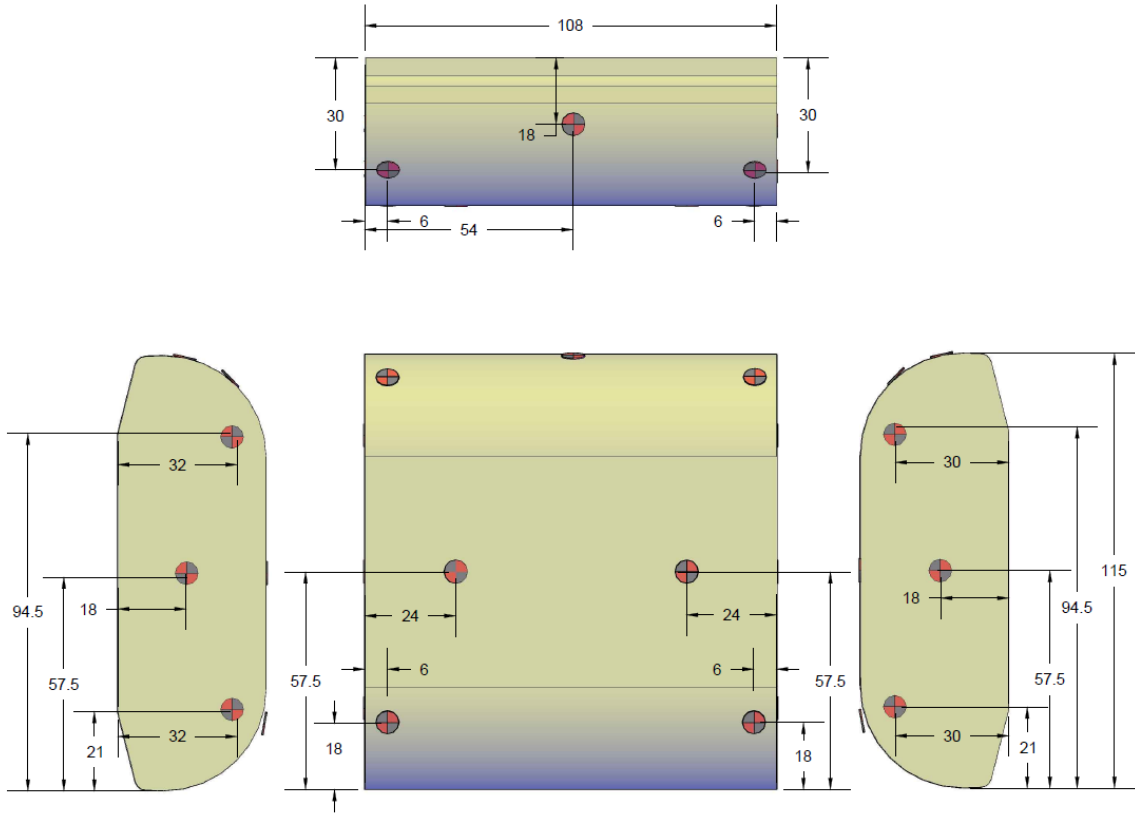


Figure A5. Target Locations (Tank 234)

Appendix B. Fuel Tank Materials

Material samples (coupons) were cut from various structures on tanks 202 and 232 after each tank's test. The nominal (engineering) stress-strain responses from each tested material are presented in Figure B1 and Figure B2, below. Three samples of each material were tested.

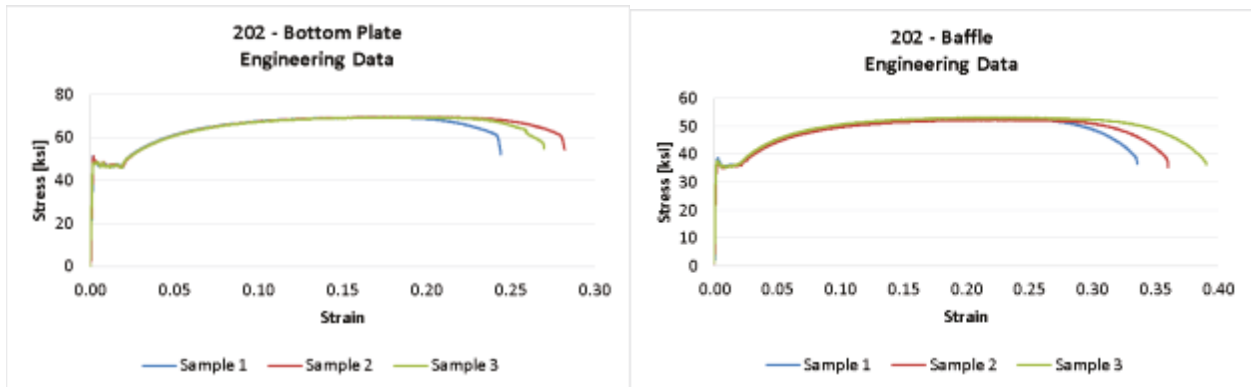


Figure B1. Engineering Stress-strain Responses from Tank 202 Members

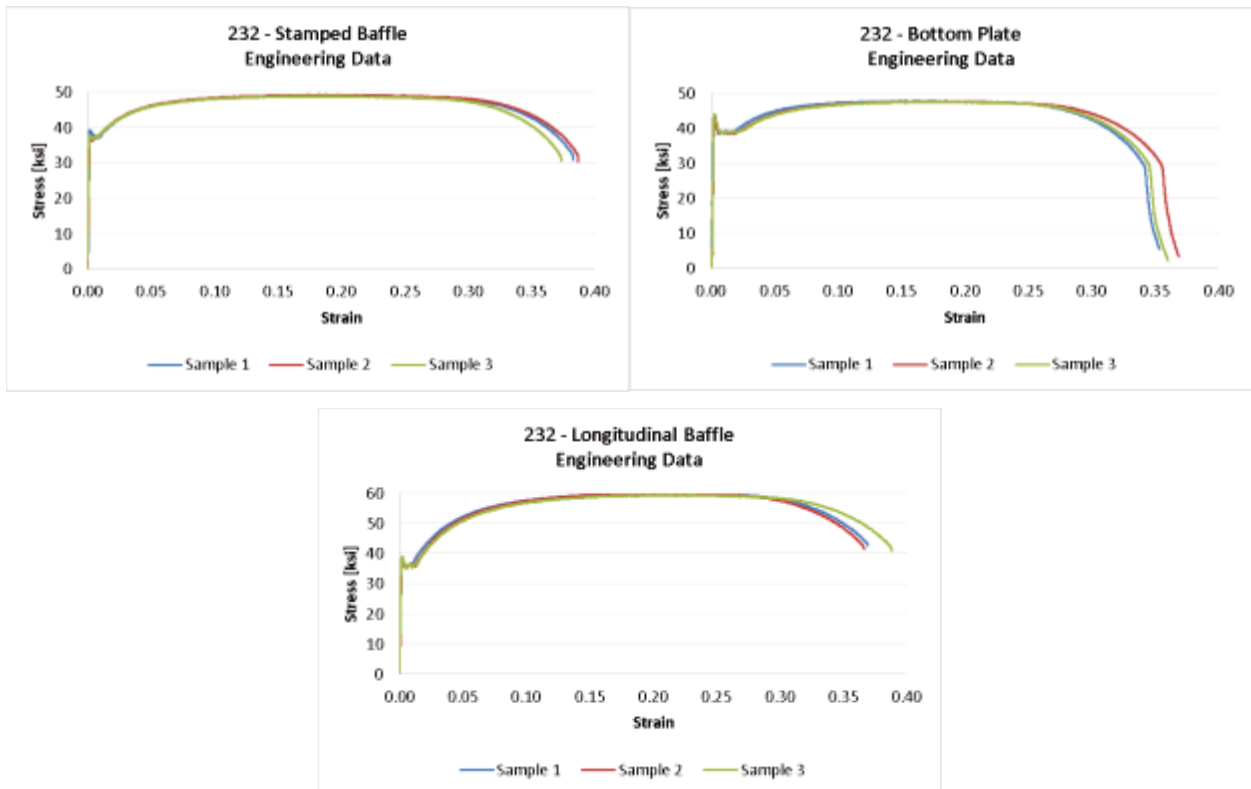


Figure B2. Engineering Stress-strain Responses from Tank 232 Members

Material Modeling In Abaqus/Explicit

For all materials used in tanks 202, 232, and 234, elasticity was modeled with $E=3 \times 10^7$ psi.

The Abaqus/Explicit FE software offers several approaches to modeling metal plasticity. Using an isotropic hardening approach, metal plasticity is defined using true plastic strain and true stress. Therefore, the engineering stress and engineering strain results obtained through tensile testing must be transformed using equations B1 and B2 before being included in the FE model.

Equations B1. and B2. True Stress and True Plastic Strain

$$\sigma_{\text{true}} = \sigma_{\text{nom}} (1 + \epsilon_{\text{nom}})$$
$$\epsilon_{\text{ln}}^{\text{pl}} = \ln(1 + \epsilon_{\text{nom}}) - \frac{\sigma_{\text{true}}}{E}$$

In addition to converting the data into the format used in Abaqus, the test data were reduced and regularized into approximately 10–15 points for each individual material. Each stress-strain curve, as input to the FE models for tanks 232 and 234, are shown in Figure B3. With the exception of the bottom sheet of tank 234, the same material characterizations were used for tank 232 and tank 234.

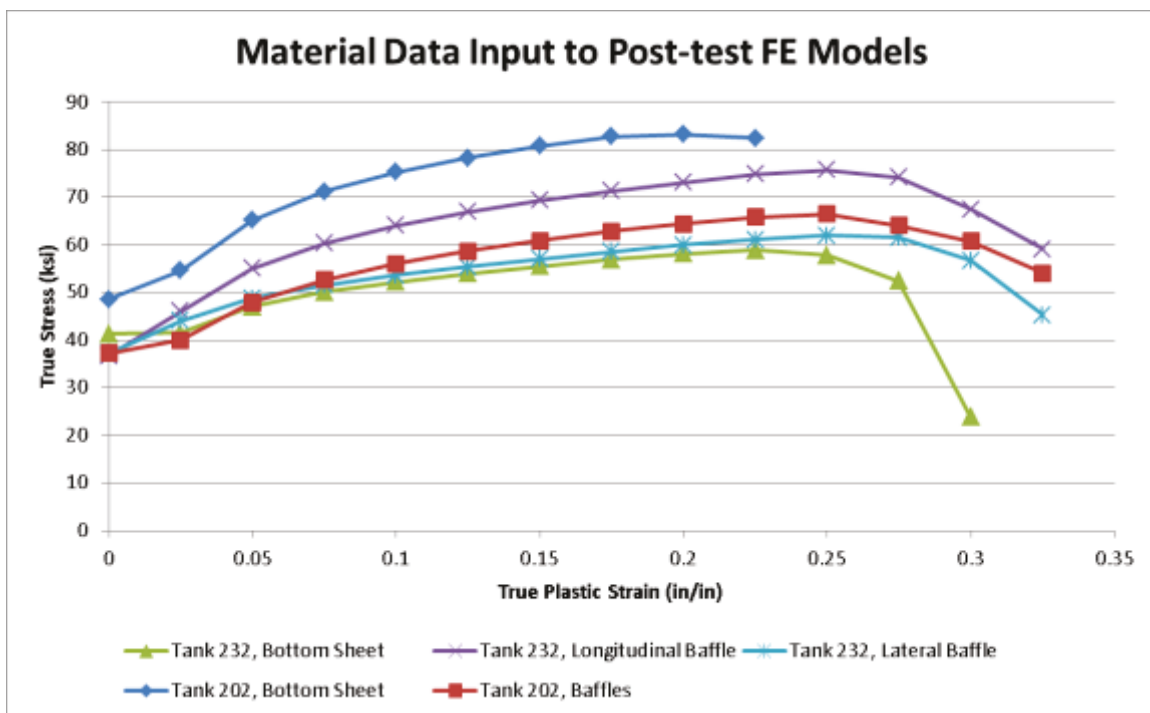


Figure B3. Stress-strain Data Defined in Post-test FE Models of Tanks 202 and 232

For tank 234, a more sophisticated material model was included in the FE model in order to include puncture capability within the model. Elasticity was modeled as before, using a modulus of 3×10^7 psi. Using the test results from tank 232's bottom sheet, a true stress, true strain curve was developed for the bottom sheet of tank 234. This curve features an increasing stress-strain relationship over the full range of strains developed during the test. While the test itself experiences a drop in stress associated with necking of the material and eventual fracture,

additional parameters will be defined within the model to capture these behaviors. The stress-strain relationship developed for tank 234's bottom sheet is shown in Figure B4.

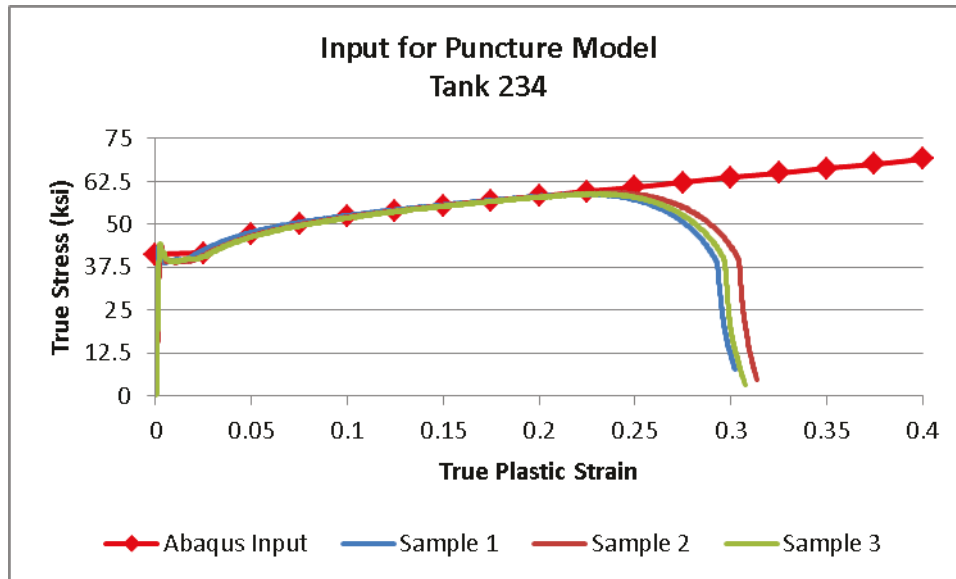


Figure B4. True Stress-strain Behavior for Tank 234 Puncture Model

In addition to elastic-plastic material behavior, damage initiation and progression characteristics were defined within the model, enabling element degradation and removal as a simulation of puncture. Previous FRA-sponsored research projects on railroad tank cars [14,18] and on end frame structures [15] have involved techniques for modeling material failure and element removal in FE models. In both programs, the failure theory developed by Bao and Wierzbicki (B-W) has been implemented within the FE model [16]. The B-W theory defines a failure initiation envelope as a function of the stress state (i.e., triaxiality) and the plastic equivalent strain (PEEQ). Extending from this theory, Lee and Wierzbicki have developed a technique for deriving the B-W envelope using the results of a uniaxial tensile test of the subject material. [17] Lee and Wierzbicki's method is referred to as the quick calibration method, and it was employed in this program to develop a failure model for the bottom sheets of tanks 232 and 234.

Once the baseline B-W envelope was derived, an FE model of a uniaxial test was used to derive additional model parameters necessary to model puncture. The first model used solid (brick) elements to model the uniaxial tension test. Once suitable results were obtained from this model, the material parameters and mesh density were used to generate a shell model of the tensile coupon. This model was then run, with appropriate adjustments made to the material characteristics using the results of the shell model. Once suitable results were obtained from the shell model of the tensile test, these material parameters were used as input to the fuel tank puncture model. Figure B5 is a flowchart showing the overall process for moving from tensile test results to the material failure model used in the fuel tank simulation.

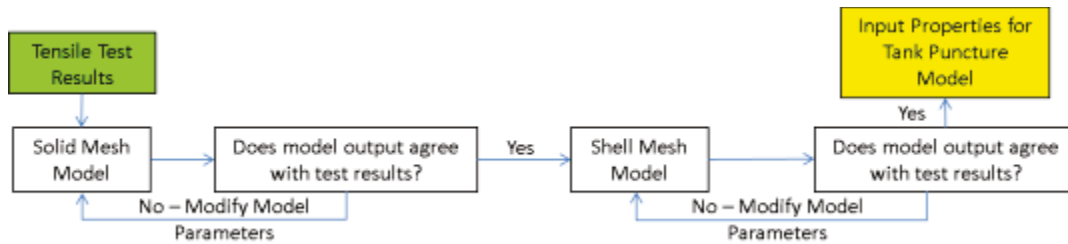


Figure B5. Process for Simulating Tensile Tests of Bottom Sheet Material

The key parameters that were varied were the mesh density (element size) and the damage evolution displacement. Within Abaqus, once the combination of PEEQ strain and triaxiality falls outside of the B-W envelope (i.e., damage has initiated), the element begins to lose its stiffness until it has zero load-carrying capacity and is removed from the mesh. The damage evolution displacement specifies the additional displacement an element may undergo once damage initiation has occurred.

Using the uniaxial tension sub-model, the tensile test was simulated. A displacement was applied to one end of the “dog bone” sample, with displacement increasing until fracture occurs in the gage length. In the solid element model, three planes of symmetry were used to speed up simulation time. The key output compared between the tests and the FEA is the nominal stress-strain relationship, including the strain at fracture. In both the test and the model, the nominal stress is the applied load divided by the initial area of the center of the sample. The nominal strain is the change-in-length of a 2-inch gage length in the center of the sample divided by the initial 2-inch length. Within the FE model, a soft (1×10^{-6} lbf/inch) spring was placed across the gage length to act as an extensometer and provide a simple way of calculating the change-in-length of the sample. Figure B6 shows the full sample’s dimensions, the symmetry used in one quadrant (note that an additional plane of symmetry exists in the plane of this page), and a focus on the fine mesh in the gage area.

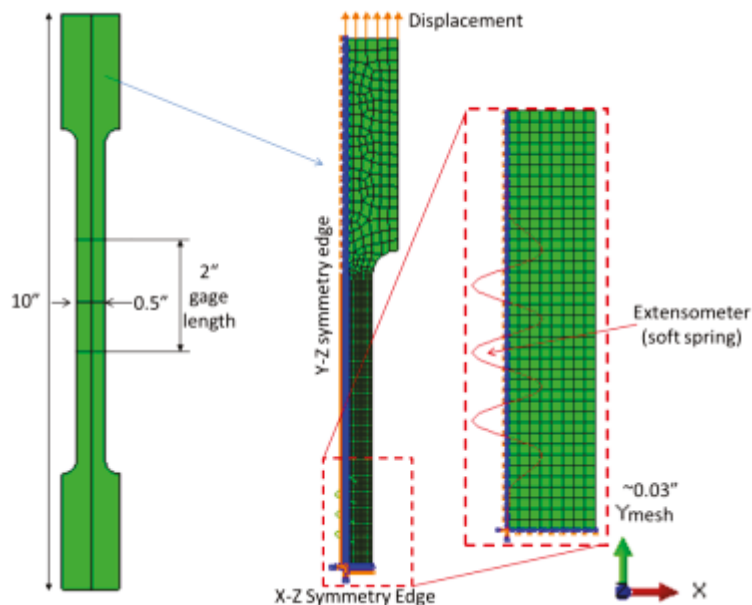


Figure B6. Uniaxial Tension FE Model (shell model shown)

While the uniaxial testing was performed quasi-statically, the Abaqus/Explicit solver was used to simulate the test. Because the ultimate goal of developing this material model was its use in a dynamic impact simulation, the material would ultimately be evaluated in an Abaqus/Explicit model. Therefore, it was important that the material’s damage characteristics be calibrated for use with this particular solver. The tensile simulation was performed at approximately 1.5 inches per second. The first model run used solid (brick) elements to mesh the coupon. The characteristics of this model are shown in Table B1.

Table B1. Summary of Properties in Solid Uniaxial Tension FE Model

Mesh	Solid (brick)
Element Type	C3D8
Number of Elements	1,596
Symmetry	Half-height Half-width Half-thickness
B-W Envelope	Baseline without adjustment
Damage progression	0.02 inch
Mesh in gage area	0.03 inch seeding

The results from the three tensile tests and the solid element FE model are shown in Figure B7. There is good agreement between the test results and the model’s response, particularly for the strain at fracture.

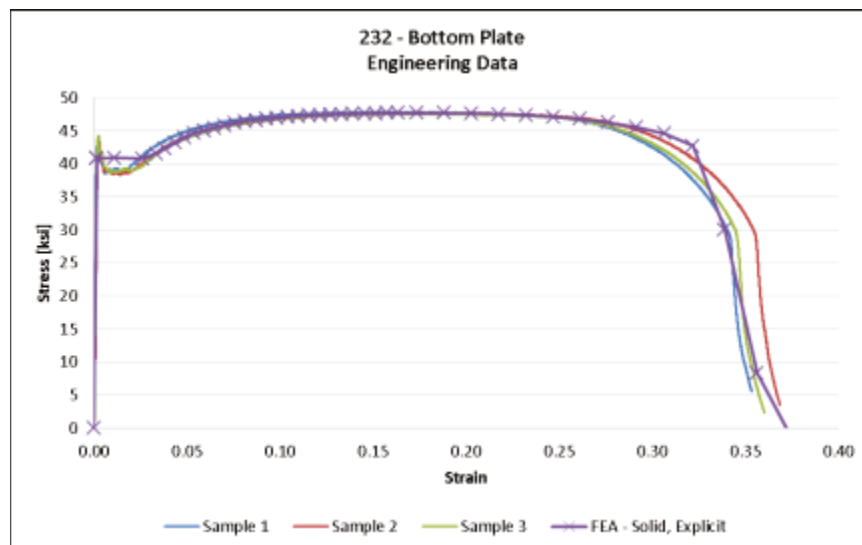


Figure B7. Stress-strain Comparison between Tensile Tests and Solid FE Model Tank 232

With satisfactory comparison between the solid FE model and the tensile test results, the tensile test was then simulated using shell elements. Because the fuel tank was to be modeled using

shell elements, it was essential to ensure that shell elements were capable of capturing the fracture behavior in a similar way as the solid elements. The mesh density and load rate were maintained at the same values as were used in the solid model. The properties of the shell model of the uniaxial test are shown in Table B2.

Table B2. Summary of Properties in Shell Uniaxial Tension FE Model

Mesh	Shell
Element Type	S4
Number of Elements	879
Symmetry	Half-height Half-width
B-W Envelope	Baseline curve OR Baseline curve with -0.1 PEEQ shift
Damage progression	0.02 inch
Mesh in gage area	0.03 inch seeding

The first simulation used the baseline B-W envelope without further modification. The stress-strain relationships for this FE model and the three tensile tests are shown in Figure B8.

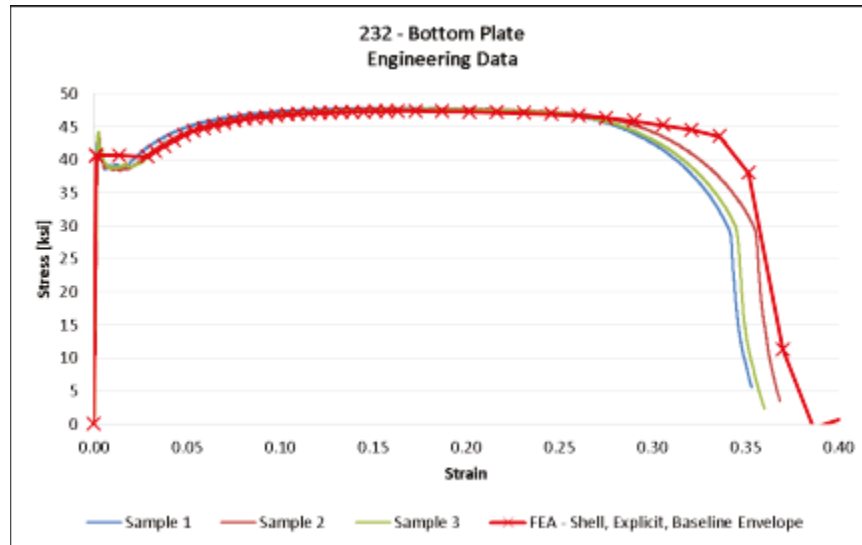


Figure B8. Stress-strain Comparison between Tests and Shell FE Model Tank 232 (Baseline Envelope)

Because shell elements cannot capture the through-the-thickness behavior in the same way that several discrete brick elements through the thickness of the coupon would, some adjustments were made to the baseline B-W envelope in order to achieve agreement between the shell model and the tests. Particularly, because the B-W- envelope uses the triaxiality of the stress state within an element, care must be taken when using this failure initiation criterion with shell elements. Regardless of the actual stress state, shell elements will experience a through-the-thickness stress of 0, which can lead to an inaccurate value for triaxiality. From the work done by

Stringfellow and Paetsch [15], the baseline B-W envelope was shifted with respect to PEEQ for use with shell elements. The baseline B-W curve was shifted downward by a PEEQ of 0.1. The baseline and shifted (shell) B-W envelopes are shown in Figure B9.

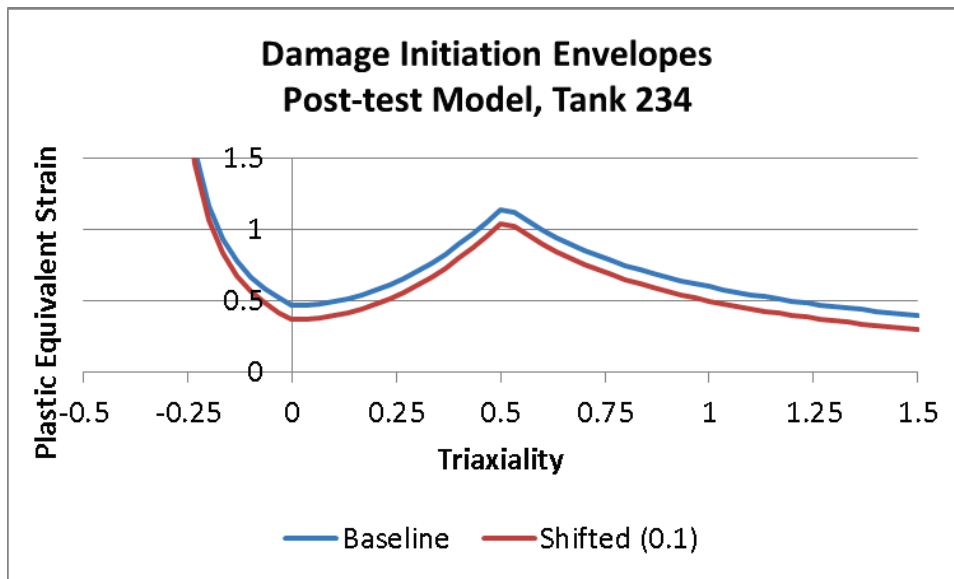


Figure B9. Baseline and Shifted Failure Initiation Envelopes

Using the shifted B-W envelope, the model was run to simulate the uniaxial tension test. The results of that simulation are shown in Figure B10.

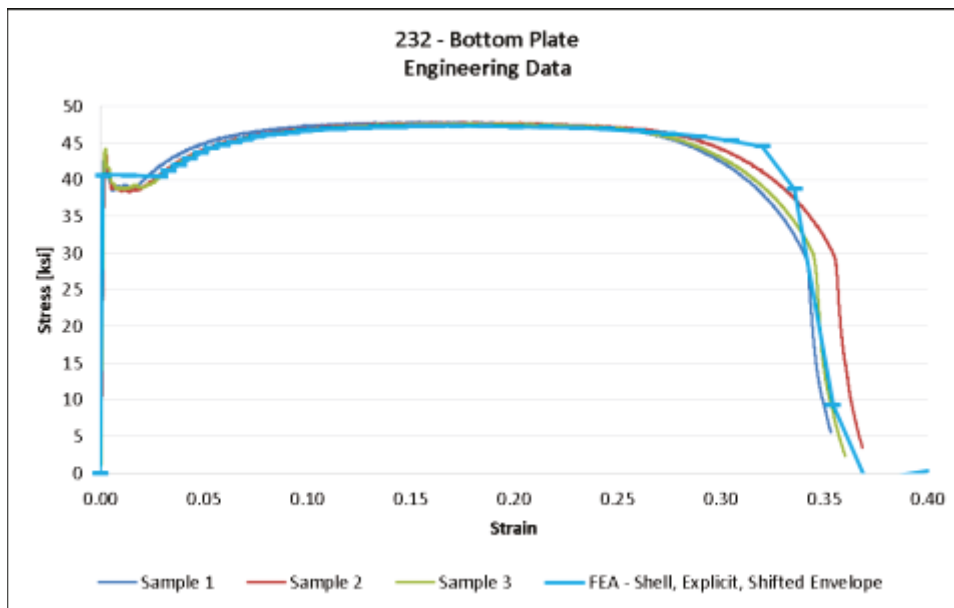


Figure B10. Stress-strain Comparison between Tests and Shell FE Model Tank 232 (Shifted Envelope)

As a further check on the quality of the material models developed, the toughness was calculated for each of the three tests and each of the three models. The toughness is calculated as the area beneath the stress-strain curve (in engineering units). The shell model with a shifted B-W envelope had a toughness that was ~0.6% higher than the average of the three test values. This

was considered acceptable correlation between test and analysis results. A plot of toughness versus strain is shown in Figure B11, and a table of values is shown in Table B3.

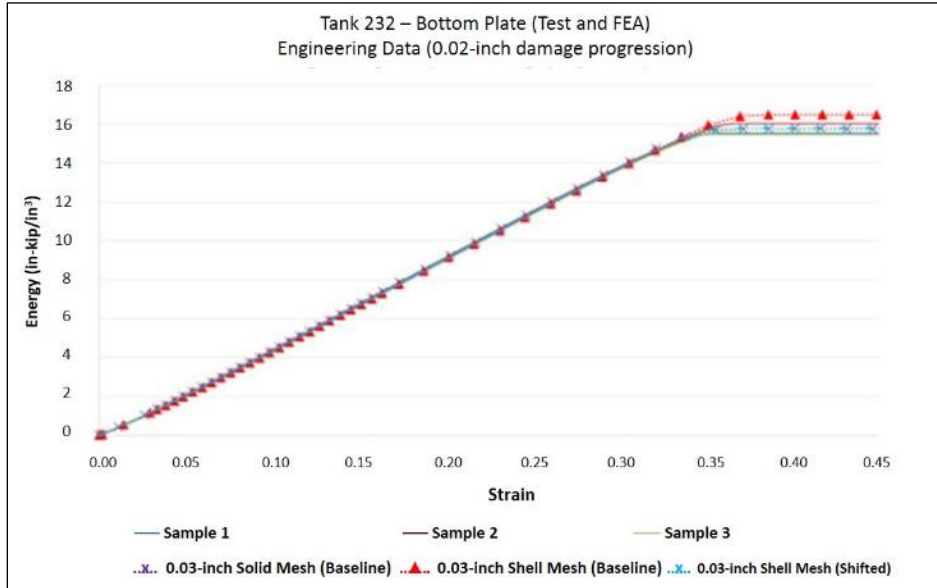


Figure B11. Tank 232 Toughness vs Strain for Each Tensile Test or Simulation

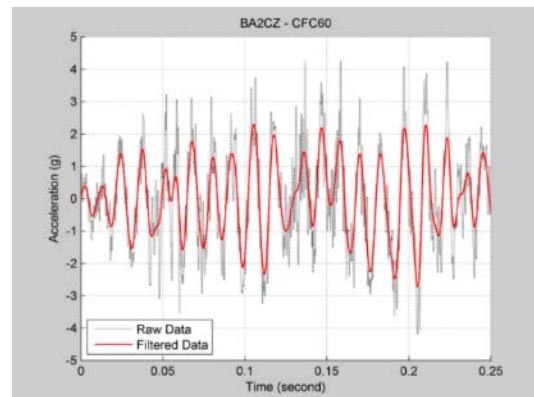
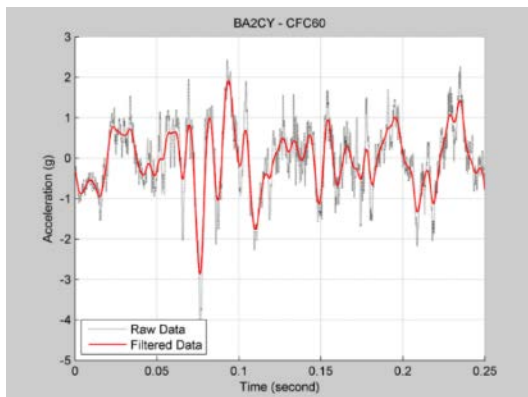
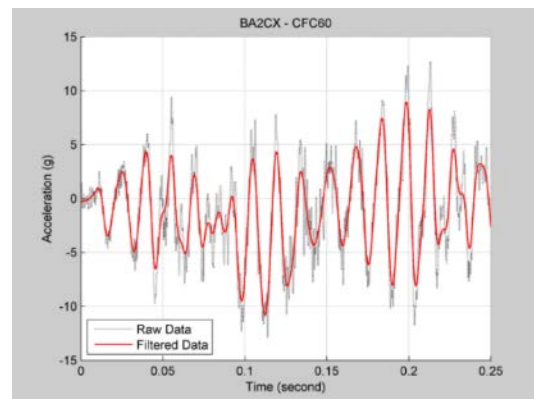
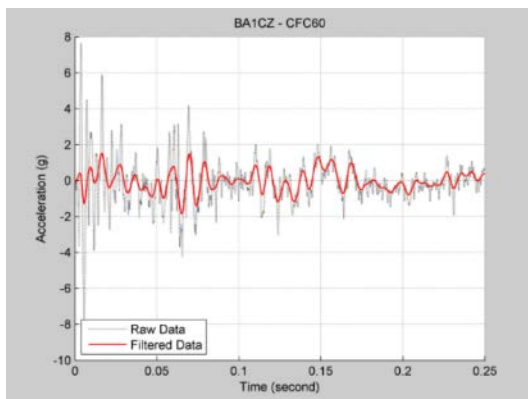
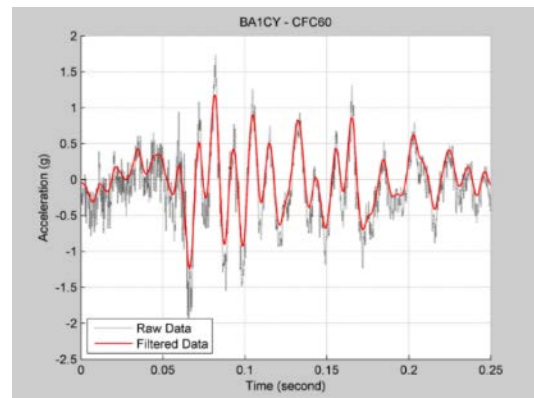
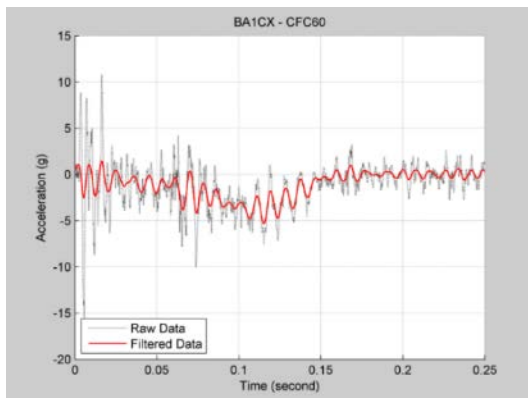
Table B3. Toughness for Each Tensile Test or Simulation

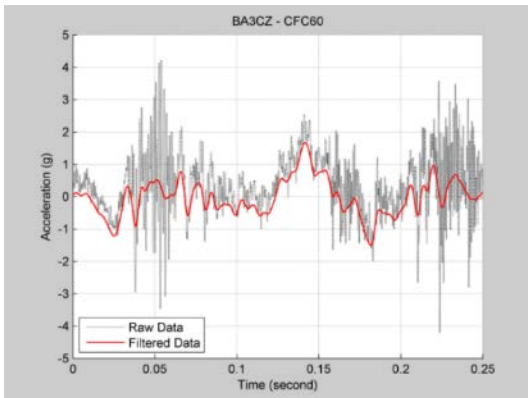
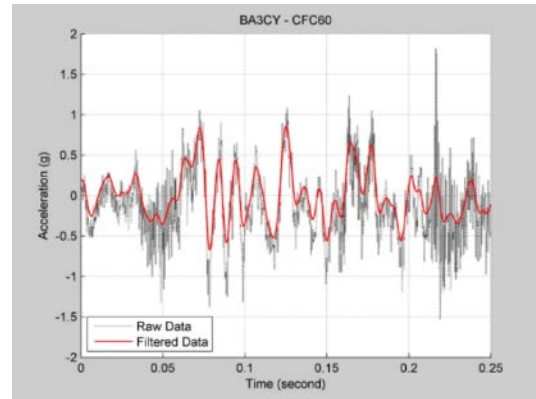
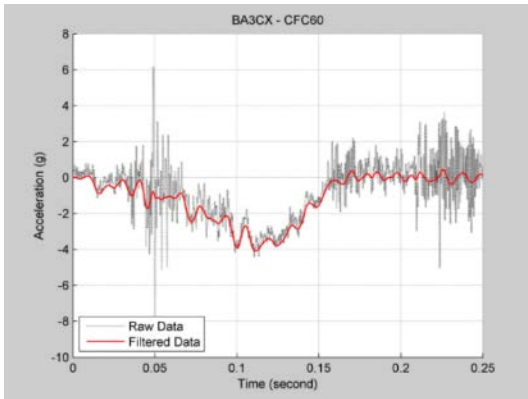
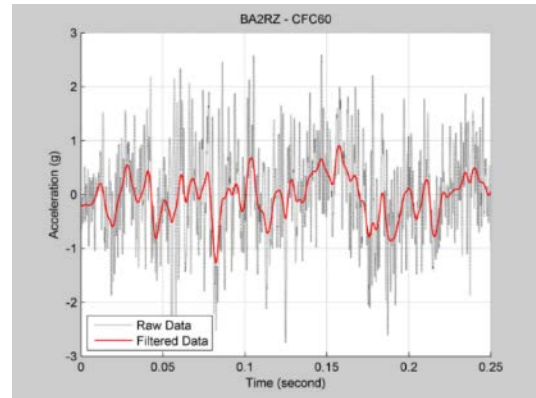
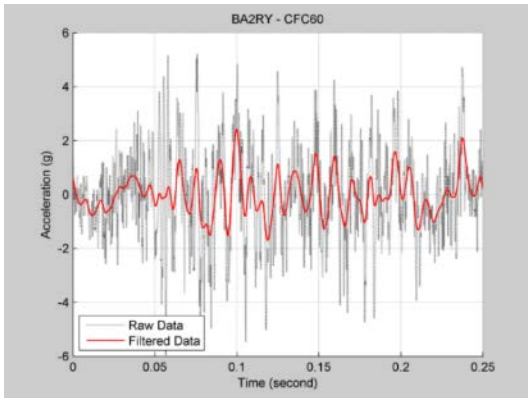
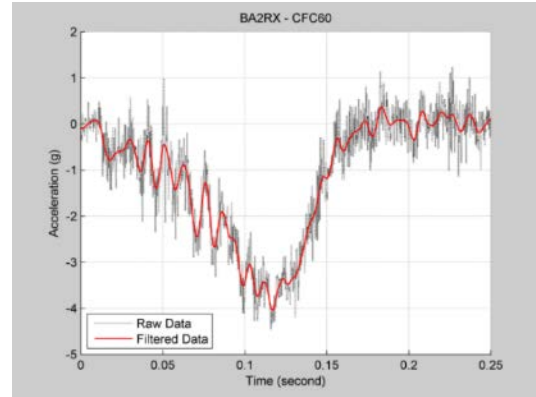
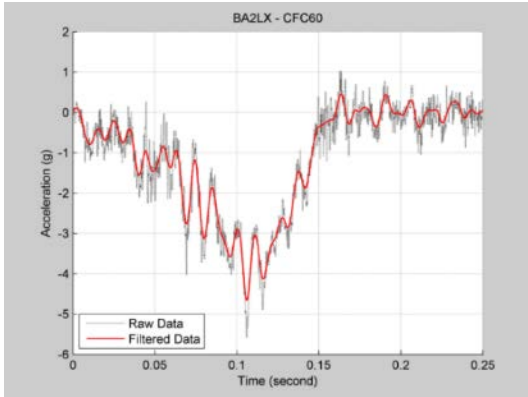
	Toughness (in-kip/in ³)	% Difference
Sample 1	15.49	-1.28
Sample 2	16.03	2.16
Sample 3	15.55	-0.881
Test Average	15.69	0
Solid Mesh (Baseline)	15.76	0.46
Shell Mesh (Baseline)	16.49	5.09
Shell Mesh (Shifted)	15.79	0.60

Appendix C. Test Data

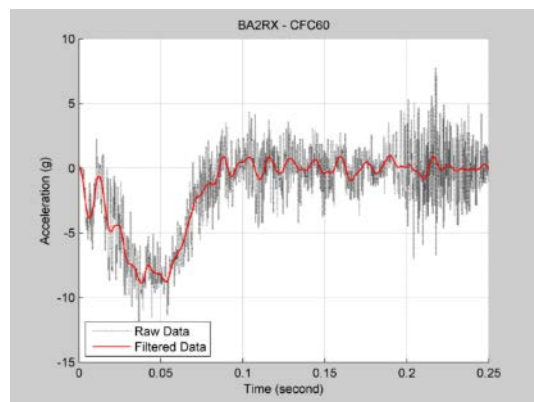
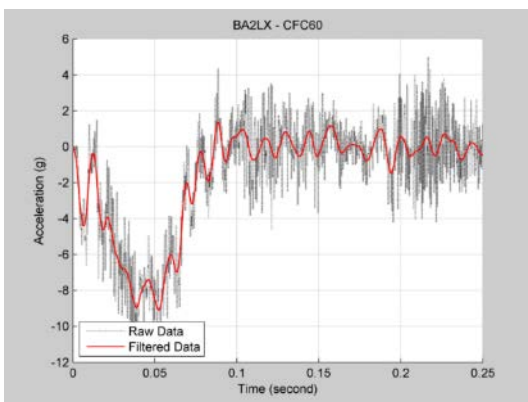
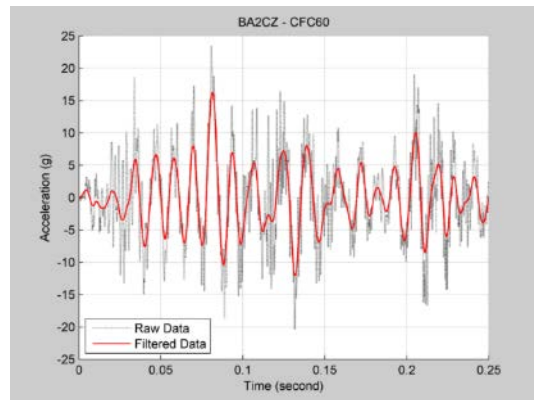
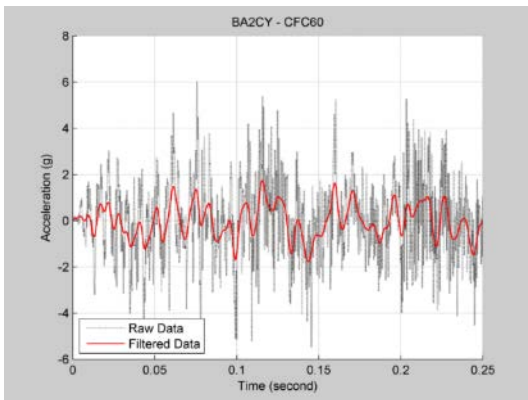
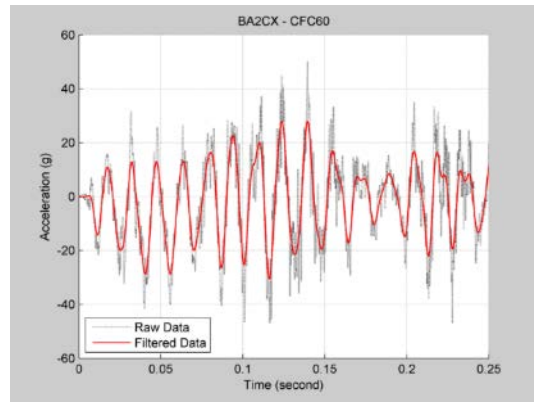
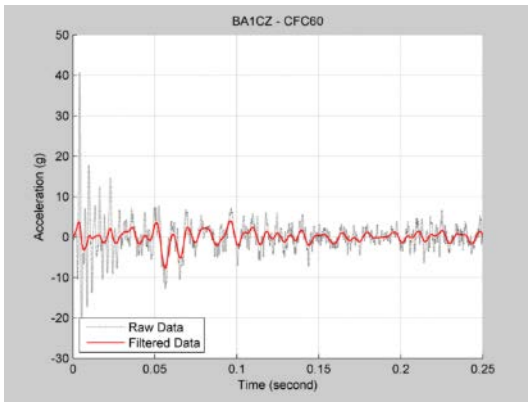
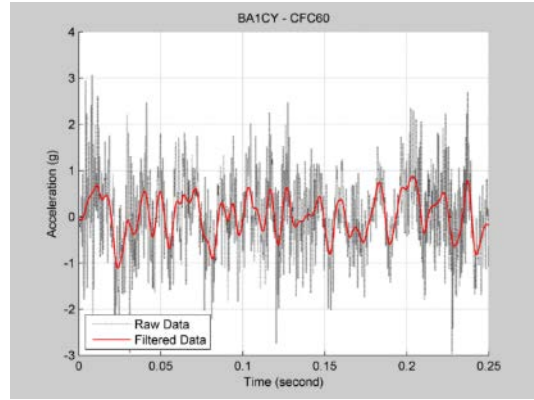
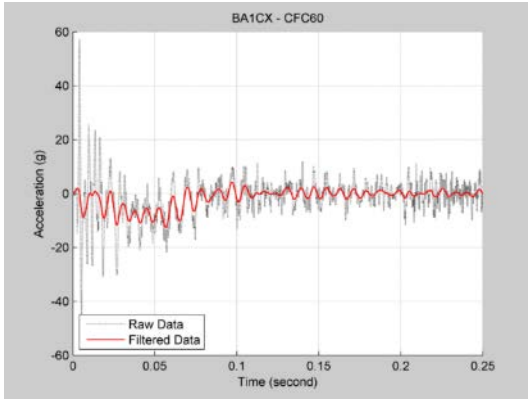
This appendix contains raw and filtered test data. The raw accelerations measured on different locations on the impact cart were processed as follows for all tests. The test data from -1 seconds to -0.1 seconds on each channel were averaged, and this value was subtracted from the test measurements in order to remove any initial offsets in the data. Each channel was then filtered to channel frequency class (CFC) 60, using the procedures given in SAE J211 [10].

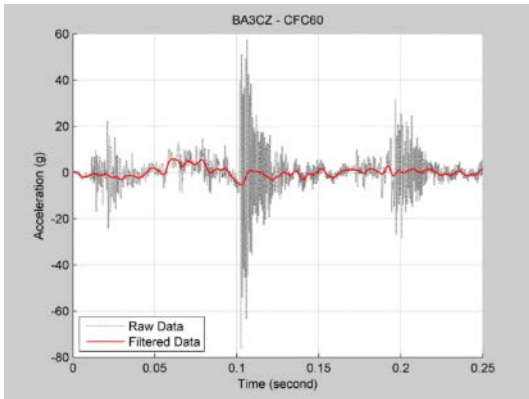
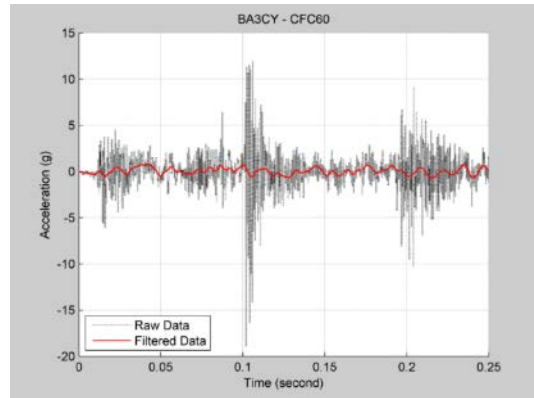
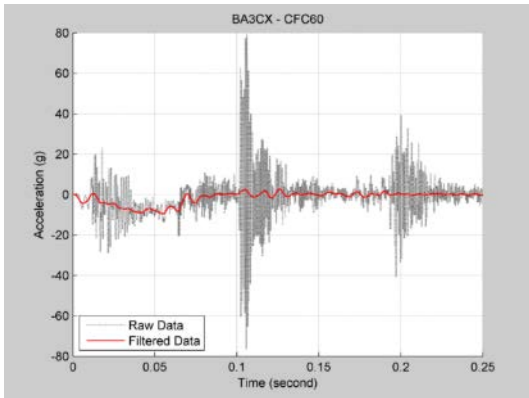
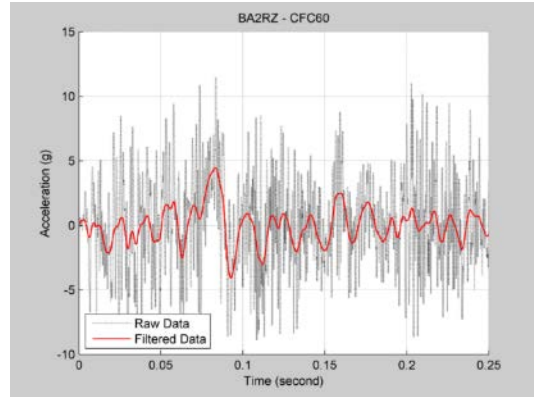
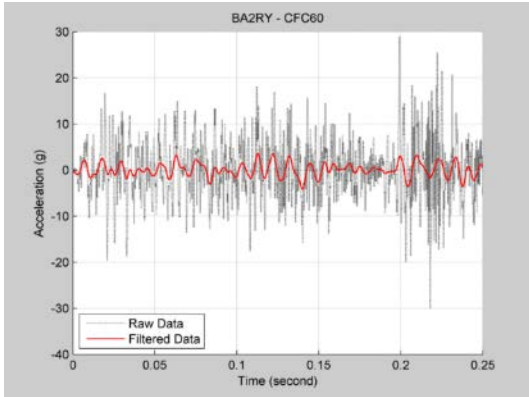
Tank 232 – Impact Speed: 4.5 mph



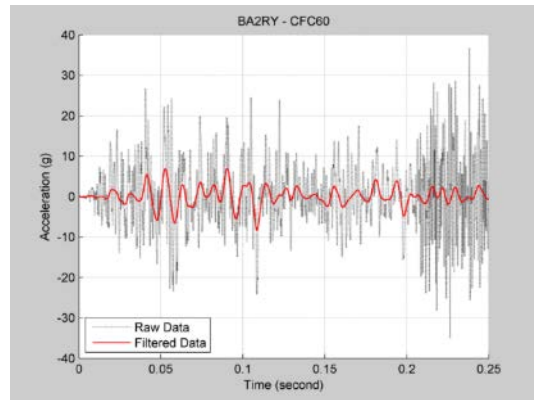
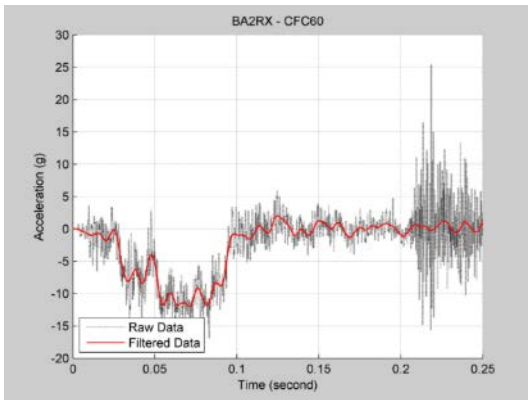
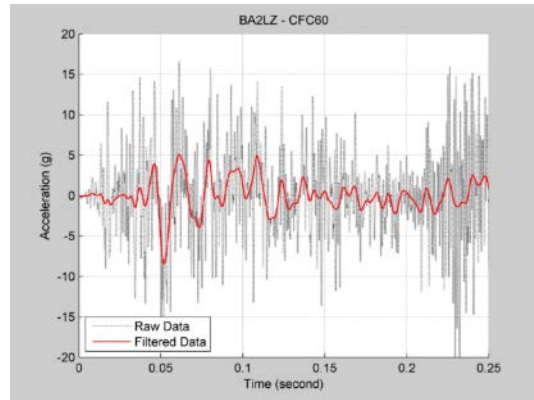
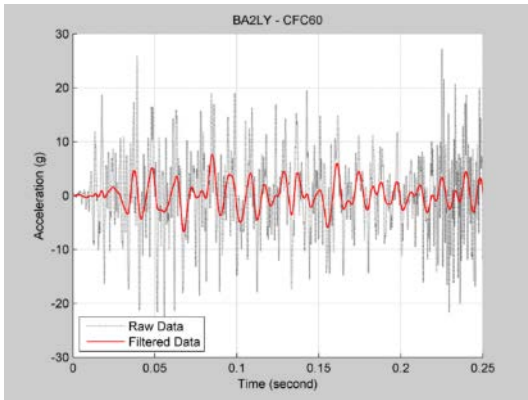
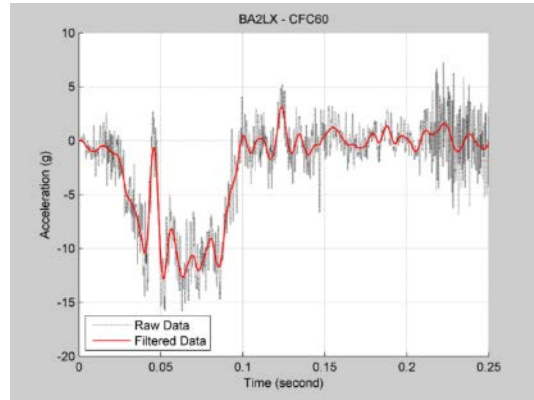
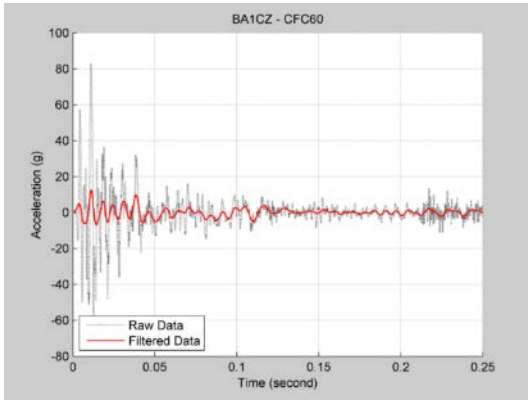
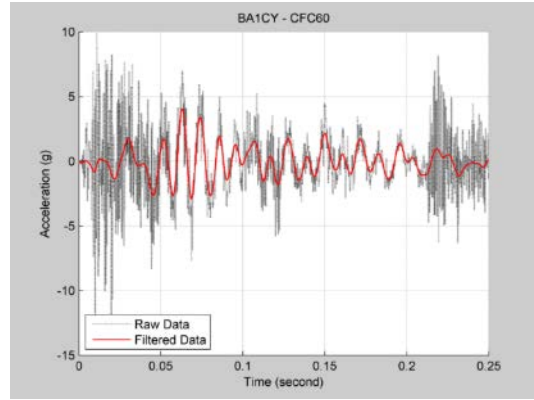
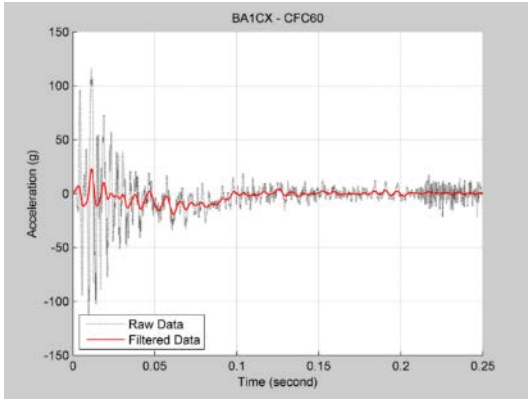


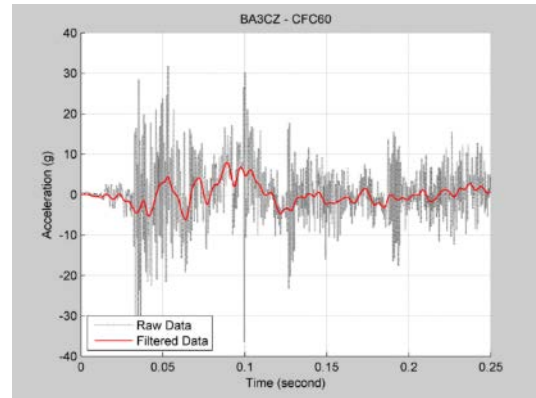
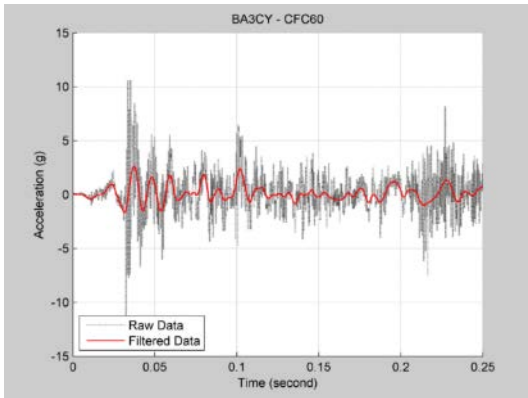
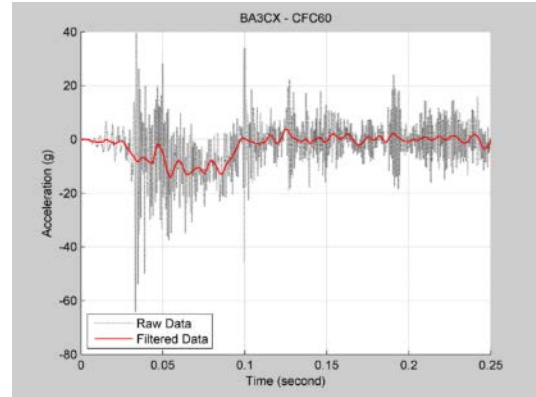
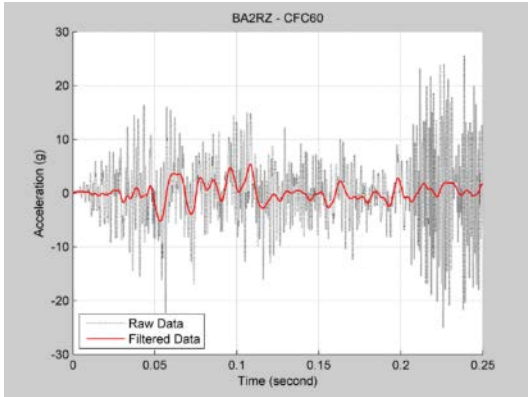
Tank 202 – Impact Speed: 6.2 mph





Tank 234 – Impact Speed: 11.2 mph





Appendix D.

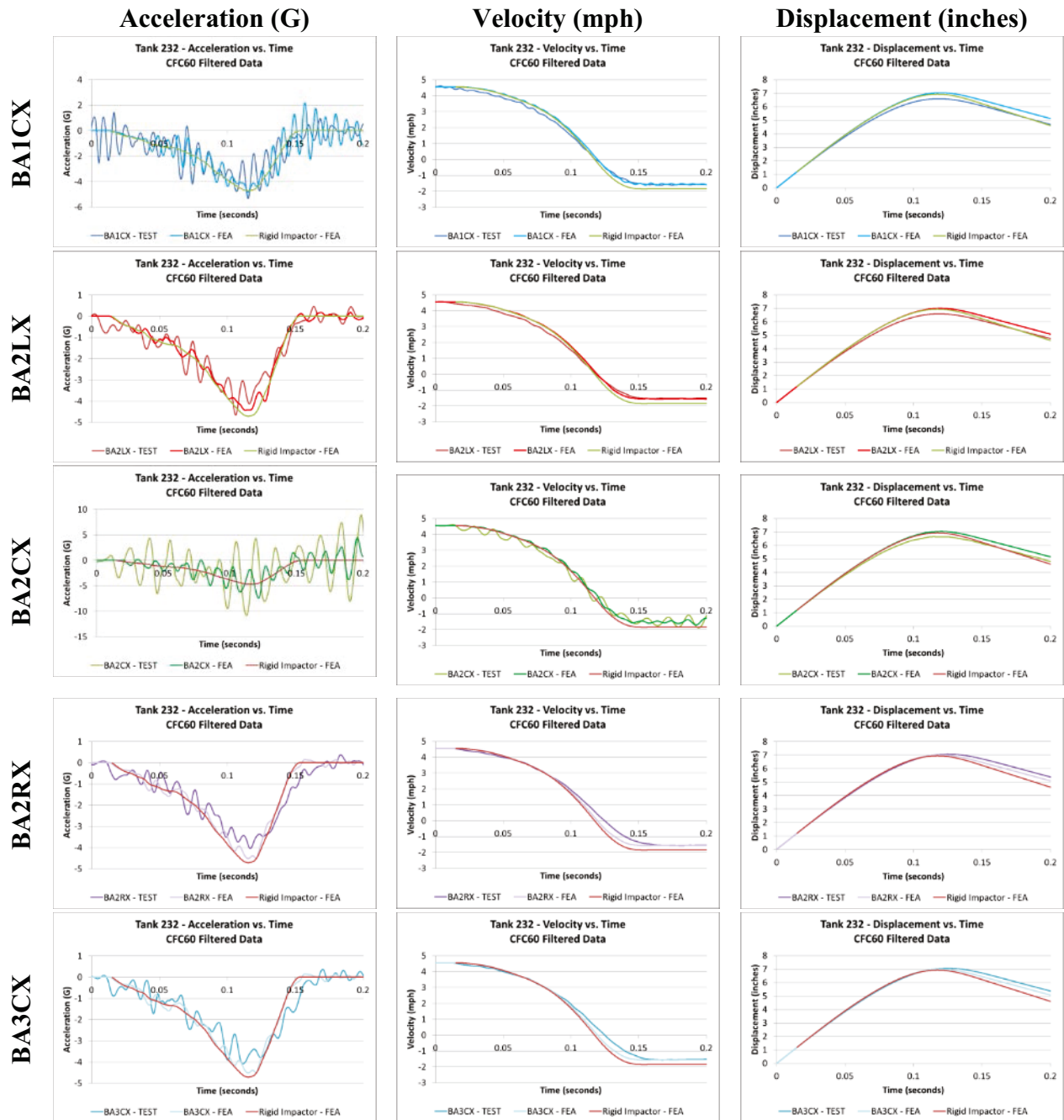
Comparison Between Test Data and Finite Element Analysis Results

This appendix contains comparisons between the filtered test data and finite element analysis (FEA) results for the longitudinal acceleration, velocity, and position quantities as obtained through the onboard accelerometers in the case of test data or derived from acceleration measurements at corresponding locations for FEA results involving a deformable impact cart. For some results, a corresponding set of FEA results using a rigid impactor with a mass equal to that of the deformable cart is also shown. Inclusion of both the rigid and deformable impactor FEA results allows the effects of cart deformation to be examined.

Velocity-time data were obtained by integrating the filtered acceleration-time history, and setting the speed at $t=0$ equal to the average time obtained by the speed trap measurements. Finally, displacement-time data were obtained by integrating the velocity-time data and setting the displacement at $t=0$ equal to 0 inches.

Tank 232 – Post-test Model

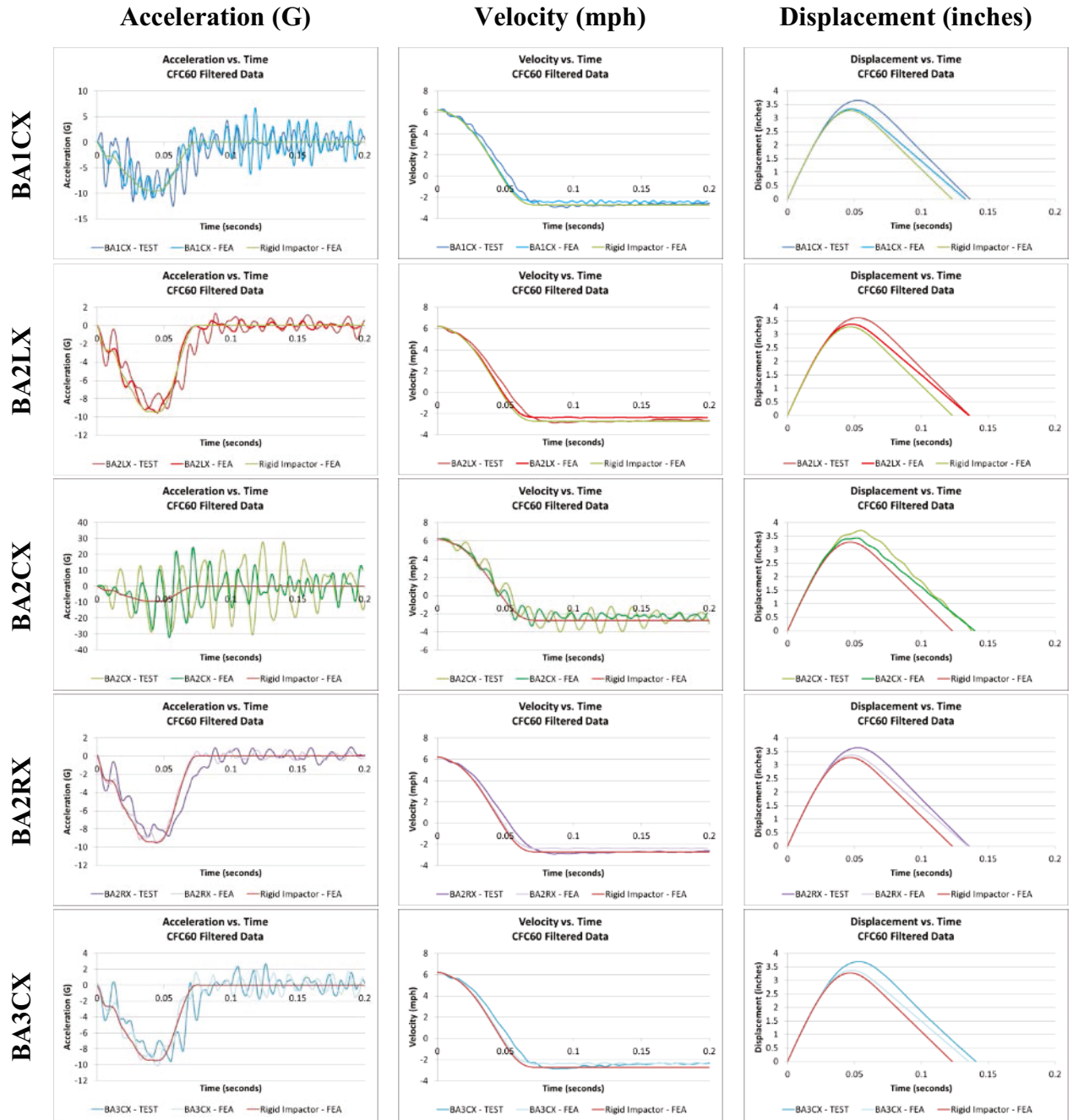
Impact Speed: 4.5 mph



* For the FE model of tank 232, the impactor was initially offset from the tank at t=0 seconds. This was done to attempt to compensate for the uncertainty between the triggering of the instrumentation and the actual contact with of the impactor with the tank, as discussed in Section 3.4.4. In the FE model, this corresponded to a time offset of 0.015 second, or approximately 1 inch.

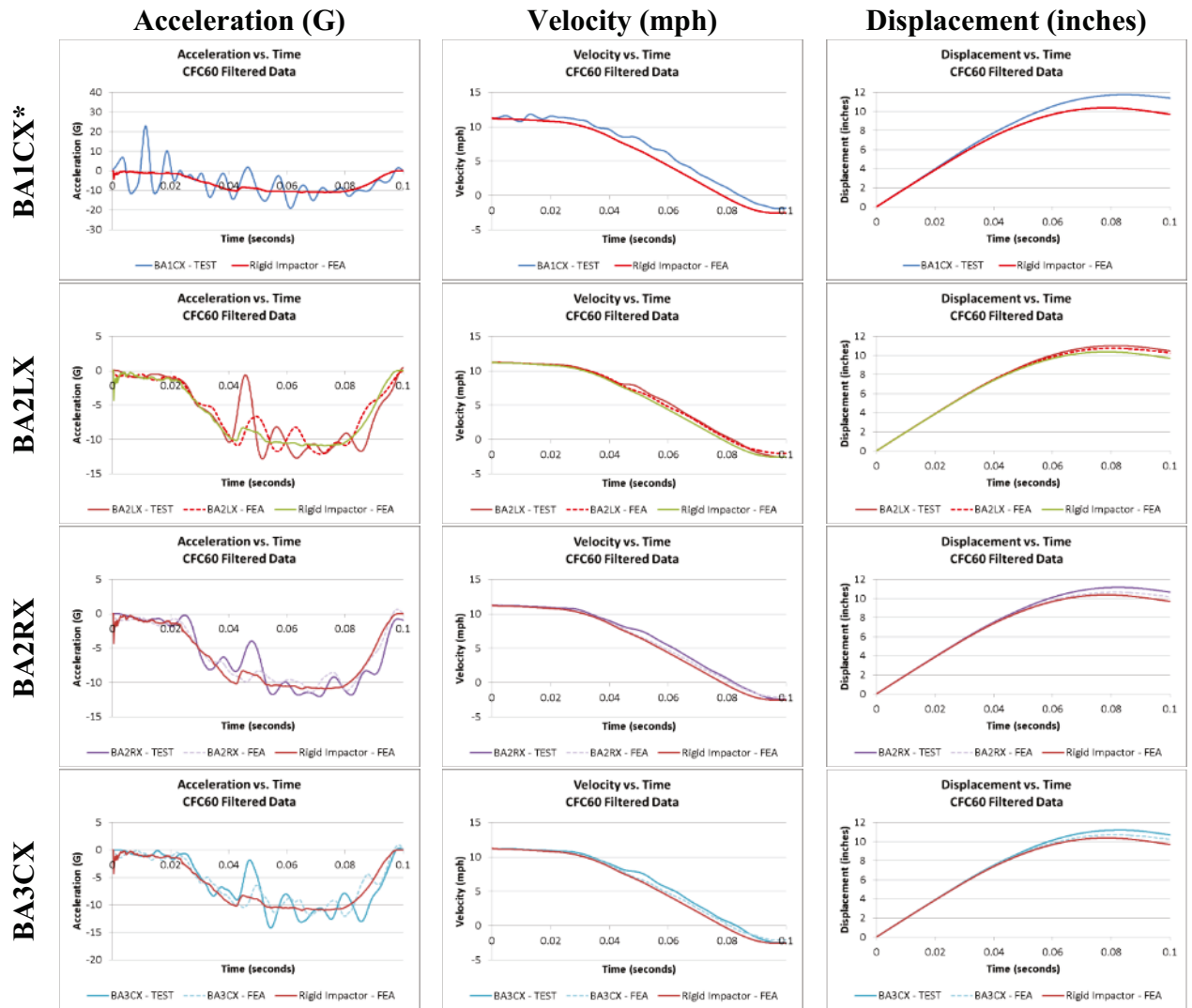
Tank 202 – Post-test Model

Impact Speed: 6.2 mph



Tank 234 – Post-test Model

Impact Speed: 11.2 mph



*Deformable FEA results not requested at BA1CX location due to high-frequency noise.

Abbreviations and Acronyms

AAR	Association of American Railroads
APTA	American Public Transportation Association
CFC	Channel Frequency Class
CFR	Code of Federal Regulations
DMU	Diesel Multiple Unit
DOF	Degrees of Freedom
EMD	Electro-Motive Diesel, Inc.
FE	Finite Element
FEA	Finite Element Analysis
FRA	Federal Railroad Administration
MBTA	Massachusetts Bay Transportation Authority
PEEQ	Plastic Equivalent
TTC	Transportation Technology Center
TTCI	Transportation Technology Center, Inc.
Volpe	John A. Volpe National Transportation Systems Center